Numerical Modelling of Fretting Fatigue Crack Initiation and Propagation
Using Extended Finite Element Method and Cyclic Cohesive Zone Model

Numerieke modellering van scheurinitiatie en -verspreiding door passingroestvermoeiing
met behulp van een uitgebreide eindige-elementenmethode
en een cyclisch samenhangend zonemodel

Kyvia de Fatima Resende Pereira

Promotor: prof. dr. ir. M. Abdel Wahab
Proefschrift ingediend tot het behalen van de graad van
Doctor in de ingenieurswetenschappen: werktuigkunde-elektrotechniek

UNIVERSITEIT
GENT

Vakgroep Elektromechanica, Systeem- en Metaalengineering
Voorzitter: prof. dr. ir. L. Dupré
Faculteit Ingenieurswetenschappen en Architectuur
Academiejaar 2019 - 2020

ISBN 978-94-6355-315-5
NUR 978
Wettelijk depot: D/2019/10.500/123

Promoter

prof. dr. ir. Magd Abdel Wahab
Ghent University
Faculty of Engineering and Architecture

Examination Committee

prof. Filip de Turck (Chair)

prof. Wim De Waele

prof. Libardo Vanegas Useche

prof. Timon Rabczuk

dr. Jacob Sukumaran

Research Institute

Department of Electrical Energy, Metals, Mechanical Constructions and Systems
Faculty of Engineering and Architecture
Ghent University
Technologiepark 903
B-9052 Zwijnaarde
Belgium

Email: KyviadeFatima.ResendePereira@UGent.be
http://www.soetelaboratory.ugent.be

Acknowledgements

Firstly, I would like to express my immense gratitude to my promoter, prof. dr. ir. Magd Abdel Wahab, for giving me the chance to work in a very interesting research topic and for his guidance during this work. I am very thankful for all his support throughout my Master's thesis and PhD research. I really appreciate all discussions and advices, that go well beyond engineering topics. Thank you also for the opportunities to present our work in international meetings and conferences; they helped me to shape my career as a researcher.

I would also like to thank my colleagues from UGent for all support and great atmosphere throughout my PhD. Special thanks to Junyan

Ni and Tongyan Yue for all delicious Chinese lunches and for always been there to share good and bad moments. Thank you also to my Brazilian lunch buddies, Leandro and Vitor. I wish you all the best and hope to see you again in Brazil, Belgium or anywhere else in the world.

Thank you also to the Laboratory Soete staff and professors for all support. Special thanks to Georgette D'Hondt for her patience and great care. Her efforts to help us, students, goes above and beyond. I really appreciate all her help, not only with administrative paperwork, but also with personal matters. Many thanks to all professors for creating such nice environment and being always willing to share their knowledge. I would like to thank Ghent University and the Doctoral Schools for promoting courses and events that allow us, students from different countries, to share our research experience, cultures and different backgrounds. This allowed me to grow not only as a researcher, but as a person.

Many thanks to the Research Foundation-Flanders (FWO) for funding my research and providing me the opportunity to be part of an European project. This was a great opportunity to work and learn from renowned researchers. Thank you for funding our meetings in Gent, Luxembourg and Slovenia, they were extremely important for the work contained in this thesis.

As a personal note, I would like thank some very important people in my life. Firstly, my parents, that even though they barely know how to read and write, they have always understood the importance of a good education. Through their hard work, they measured no efforts

to make sure that I could study and and pursue my dreams. I cannot thank them enough and I hope that they know that everything I have I owe to them both. Finally, but not least, I would like to thank the two with whom I share the same roof: my beloved husband and my dear daughter. My daughter arrived to this world while I was concluding this PhD and I must say that her laughs were what kept me going until the end. To my husband, thank you for making me smile on the toughest days and for encouraging me to move forward. I can only say that if I got to this point in my life, it is because you were always by my side. I love you both, unconditionally.

Kyvia de Fátima Resende Pereira

2019

Contents

List of Figures

List of Tables

List of Abbreviations and Symbols

a_{cont}	semi-contact width
a	crack length
a_c	critical crack length
a_i	enriched degree of freedom nodal vector
D	damage variable
$\dot{D}$	incremental damage (derivative of damage variable over time)
Δ_0	separation for which traction is maximum
Δ_f	critical maximum separation
Δ_Σ	accumulated cohesive length
$\dot{\Delta}$	increment of separation at the cohesive surfaces
$\dot{\varepsilon}$	incremental strain at the cohesive surfaces
ε_Σ	accumulated cyclic strain
ε_n	normal strain at the cohesive surface
ε_t	tangential strain at the cohesive surface
E	modulus of elasticity (Young's Modulus)
E^*	combined modulus of elasticity
f_1	quadratic traction separation criterion
f_2	maximum nominal stress criterion

ν	Poisson's ratio
F	normal load
G	fracture energy
K	cohesive stiffness of the reversible part of the traction-separation law
k_I^*	mode I stress intensity factor at the tip of a crack branch segment
k_{II}^*	mode II stress intensity factor at the tip of a crack branch segment
K_I	mode I stress intensity factor
K_{II}	mode II stress intensity factor
K_{Ic}	Mode I fracture toughness
μ	coefficient of friction
$N_i(x)$	nodal functions
N_i	initiation lifetime
N_P	propagation lifetime
N_{exp}	experimental total lifetime
N	number of cycles
$p(x)$	contact pressure distribution
p_{max}	maximum contact pressure distribution
Q	tangential load
$q(x)$	tangential shear stress
σ_{axial}	applied axial stress
σ_{bulk}	applied bulk stress
σ_f	fatigue endurance limit
σ_{eff}	effective stress acting on the cohesive surface
σ_n	normal stress at the cohesive surface
σ_t	tangential stress at the cohesive surface
σ_u	ultimate tensile stress
σ_{axial}	cyclic axial loading
$\sigma_{0.2}$	yield strength
θ_P	estimated crack propagation orientation
T	effective traction at cohesive surface
$T_{(max,0)}$	initial maximum cohesive strength
T_{max}	instantaneous maximum cohesive strength
$t_{n,c}$	cohesive strength under pure mode I condition
$t_{s,c}$	cohesive strength under pure mode II condition
$\boldsymbol{u}$	displacement vector
u_i	nodal displacements
2D	two-dimensional
3D	three-dimensional
CZM	Cohesive Zone Model
CCZM	Cyclic Cohesive Zone Model
CDM	Continuum Damage Mechanics
DENT	Double edge notched tensile
FE	Finite Element
FEM	Finite Element Method
FEA	Finite Element Analysis
FP	Findley parameter
FS	Fatemi-Socie parameter

LEFM	Linear Elastic Fracture Mechanics
MPC	Multi-Point Constraint
MTS	Maximum tangential stress
SIF	Stress intensity factor
XFEM	Extended Finite Element Method

Summary

Fretting occurs when two normal loaded contacting surfaces are submitted to oscillatory relative movement of small amplitude. Depending on service conditions, fretting fatigue may reduce significantly the life of a component. The contact interaction between bodies, non-proportional loading condition, and high stress gradient near contact are some of the characteristics of fretting that imposes difficulty in the numerical modelling of this phenomenon. Although it is a topic that has been vastly studied over the past decades, better numerical models that capture the effect of those main features in the prediction of fretting fatigue lifetime is still of great interest and is going to be the

main focus of this thesis.

As mentioned above, modelling of contact interactions and stresses are one of the main characteristics of fretting fatigue that brings extra complexity to numerical analysis of this phenomenon. Generally, predictions of fretting fatigue initiation lifetime rely on the correct estimation of those stresses at contact interface. The accuracy of those stresses greatly depends on the mesh size at interface. Therefore, aiming to guide researches on their modelling parameters, we proposed a convergence map for mesh size selection for analysis of fretting fatigue coupon tests (cylindrical pad and flat specimen configuration). Moreover, we also studied the presence of stress singularity in these conditions and we have found that there is no singularity present. Therefore, researches should be careful when approximating the subsurface stresses near contact per analytical expressions that considers singular stress fields.

When dealing with estimation of crack propagation lifetime, most work in the literature use linear elastic fracture mechanics (LEFM). Traditionally, a stepwise methodology is adopted in finite element, in which each step consists of the analysis of a full loading cycle. Based on the stresses near the crack tip at each step of the analysis, the crack is allowed to grow in a direction determined via classical orientation criteria (such as maximum tangential stress MTS). The main issue here is that those orientation criteria were developed under the assumption of proportional loading conditions, which are not valid for the case of fretting. The non-proportional loading characteristic of this phenomenon poses a difficulty in the analysis and, when it is not taken

into account, may lead to incorrect crack propagation paths. In this thesis, we implemented an appropriate orientation criterion for non-proportional loading (an extension of MTS) and checked its performance under fretting conditions. It is important to highlight that in order to properly make use of this MTS extension, we need to accurately obtain the stress at crack tip for every instant of time in the loading cycle. Under these conditions, crack faces might be in contact to each other and the proper modelling of this interaction is, therefore, essential. We also implemented an alternative way to account for crack faces in conventional finite element analysis using the commercial software ABAQUS. Our findings, for both crack propagation path and life estimates, showed a good agreement with experimental data, indicating that the non-proportional loading characteristic of fretting problems should not be neglected.

The high stresses at contact interface affect directly the crack initiation and the crack propagation phases, as a considerable amount of plasticity may be present around the contact region. Linear elastic fracture mechanics may not be the best tool to predict lives in these situations, since one of its main assumptions is the requirement of very small plastic zone around crack tip. To circumvent this problem, we proposed the use of cohesive zone model (CZM). It is a non-linear approach to model the process zone ahead of the crack tip and its main feature is that the stresses at this region are limited by the cohesive strength of the material. Therefore, there is no requirement of limited size of plasticity around the crack tip.

Firstly, we used monotonic cohesive zone models to study crack

initiation location and orientation. Our results were comparable with traditional critical plane approaches and were in good agreement with experimental data. However, the monotonic cohesive zone models are unable to capture damage accumulation under cyclic loading and a direct application of such approach may lead to crack arrest instead of propagation. To avoid this issue, one alternative is to use cyclic cohesive zone model (CCZM), an extension of monotonic cohesive zone models that allows for modelling a cycle-by-cycle damage accumulation.

We implemented and used cyclic cohesive zone model for predicting fretting fatigue lives. Firstly, we extended the ABAQUS capability by introducing a damage accumulation law to account for degradation due to loading and reloading under cyclic conditions. In this work, we implemented this law by writing user subroutines that allowed the material properties to change within the analysis. We integrated these user subroutines with extended finite element method (XFEM) and cohesive segments methodology and used them to model failure in a cycle-by-cycle analysis. The results were verified with literature data, giving confidence that the implementation is indeed correct. An interesting advantage of this technique is that it is unnecessary to divide the crack regime into initiation and propagation phases, once cyclic cohesive models treat the problem in a unified way. Nonetheless, the main drawback here is that CCZMs are extremely computationally demanding and a cycle-by-cycle approach is normally not feasible. To overcome or at least alleviate this issue, we proposed the use of CCZM in junction with an extrapolation approach that enabled us to predict lives in high cycle fatigue without dealing with all the computational

burden of a cycle-by-cycle analysis.

Based on our simulations, we concluded that our methodology (cyclic cohesive zones in junction with an extrapolation procedure) is a great alternative to model fretting problem under conformal contact (flat pad in contact with a flat specimen). We were able to correctly predict fretting fatigue lives with a narrower error band than predictions from classical approaches (continuum damage mechanics in junction with classical fracture mechanics). In addition, our results had lower mean squared error when compared with experimental data, evidencing the robustness of this method.

Finally, the main contribution of this thesis relies on proposing better approaches to accurately estimate fretting failure lifetime under different configurations and accounting for many of its complexities. Our results indicates that the non-proportional loading characteristic of fretting is an important factor that should not be neglected in the analysis. Moreover, the use of XFEM in junction with CCZM for predicting fretting fatigue lifetime seems to be a promising alternative to classical approaches.

Samenvatting

Fretting treedt op wanneer twee normaal belaste contactoppervlakken onderworpen worden aan een oscillerende relatieve beweging met een kleine amplitude. Afhankelijk van de gebruiksomstandigheden kan fretting vermoeiing de levensduur van een component aanzienlijk verkorten. Hoewel het een onderwerp is dat in de afgelopen decennia uitgebreid is bestudeerd, is een beter begrip en voorspelling van fretting vermoeiing nog steeds cruciaal voor veel technische problemen, wat de belangrijkste focus van dit proefschrift zal worden.

Numerieke modellering van fretting vermoeiing zorgt voor extra complexiteit vanwege de belangrijkste kenmerken van dit fenomeen, zoals contactinteractie en een hoge spanningsgradiënt in de buurt van deze interactie. Het is belangrijk om te garanderen dat de spanning op de contactinterface nauwkeurig wordt berekend, omdat dit voorspellingen van de start van de levensduur van de fretting vermoeiing kan beïnvloeden. We stellen een convergentiekaart voor om onderzoek te begeleiden naar de selectie van de maaswijdte voor analyse van testen van de sterkte van fretting vermoeiing coupons (cilindrische en vlakke specimenconfiguratie). Bovendien hebben we ook de aanwezigheid van singulariteit van spanning in deze omstandigheden bestudeerd en we hebben ontdekt dat er geen singulariteit aanwezig is. Onderzoekers moeten daarom voorzichtig zijn bij het benaderen van de subsurface spanning in de buurt van analytische expressies, rekening houdend met enkelvoudige spanningsvelden.

Wanneer het gaat om het inschatten van de levensduur van fretting vermoeiing, wordt in de meeste literatuur gebruik gemaakt van lineaire elastische fractuurmechanica (LEFM) om de levensduur van scheurpropagatie te voorspellen. Traditioneel wordt een stapsgewijze methodologie toegepast in een finiet element, waarbij elke stap de analyse van een volledige laadcyclus comprimeert. Op basis van de spanning nabij het scheurpunt in elke stap van de analyse laat men de scheur groeien in een richting die wordt bepaald via klassieke oriëntatiecriteria (zoals maximale tangentiële spanning of 'MTS'). Het belangrijkste probleem hierbij is dat die oriëntatiecriteria werden ontwikkeld onder de veronderstelling van proportionele laadcondities, die niet geldig zijn in het geval van fretting. De niet-proportionele

laadkarakteristiek van dit fenomeen vormt een moeilijkheid in de analyse en, zoals besproken in de literatuur, hebben veel onderzoekers die deze klassieke benadering hebben gebruikt, de propagatiepaden onder fretting niet correct kunnen voorspellen. In dit proefschrift hebben we een geschikt oriëntatiecriterium geïmplementeerd voor niet-proportionele belasting (een uitbreiding van MTS) en hebben we de prestaties gecontroleerd onder omstandigheden van fretting. Een belangrijk punt hier is dat, om correct gebruik te maken van deze MTS-uitbreiding, we nauwkeurig de spanning op het scheurpunt moeten verkrijgen op elk moment van de laadcyclus. Onder deze omstandigheden kunnen scheurvlakken in contact komen en de juiste modellering van deze interactie is daarom essentieel. We hebben ook een alternatief geïmplementeerd om rekening te houden met scheurvlakken in conventionele eindige elementenanalyse met behulp van de commerciële software Abaqus. Onze bevindingen (voor zowel propagatiepad als levensduurschattingen) lieten een goede overeenkomst zien met experimentele gegevens, wat aangeeft dat de niet-proportionele belastingskarakteristiek van fretting niet mag worden verwaarloosd.

De hoge spanningen op de contactinterface beïnvloeden de scheurinitiatie en de scheurpropagatiefases rechtstreeks, aangezien een aanzienlijke hoeveelheid plasticiteit rond de contactregio aanwezig kan zijn. Lineaire elastische breukmechanica is misschien niet het beste hulpmiddel om levensduur te voorspellen in deze situaties, omdat één van de belangrijkste veronderstellingen van deze methodologie de eis is van een zeer kleine plastisch zone rond het scheurpunt. Om dit probleem te omzeilen, stellen we het gebruik van cohesieve zonemodellen voor. Dit is een niet-lineaire benadering om de proceszone vóór

het scheurpunt te modelleren met als belangrijkste kenmerk dat de spanningen in dit gebied worden beperkt door de cohesiesterkte van het materiaal. Daarom zijn er geen aannames met betrekking tot de grootte van deze plastisch zone.

Ten eerste hebben we monotone cohesieve zonemodellen gebruikt om de locatie en oriëntatie van de scheurinitiatie te bestuderen. Onze resultaten waren vergelijkbaar met traditionele kritieke vlakke benaderingen en waren in goede overeenstemming met experimentac-cumulatie onder cyclische belasting weer te geven en pogingen om het onder deze omstandigheden te gebruiken kunnen leiden tot scheurarrest in plaats van propagatie. Om dit te omzeilen, is het nodig om het cyclische cohesieve zonemodel (CCZM) te gebruiken, een uitbreiding van een monotoon cohesief zonemodel dat het mogelijk maakt om de schade na elke cyclus te modelleren.

We stellen een innovatieve tool voor om levensduur bij fretting vermoeiing te voorspellen met behulp van CCZM. Ten eerste hebben we de Abaqus-capaciteit uitgebreid door een model te introduceren dat opgebouwde schade bevat door het laden en herladen onder cyclische belasting. In dit werk hebben we dat bereikt door gebruikerssubroutines te schrijven waardoor de materiaaleigenschappen binnen de analyse konden veranderen. We hebben deze gebruikerssubroutines geïntegreerd met de uitgebreide eindige-elementenmethode (XFEM) en cohesieve segmentmethodologie en deze gebruikt om falen te modelleren in een cyclus-voor-cyclusanalyse. De resultaten zijn geverifieerd met literatuurgegevens, wat vertrouwen geeft dat, zodra cyclisch samenhangende modellen het probleem op een uniforme manier be-

handelen, de implementatie inderdaad correct is. Een interessant voordeel van deze techniek is dat het niet nodig is het scheurregime te verdelen in initiatie- en propagatiefasen. Deze transitie van korte naar lange scheuren is niet eenvoudig en kan de voorspellingen aanzienlijk beïnvloeden. Niettemin is het grootste nadeel hier dat CCZM's extreem computationeel veeleisend zijn en dat een cyclus-per-cyclusbenadering normaal onhaalbaar is. We stellen het gebruik van CCZM voor met een extrapolatiebenadering die ons in staat stelt om levensduur te voorspellen in hoge cyclusvermoeiing zonder alle computationele last van een cyclus-voor-cyclusanalyse.

Op basis van onze simulaties hebben we geconcludeerd dat onze methodologie (cyclische samenhangende zones gecombineerd met een extrapolatieprocedure) een alternatief is voor het probleem om fretting vermoeiing te modelleren bij conform contact (vlak in contact met een vlak preparaat). We konden de levensduur van fretting vermoeiing correct voorspellen met een kleinere foutmarge dan voorspellingen uit klassieke benaderingen (d.i. continuümschademechanica in verbinding met lineaire elastische breukmechanica). Bovendien waren onze resultaten ook meer gecentraliseerd rond experimentele gegevens, wat de robuustheid van deze methode aantoont.

Ten slotte is de belangrijkste bijdrage van dit proefschrift gebaseerd op het voorstellen van betere benaderingen voor het nauwkeurig schatten van de levensduur bij fretting vermoeiing onder verschillende configuraties en rekening houdend met de vele complexiteiten. Onze resultaten geven aan dat de niet-proportionele belastingskarakteristiek van fretting een belangrijke factor is die niet mag worden verwaar-

loosd in de analyse. Bovendien lijkt het gebruik van XFEM in combinatie met CCZM voor het voorspellen van de levensduur van fretting vermoeiing een veelbelovend alternatief voor klassieke benaderingen.

1

Introduction

Fretting is a phenomenon that happens when two contacting surfaces are normally loaded and subjected to small amplitude oscillatory relative movement. This amplitude generally varies from 5 to

100 μm (Ding et al., 2004), but it can be as low as, or even below, 1 μm (Vingsbo and Söderberg, 1988b). Due to its cyclic characteristic and the high stress gradient at vicinity of contact, fretting may lead to unexpected failure due to fretting fatigue, being responsible for premature failure of many common mechanical assemblies, such as bolted joints, shrink fitted shafts and dovetail joints.

Under fretting conditions, the fatigue limit of a material may be shortened by up to 50% (Jeung et al., 2015, and references therein). It is known that, in this case, the crack growth phase is significantly different from plain fatigue propagation phase, due to the influence of contact stress distributions on the crack and vice-versa (Giner et al., 2008). These stresses at contact interface affects the crack growth, particularly for crack lengths smaller than the magnitude of the contact zone dimension and must be taken into account in any analysis of fatigue lifetime (Hills and Nowell, 1994). The contact stresses are easily computed in numerical methodologies, such as finite element models with contact algorithms. Therefore, it is not surprising that this tool has been vastly used to study fretting fatigue.

Finite element method has been used to predict fretting fatigue lives. As mentioned above, prediction of fretting lives has been of great interest due to its dramatic impact on fatigue lifetime. In this regard, the numerical estimate of lives is generally obtained by combining two different mechanisms: fretting fatigue crack initiation and crack propagation. Depending on the fretting conditions, failure may be mainly governed by the initiation phase and life estimates may be based only on this mechanism. On the other hand, propagation phase may be the

dominant phase and neglecting initiation may lead to reasonable live estimates. However, neglecting one phase may lead to poor predictions, as shown in the results from Madge et al. (2008). Their study shows that neglecting effects of wear on crack nucleation and considering life as purely dominated by propagation of long cracks can lead to erroneous results.

There has been some effort to combine both phases in life predictions (Hojjati Talemi, 2014; Navarro et al., 2003; Giner et al., 2011a; Hojjati-Talemi et al., 2014). Navarro et al. (2003) developed a procedure to combine initiation and propagation lives in order to obtain total failure life. Initiation life were obtained considering McDiarmid multiaxial fatigue criterion and propagation life were estimated Paris' law with stress intensity factors computed via analytical expressions. The results were in agreement with experimental data with reasonable accuracy, being within a x2 error band. Similar approach has been used by Giner et al. (2011a), they compare the impact of computing stress intensity factors via XFEM and via analytical expressions. Their life estimates were, for the majority of tested cases, in agreement with experimental data within a x2 error band as well. They argued that the three cases with estimated lives much smaller than experimental ones were the cases with smallest pad radius, that causes a smaller contact region and concentrate the stresses in a smaller region. This leads to greater initiation life that is not captured by their model. Hojjati Talemi (2014) computed initiation life using continuum damage mechanics and estimated propagation lives using LEFM and a Paris' law. Their results showed that initiation and propagation lives were a considerable percentage of total failure lifetime, showing the necessity

of accurately modelling both phases. Regarding to lifetime estimates, their estimates were within a x1.5 error band and in good agreement with experimental data.

Generally, total life is obtained as the sum of number of cycles to initiate a crack (initiation phase) and the number of cycle to propagate this crack until it reaches a critical length (propagation phase). However, the clear definition of when initiation phase finishes and propagation phase starts is not straightforward and needs to be properly ensured to guarantee accuracy of lifetime estimates. In the next chapter we aim to discuss different approaches used to study propagation phase under fretting conditions and their impact on the live estimates.

1.1 Objectives

One of the main objectives of this thesis is accurately estimating fretting fatigue lives, taking into consideration important characteristics of this phenomenon, such as crack face contact and non-proportional loading conditions. Although these features increase the complexity of the analysis, accounting for their effect may lead to substantially better live predictions.

The contact interactions between crack faces and the non-proportional nature of the loading conditions are considered in a linear elastic fracture mechanic (LEFM) approach. The stresses around the crack tip are modified according to the contact status of the crack faces and the non-proportional characteristic of the loading history is taken into account by a non-conventional crack orientation criterion.

The main drawbacks of LEFM are the necessity of separating crack initiation and propagation phases, the requirement of a small plasticity zone around the crack tip and also the need of relying on an empirical law (such as Paris' Law) to predict crack growth. Cyclic cohesive zone model (CCZM) comes as an alternative to circumvent those issues. It is a non-linear methodology that models failure of the process zone ahead of the crack tip. One of its main features is that the stresses at the process zone are limited by the cohesive strength of the material, having no limitations regarding the size of plastic zone around the crack tip.

In this regard, another important goal of this thesis is the implementation of cyclic cohesive zones in ABAQUS and its use to predict fretting fatigue lives.

As additional goals, we also intend to study stress singularity in a cylindrical pad configuration and propose a map to guide on the selection of adequate mesh sizes for 2-D analysis of a cylindrical pad in contact with a flat specimen. The use of monotonic cohesive law to predict crack initiation and orientation is also discussed as an alternative approach to classical critical plane ones.

1.2 Outline

This thesis is organized in the following way. Firstly, in Chapter 2 a literature review of the main methodologies used throughout this thesis is presented. We start by introducing fretting phenomena, followed by a description of coupon test configurations. Contact mechan-

ics is briefly discussed and analytical solutions for simple cases are presented. Next, we introduce some common approaches to estimate fatigue propagation lives, with emphasis to LEFM and damage models. Finally, numerical implementations of crack propagation analysis in conventional finite element, extended finite element and extended finite element with cohesive segments are also discussed.

Chapter 3 brings attention to the importance of analysing numerical errors in a finite element analysis of fretting fatigue. If not properly considered, these errors can have a large impact on the results, especially for life estimates of crack initiation where an accurate estimate of the contact stresses is essential. We also performed an analysis of stress singularity for cases of fretting in cylindrical pad and flat specimen configuration. Moreover, we proposed a map to guide researchers to better design and analyse their numerical studies.

Chapter 4 deals with propagation life estimates of fretting fatigue for a cylindrical pad in contact with a flat specimen. One of the main contributions of this study is the estimation of lives considering non-proportional loading and, therefore, the effect of potential crack faces contact. This contact interaction has a major impact on the stress around the crack tip and, therefore, on the estimates using LEFM. The choice of suitable orientation criterion that accounts for non-proportional loading allows for the correct crack propagation path estimation.

In Chapter 5, monotonic cohesive zone model is used to predict crack initiation location and orientation. Results are compared to classical critical plane approaches (the Findley (FP) and Fatemi-Socie (FS)

parametes). The implementation of both cohesive zone model and critical plane approaches are discussed and the results suggest that although monotonic cohesive zones are not capable of estimating fretting fatigue lives, they may be a reasonable alternative for predicting crack initiation and orientation.

Chapter 6 presents a novel approach for estimating fretting fatigue lives. Fretting phenomenon is modelled using CCZM, that accounts for damage accumulation during loading and reloading. This models both crack initiation and propagation in a unified way, making use of a damage accumulation law that is function of the current stress and strain state of the material. CCZM is implemented in ABAQUS through a USFLD user subroutine that modifies the material properties during the finite element analysis. Therefore, CCZM requires a cycle-by-cycle analysis, which can be computationally demanding. Thus, in order to estimate fretting lives, an extrapolation procedure is proposed. The lifetime predictions are considerably better than the ones obtained via classical approaches, such as continuum damage mechanics in junction with classic fracture mechanics.

Lastly, in Chapter 7, main conclusions and future work recommendations of the present work are elaborated.

2

Background

Fretting happens when two contacting surfaces, normally loaded, are submitted to small amplitude oscillatory relative movement. This small amplitude means that fretting can be observed in many mechan-

ical assemblies in service conditions where components may be susceptible to vibration causing alternating sliding movement between the contacting surfaces. For instance, Johnson and Bill (1974) studied failure of aircraft engine components due to fretting. They notice that fretting can happen on fan, compressor, and turbine blade mountings; also, on splines, rolling element hearing races, and secondary sealing elements of face type seals. Blade attachment areas (dovetail joints) of gas turbines are other example that may experience fretting, leading to stress concentration that promotes ultimate damage due to high cycle fatigue (Meher-Homji et al., 1998). Depending on service conditions, fretting may reduce significantly the service life of a component by fatigue (Ding et al., 2007). Laboratory measurements showed that fretting might reduce the service life by way more than 50% (Hojjati-Talemi et al., 2014). In this regard, the analysis of stresses at contact is of great importance for predicting lifetime of components.

Fretting may have major influence on the contacting bodies, leading to catastrophic failure due to fatigue (known as fretting fatigue), producing loss of fitting due to wear (fretting wear) or a combination of both. The types of failures depend primarily on the fretting regime. Vingsbo and Söderberg (1988a) used a "fretting map" to describe the behaviour of wear volume and fatigue life as function of slip displacement for different fretting regimes: stick, mixed stick-slip and gross slip (see Figure 2.1). As it can be seen in Figure 2.1, there is a synergism between fretting fatigue and fretting wear. Depending on the service conditions (normal loading and relative displacement between the surfaces), failure may be mainly due to fatigue or due to wear.

At stick condition, surfaces are considered to be stuck to each other and no visible damage is generated. For the same contact pressure, as the slip displacement increases, fretting is characterized by mixed stick-slip condition. Here, the fatigue life decreases and the wear rate is reasonably low. This indicates that the main failure in this regime is due to fretting fatigue. Damage is characterized by presence of cracks due to high stresses at boundary of stick-slip zone, but that does not mean that there is no wear under this circumstances. Plastic deformation of asperities contributes for formation of wear debris, that due to the contact conditions are trapped between contacting surfaces in the slip zone. Those cracks have greater contribution than plastic shearing of asperities on the damage mechanism. For even higher slip displacements, the regime changes to gross slip condition where a considerable increase of the wear rate can be noticed. Fretting fatigue is not significant at this regime, because the cracks nucleated are removed by the intense amount of wear. The evolution of fretting crushes those debris into smaller pieces and those pieces roll over the surfaces increasing wear damage until they are expelled of the contact region.

One possible way to relate the fretting regime in real time measurements would be, as proposed by Harish et al. (2000), the use of infra-red camera to measure subsurface temperatures near the fretting contact. Frictional heating due to microslip at the surface and coupled thermoelastic effect from strains in the material create temperature changes. An area of heating over the whole contact length, due to frictional heating, is characteristic of gross sliding conditions. For higher coefficient of frictions and as the fretting regime transition to a partial slip regime, the temperature changes are more clearly linked to

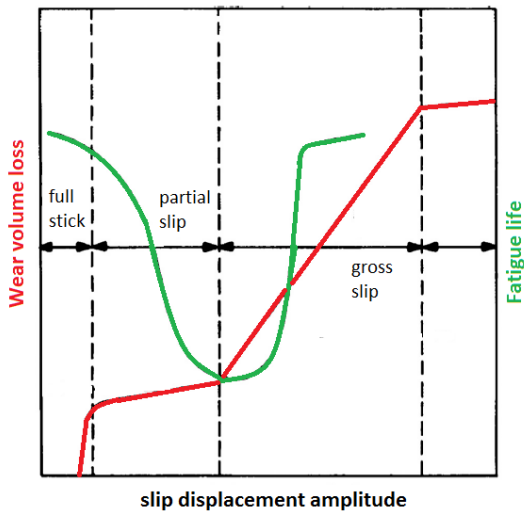

Figure 2.1: Fretting map proposed by Vingsbo and Söderberg (1988a)

strain through the coupled thermoelastic effect than through friction heating.

As discussed in Dobromirski (1992), although it has been reported that up to 50 variables might impact on the severity of the fretting process, it is possible to identify a set of "primary" and "secondary" fretting variables that govern the phenomenon. The "primary" set is composed by the coefficient of friction, slip amplitude and contact pressure. The "secondary" set are the variables that impact the "primary" set of variables, causing an indirect impact on fretting. In order to evaluate the effects of those different variables (surface finishing, coefficient of friction, normal load, relative slip amplitude, among others) on the characteristics of fretting, different laboratory tests are generally used, mainly full scale and coupon laboratory tests. Full-scale tests replicate the real service conditions and components. For instance, Conner and Nicholas (2006), Golden and Nicholas (2005) and Golden (2009)

studied the phenomenon considering test set-ups that mimic dovetails joints. Bolted or riveted lap joints are also common assemblies that are studied in full scale tests (Ferjaoui et al., 2015; Eriten et al., 2011; Oskouei and Ibrahim, 2012; Chakherlou et al., 2009).

When proposing numerical tools to predict lives it is important to verify and improve those tools based on experimental data. As coupon tests are certainly prone to less error than full-scale components, they are preferred to validate models in an initial stage of research. In addition, the controlled environment of a coupon scale test and its simplicity when compared to full-scale test are very interesting from numerical point of view, as these features also simplify the modelling. In this thesis, the estimation of fretting fatigue lives of coupon tests is of major interest. These coupon tests consist of pads that are maintained in contact with a flat specimen through the application of a constant clamping or normal force F. The specimen is fixed at one end and the other end is subjected to an oscillatory bulk stress σ_{Bulk} (an oscillatory load that is applied at one end of the specimen, sometimes also referred to as axial load σ_{axial}). The typical test configurations can be divided in three main categories, a, b and c, summarised in Figure 2.2. The first type does not provide any control of the tangential loading applied to the contact interface; only the normal load is maintained through a proving ring. In the second type, the use of compliance springs provides an alternative to obtain the tangential loading based on the other loads, i.e., bulk load and normal load. However, it still does not provide control over the applied tangential load amplitude. The third type makes use of individual actuators to apply the bulk stress and tangential loading, providing in this way a full control of

the applied load.

One of the most common configurations is a cylinder-on-pad, as illustrated in 2.2(b). In this set-up, two cylindrical pads are maintained in contact with a flat specimen through the application of a constant clamping or normal force F. The specimen is fixed at one end and the other end is subjected to an oscillatory bulk stress σ_{axial}. Upon application of the bulk stress, the compliance springs transmit an oscillatory tangential force Q at the pads. Generally, the tangential load Q is smaller than the product of the normal load F by the coefficient of friction μ and the contact is divided into two regions: a stick zone and a slip region.

For a cylinder-on-plane configuration, the stress and strain field in the specimen can be analytically estimated by contact mechanics. The stresses are estimated by a combination of the normal pressure distribution $p(x)$ (due to the normal force F) and surface traction $q(x)$ (due to the tangential and bulk loads, Q and σ_{axial}, respectively). These solutions are valid under a series of conditions, such as infinite and idealized bodies, elastic material properties, loading conditions, among others.

2.1 Contact Mechanics

Contact mechanics studies the interaction between two bodies that contacts each other in one or more points (Johnson, 1987). It has been largely discussed in the literature and it dates back to 1880s, in a seminal paper of Heinrich Hertz (Hertz, 1882). Hertz studied the con-

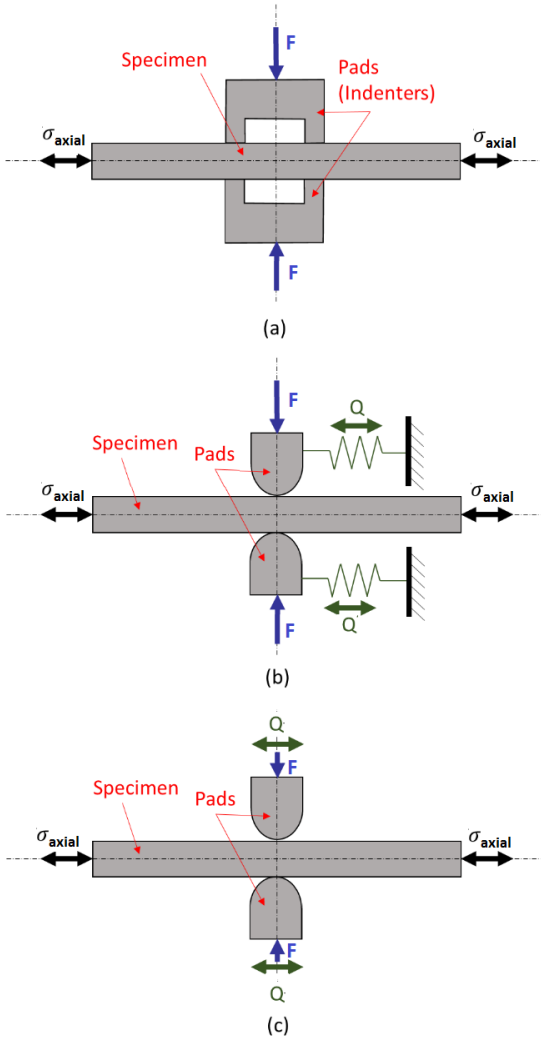

Figure 2.2: Fretting coupon scale test set-ups: (a) no controlling of slip; (b) indirect information of slip amplitude, through the compliance spring; (c) full control of the applied slip (or tangential) load.

tact between two curved surfaces that deform slightly due to imposed loads. His work set the foundations for this field and is now known as the classical or Hertzian contact mechanics. For the reader interested in a more general approach, in which near Van der Waals or adhesive interactions are considered, we refer to Bradley (1932) and Johnson et al. (1971), respectively.

In this Section, we first review the Hertzian approach to deal with smooth surfaces under normal and tangential loads. Later, we add the influence of axial loading on the stress distribution at contact interface. This Section is a review mostly centred around Johnson (1987).

2.1.1 Contact of cylindrical bodies with parallel axes

Consider a two-dimensional (2D) case, in which two smooth cylindrical bodies with parallel axes are in contact due to a normal load F. The first body has a curvature of R_1 and the second, R_2. The cross section of the two cylinders compressed together by F is shown in Figure 2.3. The plane $x-y$ is considered the contact plane and the origin of the Cartesian coordinate system $\mathbb{O}(0,0,0)$ is considered to be the initial contact line. Due to compression, cylinders 1 and 2 move towards $\mathbb{O}$ by displacements δ_1 and δ_2, respectively, with $\delta = \delta_1 + \delta_2$ defined as the total approach between the bodies. Due to the contact pressure, the surface of each cylinder is subjected to a displacement u_{y1} and u_{y2}. The elastic deformation of the surfaces results in a contact region of depth l (cylinder length) and width of $2a_{cont}$, where a_{cont}, as seen in Figure 2.3, is the semi-contact width. The contact area is rectangular and equal to $2a_{cont} \times l$.

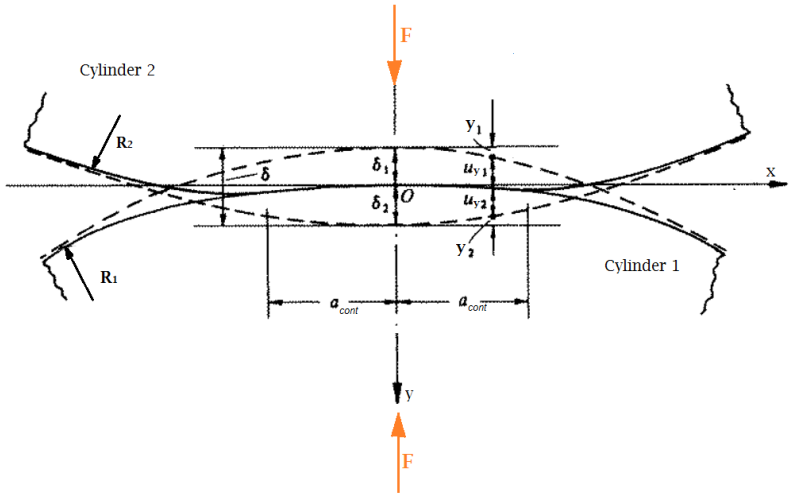

Figure 2.3: Schematics showing the contact of two cylinders with parallel axes. (based on Johnson (1987))

The combined curvature R and the combined modulus of elasticity E^* can be defined as:

$$\frac{1}{R} = \frac{1}{R_1} + \frac{1}{R_2} \tag{2.1}$$

and

$$\frac{1}{E^*} = \frac{1-\nu_1^2}{E_1} + \frac{1-\nu_2^2}{E_2}, \tag{2.2}$$

where E_i, for $i = 1,2$ are the Young's Modulus and ν_i, for $i = 1,2$ are the Poisson's ratio for the first and second bodies, respectively.

The goal is to obtain the contact pressure distribution $p(x)$ as a function of the coordinate x, at contact interface. However, to do so, the following conditions must hold:

1. Surface profiles are smooth, continuous and nonconforming;

2. Small strains at contact region;

3. Bodies can be approximated as a semi-infinite elastic half-space near the contact zone;

4. Frictionless contact.

If assumptions $1-4$ hold, this problem fits into the Hertzian contact mechanics theory and closed-form expressions for the contact pressure are available.

The pressure distribution $p(x)$ is elliptical at a distance x from the center of the contact zone and given by:

$$p(x) = p_{max}\sqrt{1-\left(\frac{x}{a_{cont}}\right)^2}, \quad \text{where} \quad p_{max} = \sqrt{\frac{FE^*}{l\pi R}} \tag{2.3}$$

where a_{cont} is the semi-contact width, p_{max} is the maximum contact pressure at the center of the contact, R is the combined curvature and E^* is the combined modulus of elasticity.

Considering that contact should occur only inside the loaded area and that the pressure must be positive, the semi-contact width a_{cont} and the applied load F are related by

$$a_{cont} = 2\sqrt{\frac{FR}{l\pi E^*}}, \tag{2.4}$$

where l is the cylinders length.

2.2 Fretting Fatigue: Analytical solutions

In this section, we consider the interface of the contact of a cylinder and a plane under normal load, representing the usual cylinder-on-plane fretting fatigue test configuration (see Figure 2.2(b)). Firstly, we present the Hertzian solutions for the pressure distribution. Later, we consider the effect of combined normal and tangential loads and we present solutions for the effect of bulk stresses on fretting fatigue conditions.

2.2.1 Hertzian solutions for the pressure distribution

The contact pressure distribution $p(x)$, due to the normal clamping force F between the pad (cylinder) and specimen (half-plane), can be calculated analytically using Equation (2.3). The flat specimen can be considered as a cylinder with an infinitely large radius $R_1 = \infty$. The combined curvature R becomes equal to the radius of the surface of the pad R_2. The elastic deformation of the surfaces results in a rectangular contact region of area equal to $2a_{cont} \times l$.

For instance, Figure 2.4 illustrates the normalized contact pressure distribution (from equation (2.3)) as a function of the normalized distance x/a_{cont} for the case of a cylinder in contact with a flat plane.

The subsurface stresses of the plane $\sigma_x(y)$ and $\sigma_y(y)$, along the x

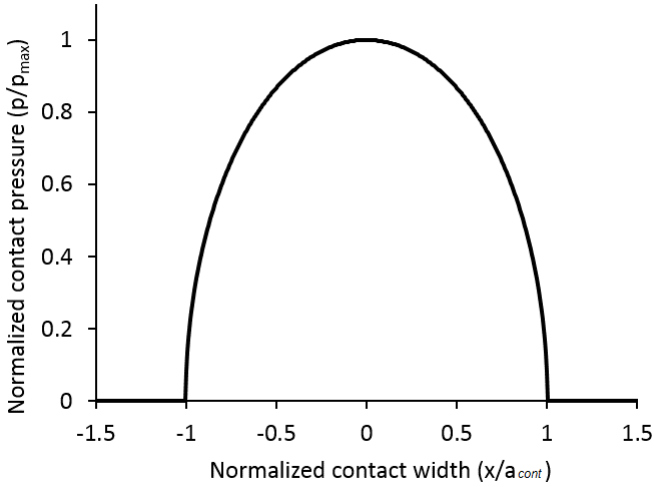

Figure 2.4: Contact pressure normalized by the maximum normal pressure p_{max} in function of the normalized distance x/a_{cont}

and y-directions, respectively, can be written as

$$\sigma_x(y) = -p_{max}\left[\frac{1+2\left(\frac{y}{a_{cont}}\right)^2}{\sqrt{1+\left(\frac{y}{a_{cont}}\right)^2}} - 2\left|\frac{y}{a_{cont}}\right|\right] \tag{2.5}$$

and

$$\sigma_y(y) = \frac{-p_{max}}{\sqrt{1+\left(\frac{y}{a_{cont}}\right)^2}}. \tag{2.6}$$

Considering plane strain conditions (null deformation in the z-direction), the stress in the z-direction ($\sigma_z(y)$) is correlated to the other components via the Poisson's ratio ($\sigma_z = \nu(\sigma_x + \sigma_y)$). Therefore,

$$\sigma_z(y) = -2\nu p_{max}\left[\sqrt{1+\left(\frac{y}{a_{cont}}\right)^2} - \left|\frac{y}{a_{cont}}\right|\right]. \tag{2.7}$$

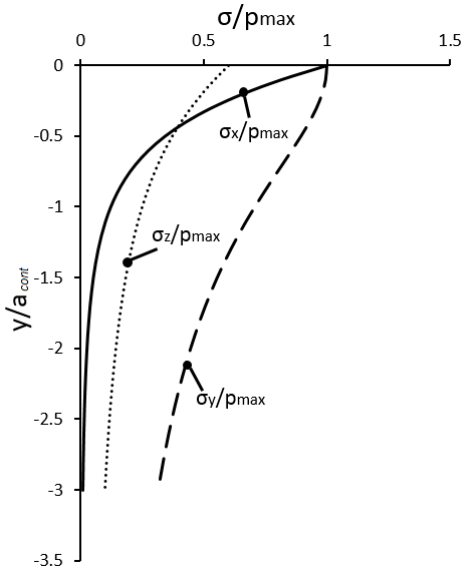

Figure 2.5: Stress components normalized by the maximum normal pressure p_{max} in function of the normalized distance y/a_{cont}

As an example, considering the case of Poisson's ratio equal to 0.3, the normalized stresses can be plotted in function of the normalized y, as shown in Figure 2.5.

2.2.2 Solutions for combined normal and tangential loads

When studying fretting, it is necessary to consider not only the normal loading condition, but also the effect of the tangential frictional force Q. The Coulomb friction law can be used to model the contact shear traction $q(x)$ at an arbitrary position x as a function of the normal contact pressure $p(x)$ and the coefficient of friction μ. If Q is smaller than the product of μ and the normal load F, the contact region will

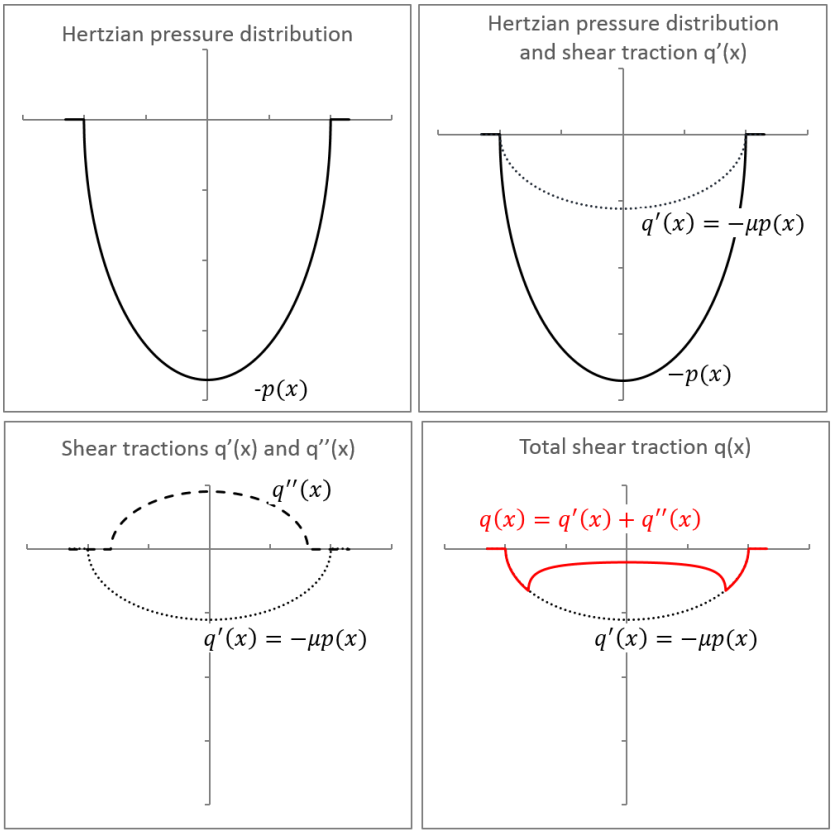

Figure 2.6: Illustration of the components of shear traction distributions

be divided into two different zones: *stick* and *slip*, in which the width of the stick zone is denoted by c. In this case, the contact shear traction can be seen as combination of two superposed shear tractions $q'(x)$ and $q''(x)$, as shown in Figure 2.6.

The complete expression for the shear traction q(x) can be written

as (Johnson, 1987; Hills and Nowell, 1994):

$$q(x) = \begin{cases} -\mu p_{max}\sqrt{1-\left(\frac{x}{a_{cont}}\right)^2} & \text{if } c \le |x| \le a_{cont} \\ -\mu p_{max}\left[\sqrt{1-\left(\frac{x}{a_{cont}}\right)^2} - \frac{c}{a_{cont}}\sqrt{1-\left(\frac{x}{c}\right)^2}\right] & \text{if } |x| < c \end{cases} \tag{2.8}$$

with

$$\frac{c}{a_{cont}} = \sqrt{1-\frac{Q}{\mu F}}.$$

2.2.3 Effect of bulk load on contact shear traction

According to Hills and Nowell (1994), the contact shear traction presented above can be adjusted for the presence of bulk stresses σ_{axial}. It causes an eccentricity to the solution presented in Section 2.2.2 and, for the case of negative shear traction, it can be written as:

$$q(x) = \begin{cases} -\mu p_{max}\sqrt{1-\left(\frac{x}{a_{cont}}\right)^2} & \text{if } c \le |x| \le a_{cont} \\ -\mu p_{max}\left[\sqrt{1-\left(\frac{x}{a_{cont}}\right)^2} - \frac{c}{a_{cont}}\sqrt{1-\left(\frac{x+e}{c}\right)^2}\right] & \text{if } |x+e| < c \end{cases} \tag{2.9}$$

where

$$\frac{c}{a_{cont}} = \sqrt{1-\frac{Q}{\mu F}} \quad \text{and} \quad e = \frac{\sigma_{axial} a_{cont}}{4\mu p_{max}}.$$

Figure 2.7 shows a typical normalized shear traction distribution for fretting fatigue conditions using equation (2.9). Note that based on this distribution, it is possible to determine the size of the stick and slip zones and also the peak values of shear stresses.

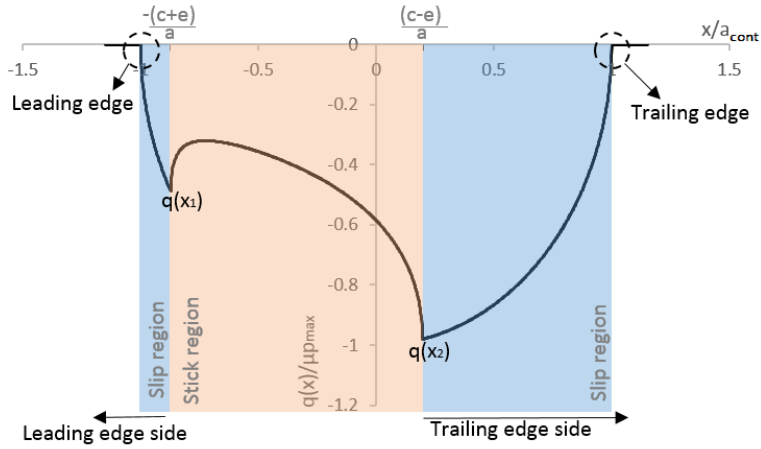

Figure 2.7: Typical normalized shear traction distribution at contact interface ($Q = 155.165$ N, $\sigma_{axial} = 100$ MPa, $p_{max} = 185.03$ MPa, $\mu = 0.4$ and $a_{cont} = 0.467$ mm)

2.2.4 Effect of bulk load on subsurface stresses

In his literature review, Mutoh (1995) mentioned studies showing that fretting fatigue crack (which propagates to material final rupture) originates in the edge of the contact area ($x = a_{cont}$), while small arrested cracks initiated near the maximum shear traction $q(x_2)$. Many other researches (Hills and Nowell, 1994; Namjoshi et al., 2002; Lykins et al., 2000) also pointed out that the principal crack initiates near the trailing edge ($x = a_{cont}$). The reason for that may be related to the contribution of the principal stress σ_{xx} in the stress state at the contact interface. As discussed by Szolwinski and Farris (1996), studies showed that the sharp peak in tangential stress $\sigma_{xx,max}$, at trailing edge of the contact region, might play a significant role on fretting fatigue crack initiation.

There are analytical solutions for subsurface elastic stresses σ_{xx} as

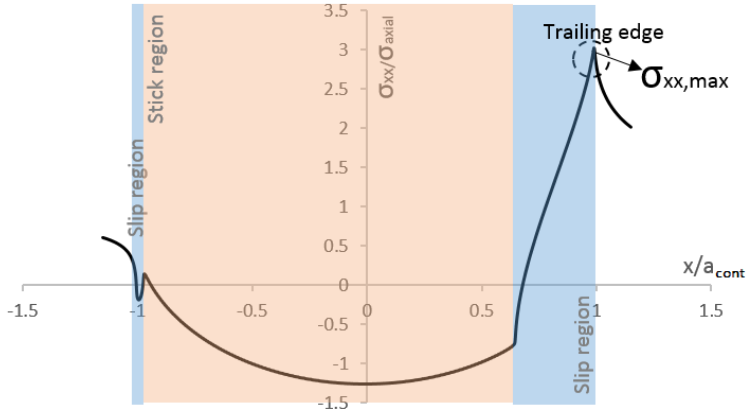

Figure 2.8: Typical normalized principal stress σ_{xx} distribution at contact interface, obtained from finite element analysis ($Q = 155.165$ N, $\sigma_{axial} = 100$ MPa, $p_{max} = 185.03$ MPa, $\mu = 0.85$ and $a_{cont} = 0.467$ mm)

function of x for given normal and tangential loads (F and Q) and coefficient of friction μ in the slip zone (Johnson, 1987; Hills and Nowell, 1994; Szolwinski and Farris, 1998). Although the addition of the bulk stress σ_{axial} brings some extra complexity to the problem, McVeigh and Farris (1997), based on the work done by McVeigh and Farris (1997), provided a simplified equation to estimate the maximum peak stress $\sigma_{xx,max}$ as:

$$\sigma_{xx,max} = 2p_{max}\sqrt{\frac{\mu Q}{F}} + \sigma_{axial}. \tag{2.10}$$

It is important to notice that the analytical expression for contact pressure distribution does not change when adding tangential and bulk stresses.

Due to the complexity of the fretting phenomenon, analytical solutions are available only for selective situations. These analytical solutions rely on assumptions that are not satisfied in most cases, such as semi-infinite elastic half-space near the contact zone and small strains at contact. In the analytical solution for tangential loading (equation (2.9)), the superimposing of shear stress due to normal load and due to fatigue load is a linear approximation and ignores the effect of interaction between both loads. In addition, equation 2.10 is only an approximation of the maximum stress σ_{xx} and may not be representative for all scenarios. Moreover, the stress field near the contact region is variable, multiaxial and non-proportional (Tur et al., 2003), which brings extra complexity to the phenomena. With the advance of computational power, numerical methodologies have become an interesting alternative to model fretting without relying on these many assumptions. In this regard, finite element method (FEM) has been greatly used.

Commercial FEM packages, such as ABAQUS and ANSYS, have powerful contact algorithms that allow an accurate computation of contact stresses. Another advantage is that advanced failure analysis (such as crack propagation and initiation) can be integrated to the modelling, considering the stresses and strains computed by FEM. In this review, firstly, in Section 2.3, the use of finite element analysis for studying fretting. Later, in Section 2.4, we briefly present recent advances in empirical and numerical analysis of failure due to fretting fatigue.

2.3 Finite element analysis of fretting contacts

The contact problem in fretting consists in the interaction of two bodies A and B, as represented in Figure 2.9. Traditionally, a classical linear elastic problem is considered, assuming that the strains are given by the first derivative of the deformation. A linear relation among the components of the stress and strain is also assumed and an isotropic linear elastic material is generally adopted. In order to obtain the stresses and strains, the conservation of linear momentum (equilibrium equation) is solved. The contact between the two bodies brings extra difficulties to the solution of the problem. For example, both displacement and contact force are unknown, meaning that the contact boundary tractions are part of the solution. In terms of contact algorithm the pad is defined as the master and specimen as slave. Contact also creates extra constraints to the problem. These constraints are derived from the physical requirements of contact, which can be summarized as follows: no penetration condition; traction condition and consistency condition.

In fretting scenarios, FE contact algorithms, that incorporate the conditions mentioned above, allow the computation of stresses at interface of fretted bodies. Since the 1990's, finite element methodology with contact algorithm (master-slave algorithm is generally used) has been vastly used to study fretting (Petiot et al., 1995; McVeigh and Farris, 1997; Lykins et al., 2000; Iyer and Mall, 2001; McColl et al., 2004; Kim et al., 2011; Shen et al., 2015). The accurate computation of contact stresses allows for a better understand of fretting phenomenon as well

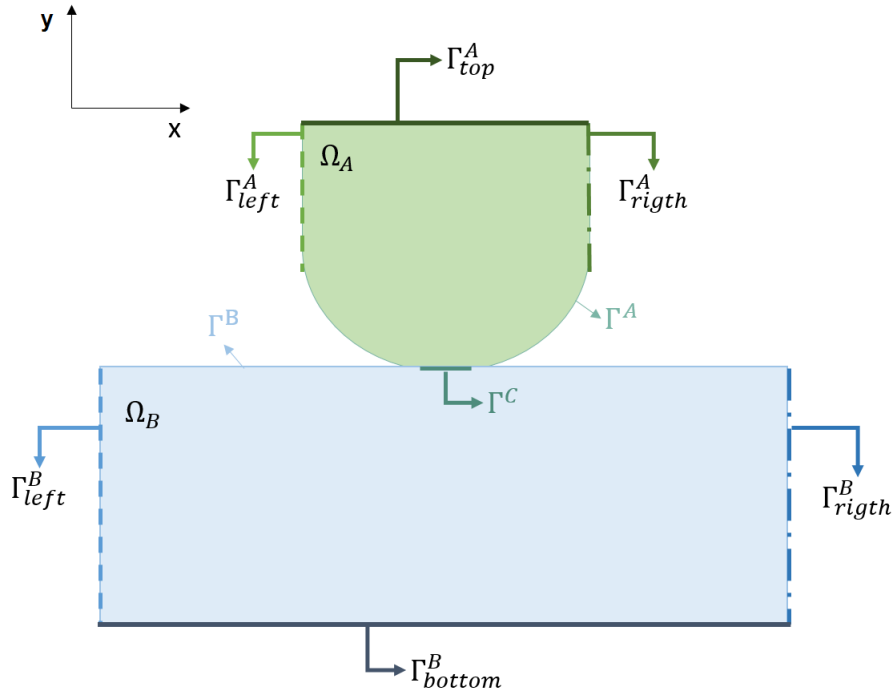

Figure 2.9: Domain definition of two bodies in contact

as the development of numerical tools to predict fretting lifetime.

One important factor in the FE analysis of contact problems is the definition of the coefficient of friction. It is normally taken as a constant on the model, although it is known that it varies as a function of various surface factors. As described by Blau (2001), the frictional behavior is influenced by many factors such as contact geometry (conformity of the components, surface roughness and waviness), fluid properties and flow (lubrication regime, viscosity, temperature and pressure influence on viscosity, shear thinning effects), lubricant chemistry (formulation of films, oxidation of lubricants), relative motion (reciprocat-

ing movement, constancy of motion, relative velocity) , applied forces (magnitude of contact pressure, constancy of loads), debris (characteristics of third-body particles), temperature (thermal effects on material and lubricant properties), stiffness and vibrations (contact compliance, damping of vibrations). Some effort have been made in the literature to account for some of these variables and their impact in fretting analysis (Chakherlou et al., 2009; Ghosh et al., 2016; Lehtovaara and Rabb, 2008; Gavrilă and Cretu, 2012; Yue and Wahab, 2017). For instance, Naboulsi and Nicholas (2003) analysed the impact of considering a constant Coulomb friction coefficient, developing a Coulomb friction model based that allows the coefficient of friction (COF) to be function of both contact pressure and slip magnitude. Their results showed that a variable coefficient of friction was able to replicate same stress state scenarios for different contact geometries, which was not able to be done considering a constant coefficient of friction.

2.4 Failure analysis of fretting fatigue

Stresses and strains obtained by finite element analysis are generally used to model failure of components under fretting. In order to understand the main features of fretting fatigue failure, firstly, we briefly review recent empirical observations of failure behaviour due to fretting. Later, we focus on numerical procedures aiming to estimate fretting fatigue crack propagation as well as lifetimes.

2.4.1 Empirical observations

Empirical observations of fretting fatigue cracks show that cracks follow a typical behaviour, being characterized by different mechanisms. In the earlier 1970s, Wharton et al. (1973) concluded that due to the localized action of fretting, crack initiation happens at the surface at very early stages, after only a few thousand fatigue cycles. At first, crack propagation happens in the region affected by the contact stresses arising from the fretting in a direction oblique to the surface. When it grows out of this zone, the crack changes direction and propagates perpendicularly to the bulk alternating stress in the specimen. Wharton et al. (1973) results show that as the amplitude of bulk load and slip increase, the combined stresses in the fretting region are considerably raised and the fretting-fatigue limit reduces significantly.

Studying carbon steel samples, Endo and Goto (1976) also concluded that fretting cracks initiate early in life and their growth to a certain depth is mainly defined by the combination of tangential (contact) stresses and the repeated axial or bulk load. Their results indicate that shear type cracks are initiated near contact edge and propagate through a small depth, defined as stage I mode. Thereafter, stage II begins and the crack grows in a direction oblique to the surface (under mixed-mode) until it reaches a depth large enough, approximately of the order of a few grain sizes. After this point, the effect of contact stresses can be neglected and the direction of propagation becomes perpendicular to the principal stress of the bulk load. This typical behaviour can be summarized in Figure 2.10 and has been also reported over the past thirty years by other researchers testing different ma-

terials and fretting conditions (Alic and Hawley, 1979; Switek, 1984; Faanes, 1995; Szolwinski and Farris, 1998; Navarro et al., 2006; Hojjati-Talemi et al., 2014; Cardoso et al., 2016).

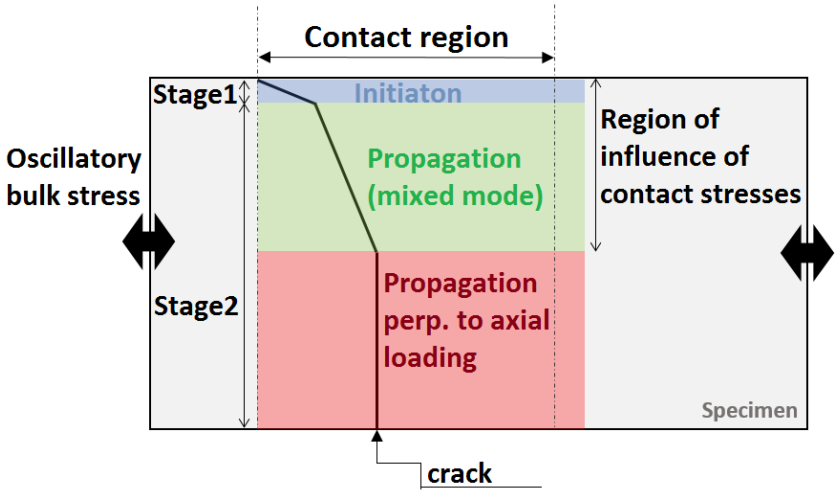

Figure 2.10: Fretting fatigue cracks behaviour

Stage I cracks are considered to be part of the crack initiation phase. At this regime, crack growth is affected by many different factors, such as plasticity, debris and wear, as in Conner et al. (2003), and microstructure. Metallography and fractography analysis of short cracks (stage I) done by Nix and Lindley (1988) showed a series of parallel ridges running in the direction of growth, suggesting a shear mode propagation. Experiments in aluminium and steel by Sato et al. (1986) showed that crack growth rate in this stage was considerably higher in comparison to plain fatigue. Their results also indicate that in this early stage of propagation, high contact pressures may induce crack closure which can cause a significant impact on the crack growth rate.

Numerical models of fretting fatigue failure consider each of these stages of crack growth (Stage I and Stage II) separately. Modelling of Stage I cracks characterizes the modelling of crack initiation phase, while modelling of Stage II cracks is associated to the modelling of crack propagation regime. Generally, total lifetime is estimated by combining crack initiation and propagation lifetimes.

2.4.2 Crack initiation lifetime

When dealing with crack initiation, important aspects of the modelling consist in defining the position of crack initiation in the model and the orientation of the initial crack. The initial crack is traditionally modelled at a fixed location, at the contact edge between pad and specimen (Noraphaiphipaksa et al., 2016; De Pannemaecker et al., 2016; Giner et al., 2014), at the location of the most severe stress.

Nevertheless, prediction of crack initiation location can be made by combining the stress distribution and slip at contact interface. Mutoh and Xu (2003) proposed that the initial crack should be located at the point with the most severe stress, in the case of a flat pad in contact with a flat specimen that is the contact edge. Hojjati-Talemi and Wahab (2013) used continuum damage mechanics approach to study initiation phase, aiming to predict crack initiation lives and location. They suggested that initial crack location should correspond to the site of maximum equivalent multiaxial damage stress in the contact region. A drawback of this methodology is the lack of sensitivity regarding changes in axial bulk loading. In a follow up study, Hojjati-Talemi et al. (2014) extended their methodology considering the location being the

one that dissipates most energy in one full fretting cycle. Recently, Noraphaiphipaksa et al. (2017) considered different pad geometries (flat and cylindrical) and compared the initial location predicted by two approaches (maximum relative slip amplitude and maximum shear stress range) with experimental data. They concluded that for flat pads, both approaches predict crack location in agreement with laboratory tests. However, for cylindrical pads, the maximum shear stress range method fails to predict the correct location and the maximum relative slip amplitude is recommended.

Although there is no consensus in the literature in which methodology is best for predicting crack initiation location, the location that dissipates more energy in one full fretting cycle seems to be a good option when dealing with initiation phase. It has been used to predict crack initiation locations and found to be in good agreement with experimental data for both pad configurations (flat and cylindrical) (Hojjati Talemi, 2014).

2.4.3 Crack propagation lifetime

Most works in literature uses LEFM to model long crack propagation phase under fretting conditions (Noraphaiphipaksa et al., 2016; Giner et al., 2009; Araujo and Nowell, 2002). The applicability of LEFM methodology requires the pre-existence of a crack of suitable length in the model, where assumptions of LEFM are satisfied.

Figure 2.11 shows a flow chart of a traditional finite element analysis of fretting fatigue crack propagation using LEFM. Firstly, a model

with a predefined crack is analysed, considering the whole cyclic loading condition. For a 2-dimensional analysis (most analyses of fretting fatigue coupon tests can be simplified considering plane strain conditions), the stresses and strains around the crack tip are used to estimate stress intensity factors for Mode I (K_I) and Mode II (K_{II}). The crack is allowed to grow, in a specific orientation, by a predefined length a_{inc}. The direction of crack growth is defined considering an orientation criterion computed by the stress intensity factors. Later, the incremental lifetime is obtained by integrating an empirical crack growth law, considering the previously calculated values of K_I, K_{II} and a_{inc}. A stepwise procedure is considered. The new model with increased crack length is analysed and stresses and strains are used to compute the new values of K_I and K_{II}. Again, crack is allowed to grow and incremental number of cycles is computed. This procedure is repeated until crack length has reached a critical value. The total lifetime is obtained by adding the incremental values computed in each step of the analysis.

This stepwise procedure is affected by many factors, such as: how mode mixity (interaction of contact loads and axial loading in fretting) impacts the modelling; where the initial crack should be located and how long it should be; which orientation criterion should be adopted; the crack growth rate quantification. A brief overview of these parameters and their effect on the analysis is given in the next Section.

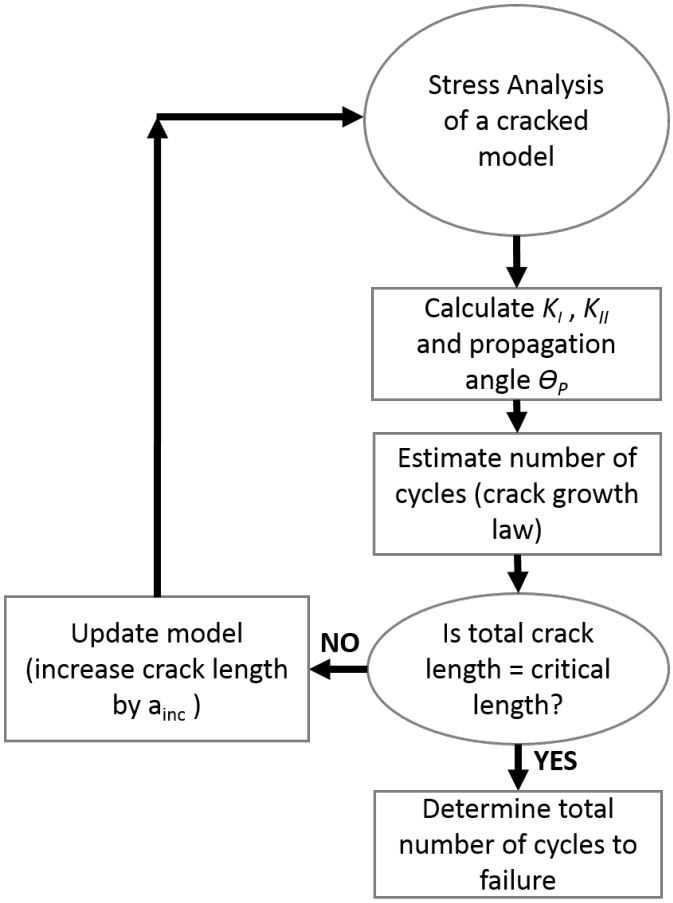

Figure 2.11: Analysis of fretting fatigue using LEFM

2.4.4 Parameters that affect LEFM modelling

2.4.4.1 Mode mixity

It is a common approach to consider the crack growth purely in Mode I condition, ignoring the mixed-mode effect present in fretting fatigue Stage II cracks. In this approach, crack growth is in a verti-

cal direction to the contact surface, perpendicular to the applied bulk stress. For instance, Hattori et al. (1988) used FEM model to obtain stress distributions at contact interface. Those stresses were later used together with fracture mechanics concepts to evaluate stress intensity factors at the crack tip. In their analysis, the fretting crack was approximated by a crack in the edge of a half plane, perpendicular to the surface and subjected to point loads. The computed stress intensity factors were compared with threshold stress intensity factors and adjusted for short crack behaviour. Their numerical results estimated the influence of mean stress in the fretting fatigue limit, which agreed well with their experimental results. Hills et al. (1988) also modelled fretting fatigue cracks as a crack edge of a half plane, perpendicular to the surface and found that cracks are generally closed and most likely to propagate in mode II.

Szolwinski and Farris (1996, 1998) also considered the propagation of an initial crack at edge of contact, perpendicular to the surface, under pure mode I. Their prediction of propagation lives was used to estimate the initiation live of test samples, by simply subtracting the total life measured in laboratory to this calculated propagation life. They also calculated initiation lives using multiaxial fatigue criteria and compared their predictions with the adjusted experimental data.

Navarro et al. (2003) proposed a procedure for estimating the total fatigue life in fretting fatigue, combining initiation and propagation lives and accounting for short-crack growth phase. In this proposed methodology, they also assumed a vertical initial crack. For estimation of the stress intensity factors (SIFs), they used weighted functions,

valid for mode I propagation. Hence, they neglected the influence that the contact stresses may have on the crack. This approach was also used for Munoz et al. (2007), with reasonable accuracy, in their approximations of fatigue curves for fretting conditions in aluminum alloy samples, under spherical contact. In the same line, Golden and Grandt (2004) proposed a methodology to predict fretting lives considering only the remote stress range, using a crack propagation analysis tool combined with contact mechanics software to estimating the stress at interface. The SIFs were also estimated by a weight function with a modification to account for a semi-elliptical crack. Their results showed that the combination of initiation and propagation lives provided a good estimate of total life.

Following up their research, Giner et al. (2011a) carried out XFEM analysis of fretting conditions and evaluated the impact of interaction of contact stresses on the SIFs estimates. Stress intensity factors obtained by weighted functions were under or overestimated in comparison to SIFs numerically calculated by XFEM. They also indicated that the life predictions obtained by XFEM were generally better than the ones obtained using weighted functions, pointing in the direction that the choice of weighted functions might influence the reliability of the estimation.

Although the assumption of pure mode I propagation may seem reasonable, fretting fatigue tests showed that crack propagates in a direction oblique to the surface, especially at the initial stage I of propagation (Wharton et al., 1973; Endo and Goto, 1976; Conner et al., 2003; Nix and Lindley, 1988). Therefore, another methodology is to insert

an inclined crack at a location calculated based on the stresses at contact and then assess its propagation. Faanes (1995) was one the first researchers to consider an initial inclined crack and attempted to compute the error of considering it in a vertical direction instead of oblique one. Based on his findings, in most of cases, the assumption of pure mode I propagation is valid. However, under conditions of high contact pressure, where crack closure may happen, the assumption of pure mode I may lead to very conservative life estimates. In the same line, Lamacq et al. (1996) proposed a theoretical approach to analyse crack propagation direction under fretting conditions, taking into account the non-proportional loading and mixed mode condition. One of the conclusions of their study is that depending on the loading conditions, either mode I or mode II may be dominant. They also show that mode II, under a spherical contact situation, is mainly due to the interaction between the two cracks that appear symmetrically in the problem.

Regarding the orientation angle of this initial oblique crack, a common approach is to introduce the crack in a direction based on experimental data. Some researches attempted to predict the orientation angle of this initial oblique crack, mainly based on the stresses near contact interface. In the work of Mutoh and Xu (2003), the authors suggest that it should be oriented in the direction of maximum tangential stress, ignoring the initial shear crack type. With respect to the flat pad/flat specimen contact, Giner et al. (2014) considered an initial crack at the edge of the contact, oriented in the direction which minimizes the shear stress range over the fretting cycle at the crack tip. This leads to two orthogonal planes, from which the one with the maximum normal stress range is chosen, because it is the orientation with

less energy loss due to frictional work. The effect of non-proportional loading is incorporated in their predictions of location and orientation by considering how the contact stresses vary over the entire fretting fatigue cycle .

2.4.4.2 Initial crack length

Fracture mechanics approach for propagation depends upon the definition of a "crack initiation length", which separates the initiation and propagation phases. Most of the work in literature (Madge et al., 2008; Cardoso et al., 2016) considered this length as the critical minimum crack length for which fracture mechanics could be used. It was determined by El-Haddad parameter (El Haddad et al., 1979) as:

$$a_0 = \frac{1}{\pi}\left(\frac{\Delta K_{th}}{\sigma_A}\right)^2 \tag{2.11}$$

where ΔK_{th} is the minimum stress intensity factor threshold that gives rise to crack propagation and σ_A is the fatigue limit of the material.

As discussed by Navarro et al. (2003), the issue with this approach is that the "crack initiation length" is arbitrarily chosen from a phenomenological perspective and it is generally kept constant, ignoring the effect that the size of contact and the gradient of stresses might have on it.

Noraphaiphipaksa et al. (2013) found out, through a sensitivity study, that their numerical results were in better agreement with experimental data when the initial crack length was chosen to be half of the critical length predicted by El-Haddad parameter.

2.4.4.3 Propagation direction and orientation criteria

One important point of modelling propagation phase is the definition of propagation direction, which can be done by considering an orientation criterion. There are several crack propagation direction criteria available in the literature that are used for proportional mixed-mode fatigue. A summary on the subject can be found in (Rozumek and Macha, 2009). Here, we focus on two of the most widely used criteria: maximum tangential stress (MTS) criterion and maximum energy release rate (MERR).

The MTS was originally proposed by Erdogan and Sih (1963) in the early 1960s. It states that crack growth is in the radial direction θ_P of greatest tension, i.e., in the direction along which the tangential stress $\sigma_{\theta\theta}$ is maximized and exceeds a critical value σ_c (a material property). Considering the analytical expressions for the stress field near the crack tip, the tangential stress can be written as function of the stress intensity factors K_I and K_{II} as

$$\sigma_{\theta\theta} = \frac{1}{\sqrt{2\pi r}} \cos\left(\frac{\theta}{2}\right) \left[K_I cos^2 \frac{\theta}{2} - \frac{3}{2} K_{II} \sin\theta \right]$$

where r and θ are cylindrical coordinates, as represented in Figure 2.12.

Imposing the conditions $\partial\sigma_{\theta\theta}/\partial\theta = 0$ and $\partial^2\sigma_{\theta\theta}/\partial\theta^2 < 0$, the direction of propagation θ_P can be obtained as function of K_I and K_{II} as:

$$\theta_P = \cos^{-1}\left(\frac{3K_I^2 + \sqrt{K_I^4 + 8K_I^2 K_{II}^2}}{K_I^2 + 9K_{II}^2} \right)$$

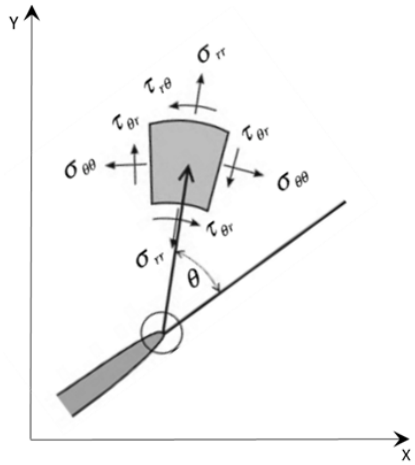

Figure 2.12: Stresses at a fixed position ahead of crack tip in cylindrical coordinates (based on (Kuna 2013))

The MERR was introduced independently by Hussain et al. (1974) and Palaniswamy (1978). It is based on the following hypotheses: crack will propagate at the crack tip in a radial direction θ_P along which the energy release rate $G(\theta)$ is maximized. For a co-planar crack growth under mixed mode, $G(\theta)$ can be written as

$$G(\theta) = \frac{1+\kappa}{8\mu}(K_I^2(\theta) + K_{II}^2(\theta))$$

where κ is a function of the Poisson's ratio and the stress state (plane stress or plane strain), μ is the shear modulus and $K_I(\theta)$ and $K_{II}(\theta)$ are the stress intensity factors associated to the new crack tip at a branched crack from the original crack. Based on the hypothesis of this criterion,

the propagation direction can be predicted by the solution:

$$\begin{cases} \left.\frac{\partial G(\theta)}{\partial \theta}\right|_{\theta=\theta_P} = 0 \\ \left.\frac{\partial^2 G(\theta)}{\partial \theta^2}\right|_{\theta=\theta_P} \leq 0 \end{cases}$$

As discussed by Lamacq et al. (1996), fretting fatigue problems are subjected to non-proportional loading, invalidating the application of those criteria and increasing the complexity for modeling crack propagation phase. Various researchers tried to make use of traditional LEFM orientation criteria using numerical models, but their fretting fatigue path predictions were not in agreement with experimental observations (Hojjati-Talemi et al., 2014; Giner et al., 2014, 2008).

Dubourg and Lamacq (2000) proposed that crack growth direction is the one with the maximum effective amplitude of tangential stress at crack tip during the entire load cycle. Their predictions were validated with experimental data from tests conducted in a fretting wear machine with pre-stressed specimen. As a conclusion, their work pointed out the necessity to account for non-proportional loading when estimating propagation paths. Their predictions were in better agreement with experimental data when using their proposed orientation criterion.

Noraphaiphipaksa et al. (2016) and Noraphaiphipaksa et al. (2013) used the same methodology proposed by Dubourg and Lamacq (2000), which states that the propagation direction is going to be defined by the one with the maximum effective amplitude of tangential stress at

crack tip. Those stresses are extracted in a circular path centred at the crack tip with radius r. Noraphaiphipaksa et al. (2013) considered a sensitivity analysis to study the influence of the results of the analysis with respect to the radius of this circular path, where the stresses are extracted. , where the stresses are extracted. Their results were significantly affected by the selection of r and they have also compared the predictions of crack path with experimental data to select an appropriated value of r. They found that, for the case of flat pad/flat specimen in steel, the radius that provided better accuracy when comparing predicted paths with experimental data was equal to half of the critical smallest crack length. In addition, the results were best when this critical smallest crack length was also used as length of the initial propagating crack and as the increment length of the fretting fatigue crack propagation for every analysis step. They also studied the influence of stress amplitude on paths. For the same contact pressure, they concluded that higher stress amplitude led to paths turning into perpendicular direction to bulk load in an earlier stage. Lives were calculated with good agreement with experimental data, but not very accurate estimates were obtained for cases with high stress amplitude. In these cases, the predictions were higher than the measured lives. They justified the mismatch by the fact that plasticity zone ahead of crack tip was neglected in their simulations.

Instead of dealing with stresses at crack tip, another approach is to define an orientation criterion based on stress intensity factors. Hourlier et al. (1985) proposed three extensions of the classical MTS criterion for non-proportional loading, based on the values of mode I stress intensity factor in a branched crack k_I^* along the fatigue cycle. The stress

intensity factor k_I^* and k_{II}^* are calculated at the tip of an infinitesimally small crack segment, branched from an original crack and they can be expressed as a linear combination of K_I and K_{II} (stress intensity factors at the tip of the original crack), as proposed by Ribeaucourt et al. (2007). The first extension proposes that the propagation direction would be the one that maximizes mode I stress intensity factor in a branched crack, considering the entire loading cycle, i.e., crack propagates in the direction θ that maximizes $k_I^*(\theta)$. Under proportional loading, this criterion is the same as the classical MTS. The second extension considers the direction that maximizes the amplitude of $k_I^*(\theta)$, i.e., the orientation that provides maximum difference between $k_I^*(\theta)$ for the instant of maximum load and at minimum load, $\Delta k_I^*(\theta)_{max}$. A major drawback of both extensions described above is their inability to account for the effects of mean stresses. In order to solve that, the third extension proposes that crack propagates in the direction θ that maximizes the crack growth rate, i. e., $(da/dN)_{max}$.

Baietto et al. (2013) developed a methodology based on the combination of experimental data and numerical modelling to predict crack initiation and propagation. Crack face contact and friction were considered in their numerical scheme (Baietto et al., 2010). They compared the extensions of MTS criterion proposed by Hourlier et al. (1985) and predicted propagation behaviour for 2D and 3D cases. Their results showed that crack paths could be accurately estimated using either the second or the third extensions ($\Delta k_I^*(\theta)_{max}$ or $(da/dN)_{max}$). Nevertheless, the first extension $k_{I,max}^*$ failed to predict correct paths.

2.4.4.4 Crack faces contact

It is known that crack faces contact can influence the crack growth rate. Consequently, it has a direct impact on the life predictions obtained by fracture mechanics, as described in Giner et al. (2011b). In later works, Giner et al. (2016, 2014) accounted for the effect of crack faces interaction on the estimation of crack path under fretting conditions, considering a constant coefficient of friction between them. They proposed an orientation criterion based on the minimization of the shear stress amplitude at crack tip over the loading cycle stress range, accounting for non-proportional loading. Considering a flat pad in contact with a flat specimen configuration, their numerical predictions of crack propagation path were in agreement with experimental observations. Their numerical simulations indicated the necessity of considering crack face contact, especially under compressive bulk stresses, where mode II plays a significant role in the propagation. Similarly, Martínez et al. (2017) implemented an XFEM approach to model propagation phase, incorporating the effects of crack closure on their prediction. By doing so, they correctly estimated the propagation path of a fretting fatigue crack in a Chinese railway axle.

Dealing with fretting in steel samples, Noraphaiphipaksa et al. (2014) showed that crack opening/closure behaviour of cracks under fretting may be significant. In a latter study, Noraphaiphipaksa et al. (2016) conducted experiments and finite element simulations of fretting fatigue of a flat pad in contact with a flat specimen configuration, aiming to evaluate the impact of crack closure behaviour under those conditions. Using strain gauges near the crack mouth and the rela-

tionship between those measurements and the applied bulk stresses, they were able to determine the crack opening load. They were able to detect experimentally that crack opening may happen under alternating compressive bulk load, due to the influence of contact stress on the crack behaviour. This idea was further supported by their numerical analysis. They determined numerically the crack opening ratio α based on the stresses at crack mouth at maximum load σ_{max} and at opening load σ_{OP}:

$$\alpha = \frac{\sigma_{max} - \sigma_{OP}}{\sigma_{max}}.$$

The crack opening load was numerically determined as the loading that caused the stress normal to the crack surface (at 10 μm away from the crack mouth) to vanish. In their study, they incorporated the crack opening/closure through a maximum effective stress intensity factor $\Delta K_{(max,eff)}$ given by:

$$\Delta K_{(max,eff)} = \alpha K_{max},$$

where K_{max} is the maximum stress intensity factor obtained by contour integral at the condition of maximum load. This effective stress was later on used in combination with a fatigue crack growth law to predict lives under fretting conditions and the results using $\Delta K_{(max,eff)}$ produced estimates in better agreement than using the traditional K_{max}.

Recently, Noraphaiphipaksa et al. (2017) used the above methodology to study the impact of different pad geometries (flat and cylindrical with two different radii) on live estimates, incorporating the phenomenon of crack opening and closure (considering frictionless con-

tact between crack faces) and its impact on the fatigue crack growth. Their predictions of propagation path were in excellent agreement with experimental observations. However, shorter lives were obtained for cylindrical contact when compared with flat pad. Regarding total life estimates, they agreed with experimental observations, being slightly smaller. Authors argued that this was because they neglected plasticity-induced crack closure phenomena.

2.4.4.5 Crack growth law

Fracture mechanics has been widely used to predict crack growth of problems under mode I loading conditions, implying that propagation is co-planar and perpendicular to the loading direction (Plank and Kuhn 1999). However, most engineering applications are subjected to a combination of normal and shear loading (mixed-mode I and II conditions) and a definition of a propagation criterion and crack growth rate that takes into account this loading scheme is necessary.

Most of crack propagation modelling using fracture mechanics has been based on Paris' type fatigue crack growth law. For this type of law, the relationship between the rate of propagation of a fatigue crack (da/dN) and the applied range of stress intensity factor ΔK, related with the crack and the cyclic loading, can be expressed as:

$$\frac{da}{dN} = C\left(\Delta K\right)^m,$$

where C and m are material constants determined by curve fitting.

The propagation life N_p is then obtained by integrating the above

equation, leading to:

$$N_p = \int_{a_0}^{a_f} \frac{da}{C\Delta K^m} \tag{2.12}$$

where a_0 is an assumed initial crack length and a_f is a critical length, that can either be the total crack length to failure or the length at which ΔK is equal to K_c, with K_c being the fracture toughness of the specimen.

Although fretting fatigue cracks behaviour are influenced by a mixed-mode conditions, the fatigue crack growth data under pure mode I is commonly used to predict propagation life (Araujo and Nowell, 2002; Szolwinski and Farris, 1998; Navarro et al., 2003; Giner et al., 2011a; Mutoh et al., 2003; Navarro et al., 2008). Generally, in Equation (2.12), ΔK is taken equal to the maximum amplitude of mode I stress intensity factor in a loading cycle:

$$\Delta K = \Delta K_{eff} = \Delta K_{I,max},$$

Mutoh and Xu (2003) compared fatigue crack growth curves of a fretting case and a pure mode I condition. They argued that the pure mode I growth curve is a satisfactory assumption except for the initial part of the propagation, where small crack behaviour and mean stress play a significant role. However, the general fracture path exhibits a clear region under mixed-mode conditions, which may influence the reliability of estimates based on pure mode I opening. Therefore, some researchers incorporated the effect of mixed-mode conditions in their estimates. For instance, Baietto et al. (2013) introduced the effect of

loading mixity by replacing ΔK in equation (2.12) by an effective stress intensity range given by:

$$\Delta K = \Delta K_{eff} = \sqrt{\Delta K_I^2 + b\Delta K_{II}^2},$$

where b is function of the loading mixity and ΔK_I and ΔK_{II} are, respectively, the mode I and mode II stress intensity factors ranges computed during the analysis of a full fretting cycle analysed and obtained by

$$\Delta K_I = K_{I,max} - K_{I,min}, \quad \text{with} \quad K_I \geq 0$$

$$\Delta K_{II} = K_{II,max} - K_{II,min},$$

where the subscripts max and min refer to the maximum and minimum values of stress intensity factor for any given fretting cycle, respectively. Madge et al. (2008), Hojjati-Talemi et al. (2014) and Hojjati Talemi (2014) incorporated mixed-mode effects in their predictions assuming the variable b constant and equal to unity.

Navarro et al. (2003) studied the impact of introducing crack growth threshold effect ΔK_{th} on life estimates. They considered the classical Paris' law and two of its adjustments. The first one is done by simply subtracting ΔK_{th} from ΔK, as:

$$\frac{da}{dN} = C\left(\Delta K - \Delta K_{th}\right)^m,$$

and the second one is:

$$\frac{da}{dN} = C\left(\Delta K^m - \Delta K_{th}^m\right),$$

Their results showed that, for tests that failed, the Paris' Law gives reasonable estimates, even though it neglects the threshold effect. They also pointed out the necessity of including short crack effects in the estimates.

Short cracks can propagate at stress intensity factor ranges below the threshold ΔK_{th} and they grow faster than long cracks. This behaviour is indeed experimentally observed in aluminium alloys for cracks whose length is comparable to the size of microstructural features and for relative low stress intensity factor ranges (Suresh and Ritchie, 1984). To account for this behaviour, several researchers used an approximated form of the stress intensity factor, considering that (Navarro et al., 2003; Madge et al., 2008; Munoz et al., 2007). In this methodology, growth of a crack of length $(a + a_0)$, where a_0 is defined in equation (2.11) is used to describe the growth of a short crack of length a. Under this assumption, the effective stress intensity range adjusted for short crack growth $\Delta K_{eff,short}$ is approximated by

$$\Delta K = \Delta K_{eff,short} = \Delta K_{eff} \sqrt{\frac{a + a_0}{a}}.$$

2.4.5 Cohesive zone models

In general, as discussed above, fretting failure is modelled considering both crack initiation and propagation phases separately. Propagation is normally modelled under LEFM assumptions, that might not hold for all situations. An alternative approach that is less restrictive than LEFM is the use of cohesive zone models.

The cohesive zone model (CZM) deals with the modelling of a non-linear process zone ahead of the crack tip, not requiring a small-yield plastic zone size. In addition, CZMs may account for both initiation and propagation phases in a unified way, therefore, there is no necessity of separating those two regimes.

In fretting fatigue, there has been some effort to use cohesive zone model. Kim and Yoon (2014) used a bilinear cohesive law with stiffness and fracture energy dependent of the number of cycles for model fretting fatigue failure. They used a jump cycle scheme to predict to predict S-N curves. Although their results were in good agreement with experimental data, with a maximum 20% error, there methodology a major drawback of their proposed methodology is that the crack propagation requires the knowledge of the crack path prior to the analysis. This is due to the fact that they used interface cohesive elements between continuum elements that must be located in this pre-defined path.

A more robust analysis has been proposed by Zhang et al. (2015). They used XFEM with cyclic cohesive zone models to study the effect of residual stress on fretting fatigue strength. In their approach, the cohesive law is embedded into the material properties of the XFEM element, allowing the crack to propagate in an arbitrary orientation defined by the stresses ahead of the crack tip. Therefore, their simulation is not restricted to a pre-defined path as in Kim and Yoon (2014). Their results showed that residual stress tend to enhance fretting fatigue propagation lives, although no attempt to predict total lives nor comparison with experimental data have been provided.

In a later paper, Zhang et al. (2016) used the same previous methodology to study the influence of tangential force on fretting fatigue. Their results showed that increasing tangential load leads to an increase of initiation life, change on propagation paths (increase on the knee depth of the path) and increase in total life. Their analysis was based on only a few hundred cycles of fretting, which is a rather short number for high cycle fatigue scenarios. Moreover, they did not aim on correctly predict lives and their results were not validated with any experimental data.

2.5 Conclusions

In this chapter, we presented an overview of the main analytical solutions for computing stress at contact interfaces at bodies subjected to fretting loadings. Firstly, we showed the classical hertzian solution for pressure distribution due to contact of two cylindrical bodies under normal loading. Coulomb friction law is used to obtain closed form solutions for stresses at contact due to the combination of normal and tangential loading. Finally, the effect of axial loading (present in fretting conditions) is incorporated and an approximated solution for obtaining the maximum tangential stress at contact is discussed.

Analytical solutions are restrictive and subjected to many unrealistic assumptions. To circumvent this issue, stresses at contact interface of bodies under fretting conditions are generally estimated using numerical approaches, such as finite element method. In this regard, we discussed the main idea behind the contact algorithm in a finite ele-

ment approach, highlighting the difficulties of modelling such problem. Another difficulty that will be discussed in the next chapter, is numerical stability. These are complex problems, that may often lead to convergence issues and if not properly considered.

In this chapter we also presented a brief review of the most traditional approaches to model failure under fretting conditions. Most numerical models of fretting failure are based on LEFM and must rely on restrictive assumptions, such as small plastic zone ahead of crack tip and an empirical crack growth law for life predictions. As mentioned in the previous section, an interesting option to alleviate those assumptions is use of cyclic cohesive zone models (CCZM). In Chapter 6, we present this model in detail and discuss its implementation in ABAQUS. Our main goal is to accurately predict total fretting fatigue lives and crack propagation paths, validating our methodology with experimental data.

3

Convergence study

As discussed in previous chapters, estimating the lifetime of fretting fatigue is of great importance in many industries. It requires, however, complex modelling, making analytical solutions nearly in-

tractable. Numerical methodologies have, therefore, become the standard approach to evaluate the stresses at contact as well as to estimate their impact on fretting fatigue lifetime. One example of a successful numerical methodology is FEM. For instance, McVeigh and Farris (1997) used finite element analysis to study the influence of the bulk loading σ_{axial} on the contact stress distributions and compared the results with analytical approximations. Tsai and Mall (2000) treated the problem considering the effects of plasticity on the contact stress distribution for a Titanium material and analysed the impact of plastic deformations on the size of the stick zone and peak stresses. They concluded that plastic zone started at trailing edge and that the effects of contact stresses decay rapidly as the distance from the contact increases.

Numerical methodologies accept a richer characterization of the model with less strict assumptions as those needed in analytical approaches. The researcher is allowed to model a wide variety of problems, with several complexities that resembles what we see in real life. This gain in applicability, however, comes with a price in higher computational efforts and complex algorithms that may sometimes fail to converge. As pointed out by Ainsworth and Oden (1997), although aware of the existence of numerical errors, the analyst is seldom interested in quantifying them. In fretting fatigue, the quality of a simulation is generally assessed by visual comparison between finite element results and analytical solutions and rarely some information regarding the error is provided, as in Tsai and Mall (2000), Iyer and Mall (2001) and Massingham and Irving (2006). The fretting contact stresses calculations is of significant importance as these stresses impact directly

on the crack propagation phase. Therefore, estimating errors for those stresses is of great interest to ensure accurate analysis.

In this chapter we study different element sizes at the contact surface and their influence on the stresses calculated from finite element analysis (FEA) of fretting fatigue cylinder-on-plane test configuration. A FE model of a cylindrical pad and flat specimen configuration was created and stresses at contact interface were monitored and compared with analytical solutions for different mesh sizes and fretting contact conditions. A convergence map is proposed in order to provide some guidance on the selection of the appropriate mesh size for 2D simulations of these type of coupon tests.

Additionally, the existence of stress singularity at the stick-slip zone in fretting fatigue conditions is studied using FEM, as follows. The evolution of numerical errors is captured as function of the number of nodes at contact (proportional to the number of degrees of freedom). Singularity checks are then performed.

This chapter is organized as follows. Firstly, FE models are constructed and discussed in Section 3.1. Results are presented and discussed in Section 3.2 and followed by a conclusion in Section 3.3.

3.1 Finite Element Model: Cylinder on flat

A parametric 2D finite element model was created in ABAQUS version 6.14 and a static analysis of the fretting cycle was performed, aiming to study the model response to different mesh sizes. Three cases

of coefficient of friction were studied 0.3, 0.85 and 2.0. This range of coefficient of friction allows the simulation of a wide range of stick slip ratio sizes c/a_{cont} that could happen on reality depending on the loads and surface conditions. By selecting a range of coefficient of friction from 0.3 to 2.0, it was possible to obtain c/a_{cont} ratios from 0.2 to 0.9. Therefore, being able to simulate different profiles of shear tractions without having to vary many parameters in the model, such as the tangential load and normal load (see equation (2.9)). This allowed us to study various fretting scenarios and stresses profiles that could happen in real situations, depending on the combination of normal and tangential loads, for a fixed coefficient of friction.

Details of the model, such as geometry, material properties, mesh details, boundary conditions and loading history are presented here. We first created two FE models, with dimensions and boundary conditions as depicted in Figure 3.1. These models were composed of only two parts: a pad and a specimen, representing half of the experimental set-up, due to symmetry. In order to check the influence of different geometries, the radius of the pad was set to two different values: 50 mm and 10 mm. Both parts were made of aluminium 2420-T3, with material properties as summarized in Table 3.1. One objective of this chapter is to verify the presence of stress singularity at contact interface. In order to achieve that, the methodology presented by Sinclair (2004) has been used, that requires an elastic analysis. Therefore, plasticity effects have been neglected in this study.

Stress analyses were carried out by applying a normal load ($F = 543$ N) and oscillatory axial and reaction stresses to the specimen, reflect-

ing a fretting cycle. The master-slave algorithm in ABAQUS was used

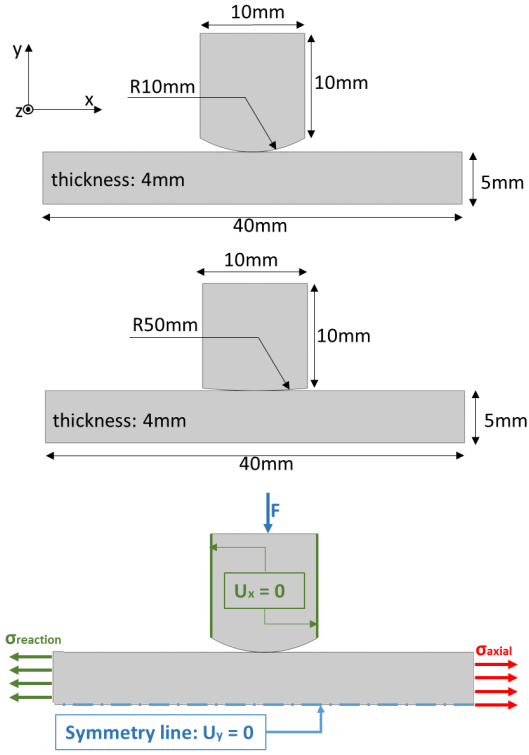

Figure 3.1: Details of the dimensions of the two FE fretting fatigue models, loading and boundary conditions

to describe the contact behaviour and the Lagrange multiplier formulation was used to define the tangential behaviour of the contact pair. The surface-to-surface and finite sliding options were used to define the contact interaction.

A 2D quadrilateral, 4-node (bilinear), plane strain, reduced integration element (CPE4R) was used in both models. CPE4R is a two-dimensional solid element continuum element with plane strain formulation. It is a first-order quadrilateral isoparametric element and not a rectangular/square element. Isoparametric interpolation in Abaqus

E	Modulus of Elasticity [GPa]	72.1
ν	Poisson's ratio	0.33
$\sigma_{0.2}$	Yield Strength [MPa]	506 ± 9

Table 3.1: Material properties for aluminium 2420-T3 (data from Hojjati Talemi (2014) and Hojjati-Talemi et al. (2014))

is defined in terms of the isoparametric element coordinates g, h (Figure 3.2). These are material coordinates that vary from -1 to +1 in an element.

The interpolation functions are as follows for a first-order quadrilateral:

$$u = \frac{1}{4}(1-g)(1-h)u_1 + \frac{1}{4}(1+g)(1-h)u_2 + \frac{1}{4}(1+g)(1+h)u_3 + \frac{1}{4}(1-g)(1+h)u_4$$

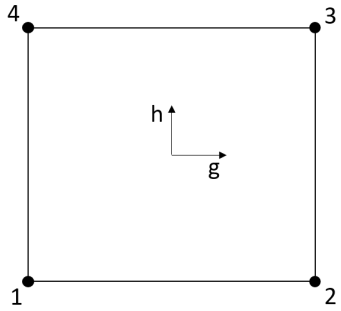

Figure 3.2: CPE4R element in Abaqus

For the first-order elements the single-point reduced-integration scheme is based on the "uniform strain formulation": the strains are not obtained at the first-order Gauss point but are obtained as the (an-

alytically calculated) average strain over the element volume.

The choice of reduced integration was mainly due to the high computational cost of the simulations with small mesh size. We have not considered second-order elements (CPE8 or CPE8R). This is due to the fact that, when dealing with contact problems, first-order elements may have improved convergence than second-order. This is because if one corner and one edge node of the second-order elements are in contact, the interpolation of the displacement of the element edge causes overlaps Bäker (2018).

Different mesh sizes were considered at the contact interface and increased as the distance from the contact region increases. In order to create a fine mesh at the contact region, the models were partitioned and the edges were seeded. The values of the mesh at the contact region varied according to the following list: (20, 10, 5, 2.5, 1.25, 0.625 and 0.3125) $\mu\mathrm{m}$. Details of the seeding used to generate the mesh and of the model partition dimensions are shown in Figure 3.3. The partition dimensions depend on the radius of the pad, being calculated based on the semi-contact width a_{cont}, from equation (2.4). An illustration of one of the meshes used in this study is also presented in Figure 3.3.

Due to the symmetry of the problem, the bottom of the specimen (which represents the axial centreline of the specimen) was restricted from vertical movement in the y direction ($U_y = 0$). The sides of the pads were restricted from horizontal movement in the x direction ($U_x = 0$) and also the MPC tie constraint was used at the top surface of the pad to guarantee that it would not rotate due to the applied

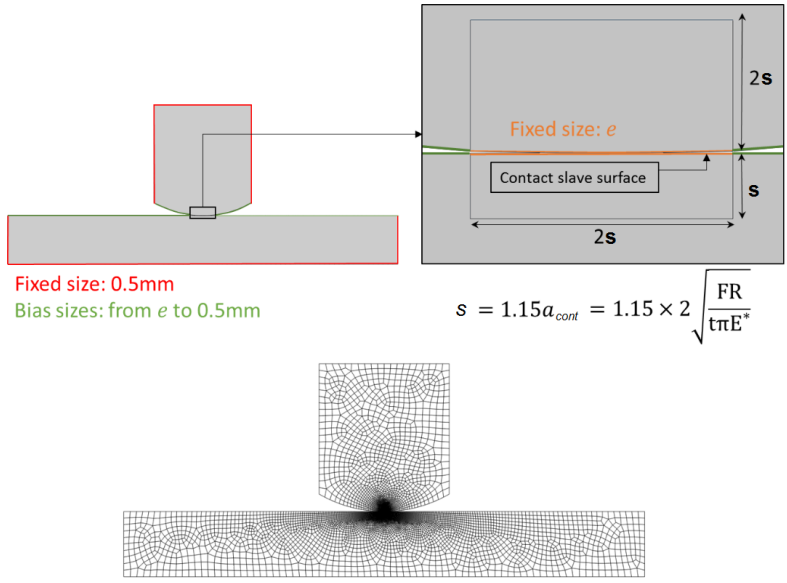

Figure 3.3: Details of the partition in the models, the edges seeding (element size e varied from values: 20, 10, 5, 2.5, 1.25, 0.625, 0.3125 μm) and also an illustration of one of the meshes used in this study.

concentrated load F.

The effect of the compliance spring and tangential load Q were modelled as a cyclic reaction stress ($\sigma_{reaction}$). This reaction stress is obtained as:

$$\sigma_{reaction} = \sigma_{axial} - 2\frac{Q}{bt}, \tag{3.1}$$

where b is the specimen width ($b = 10$ mm) and t is the specimen thickness ($t = 4$ mm). The values $Q = 155.165$ N and $\sigma_{axial} = 100$ MPawere obtained from experimental data (Hojjati-Talemi et al., 2014).

In order to simulate fretting conditions, the fretting cycle was divided into three steps (see Figure 3.4). In the first step, the top pad was pressed against the specimen surface by a normal load $F = 543$ N and

this compressed condition was held constant until the end of the cycle. Then, both axial and reaction maximum stresses were applied to the sides of the specimen. Finally, in the third step, both axial and reaction minimum stresses were applied.

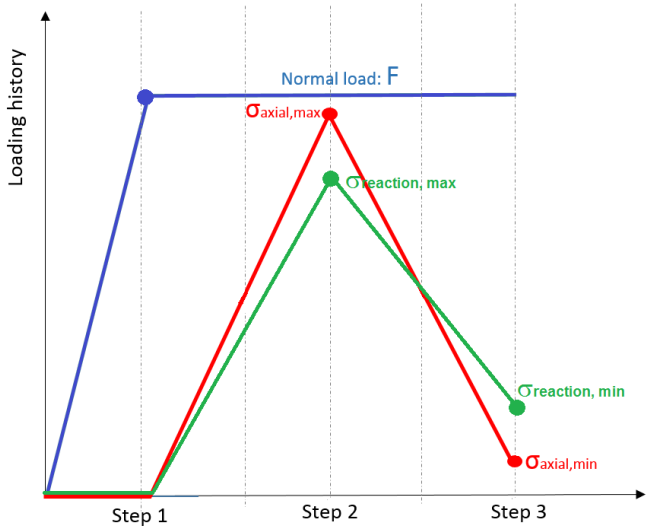

Figure 3.4: Fretting simulation: Loading variation as a function of time.

3.2 Results and Discussion

In order to evaluate the presence of singularity, we adopted the methodology presented in Sinclair (2004). Accordingly, the element size in the models was successively halved for a sequence of seven analyses and the magnitude of maximum stress values was examined. The following stress components were monitored at the maximum axial loading condition (end of loading step 2): the contact shear traction peak at trailing edge $q(x_1)$ and at leading edge $q(x_2)$ (see Figure 2.7) and also the peak tangential stress in the x direction $\sigma_{xx,max}$ (see Fig-

ure 2.8). The influence of the mesh size on the values of the ratios between stick and slip zones sizes (c/a_{cont}) was also considered. The slip zone size c was obtained by measuring the position in the contact that have non-zero values of slip and the contact width a_{cont} was obtained by the position in the x direction of the edges of the contact region, both calculated from ABAQUS.

The results of various stress components and for the ratios between stick and slip zones sizes (c/a_{cont}) are presented in Table 3.2, for different values of coefficient of friction and different radii of cylindrical pad. FEA results were also compared with analytical solutions (presented in Section 2.2). The values of shear traction at trailing and leading edges seem to converge to the analytical solution for all values of coefficient of friction. The values of peak tangential stress $\sigma_{xx,max}$ seem to converge, but to a different value than the estimated from equation (2.10). This is reasonable, since this equation provides only an approximate value of $\sigma_{xx,max}$. Note that the non-dimensional parameter (c/a_{cont}) also converged to the analytical solution for all values of coefficient of friction and pad radius.

To examine convergence in Table 3.2, the relative error between FE and analytical solutions was considered. We discuss them in detail in Sections 3.2.1 and 3.2.2.

3.2.1 Influence of mesh size on stress components

In order to analyse the influence of mesh size on the contact shear traction, the analytical solution was chosen as a reference value. The

		Pad Radius							
		50mm	10mm	50mm	10mm	50mm	10mm	50mm	10mm
COF	Mesh size [μm]	$q(x_1)$ [MPa]		$q(x_2)$ [MPa]		$\sigma_{xx,max}$ [MPa]		c/a_{cont}	
0.3	20	38.81	107.02	53.72	119.93	167.49	208.72	0.167	0.136
	10	40.72	108.69	54.11	122.34	182.87	242.57	0.200	0.136
	5	41.01	110.40	54.23	123.19	192.96	268.70	0.206	0.174
	2.5	41.30	111.21	54.38	124.29	200.09	290.50	0.211	0.207
	1.25	41.47	111.44	54.24	124.33	205.33	307.81	0.212	0.211
	0.625	41.54	111.97	54.27	124.39	208.99	320.33	0.212	0.212
	0.3125	41.57	111.99	54.27	124.44	212.00	329.94	0.211	0.213
	Analytical	**41.29**	**112.68**	**53.99**	**124.11**	**208.35**	**342.28**	**0.218**	**0.218**
0.85	20	24.89	113.00	112.64	209.21	222.91	279.65	0.702	0.727
	10	30.33	142.02	115.31	216.27	254.12	349.91	0.779	0.750
	5	33.31	146.77	117.18	226.39	274.64	398.69	0.788	0.779
	2.5	36.73	155.01	118.06	230.10	287.93	440.60	0.805	0.799
	1.25	37.54	158.98	118.50	233.62	297.38	474.40	0.806	0.804
	0.625	38.34	160.91	118.89	234.83	303.26	496.58	0.808	0.808
	0.3125	38.80	162.08	119.01	235.81	308.06	513.08	0.808	0.809
	Analytical	**38.09**	**163.18**	**119.20**	**235.12**	**283.90**	**507.82**	**0.811**	**0.815**
2.0	20	17.53	123.20	165.85	240.56	275.64	322.49	0.893	0.667
	10	22.50	162.01	175.64	318.97	336.52	441.20	0.905	0.864
	5	28.59	195.58	181.98	327.15	373.08	537.49	0.91	0.895
	2.5	41.18	207.99	185.62	347.98	399.72	612.33	0.92	0.911
	1.25	44.39	227.64	187.36	357.64	417.17	683.24	0.918	0.917
	0.625	45.85	236.01	189.13	362.74	428.46	719.75	0.921	0.92
	0.3125	47.72	239.73	189.43	366.06	436.21	750.50	0.921	0.921
	Analytical	**46.52**	**242.70**	**190.72**	**368.12**	**382.10**	**725.56**	**0.925**	**0.926**

Table 3.2: FEA results and analytical solution for different coefficients of friction, different pad radius and different mesh sizes at the contact surface

relative error between FE and analytical solutions $e_{rel,an}$ was calculated as:

$$e_{rel,an} = \left| \frac{\phi^a_{max} - \phi^i_{max}}{\phi^a_{max}} \right|, \tag{3.2}$$

where ϕ^i_{max} is the maximum variable output (contact shear stress, maximum tangential stress or ratio between stick slip zone sizes) in the ith model and ϕ^a_{max} in the analytical solution (see Table 3.2).

Higher coefficient of friction simulates a situation with large gradients in the stress distribution, as the stick zone increases for the same size of contact. The relative error between FE and analytical solutions for the contact shear traction stress component for different coefficients of friction and pad radius are presented in Figures 3.5 and 3.6. The results show that the error is decreasing as the mesh size reduces, independently of the value of the coefficient of friction and pad radius. Thus, the analysis is converging, even if only slowly, and no singularity was found for any of the tested loading conditions, pad radius and coefficients of friction.

Moreover, it can also be seen that the rate of convergence is dependent on the coefficient of friction for both cases of pad geometry. As different values of coefficient of friction represent different loading conditions (various sizes of stick zone in comparison with the contact dimension), one might conclude that the rate of convergence of the solution depends upon the loading condition.

For the smallest coefficient of friction, a relative coarse mesh (around 20 μm) at the contact is sufficient for obtaining reasonable accurate shear stresses, with relative error smaller than 10% for all cases anal-

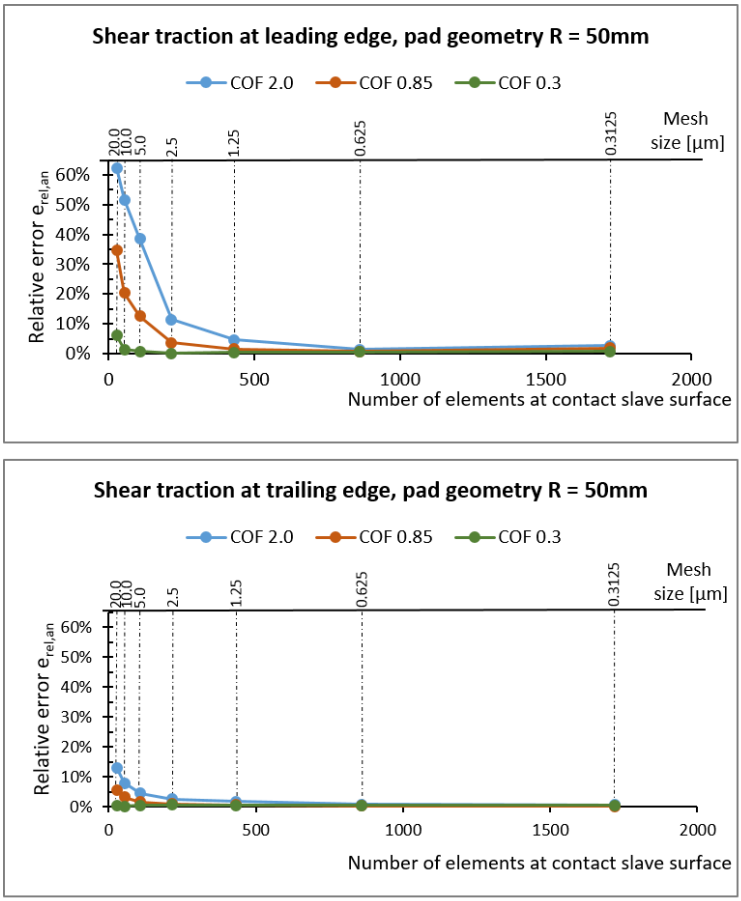

Figure 3.5: Mesh convergence curves for contact shear tractions, for different cases of coefficient of friction and pad radius equal to 50mm

ysed. For higher coefficients of friction, the rate of convergence reduces and it is necessary to use finer meshes to guarantee reasonable results. For instance, for coefficient of friction equal to 2.0, a mesh size of 1.25 µm is enough to guarantee that the relative error on the shear traction peak is smaller than 10% for all cases analysed. However, for the same coefficient of friction and a mesh size of 5 µm, the error can increase to almost 40%, for the contact shear traction peak at leading edge.

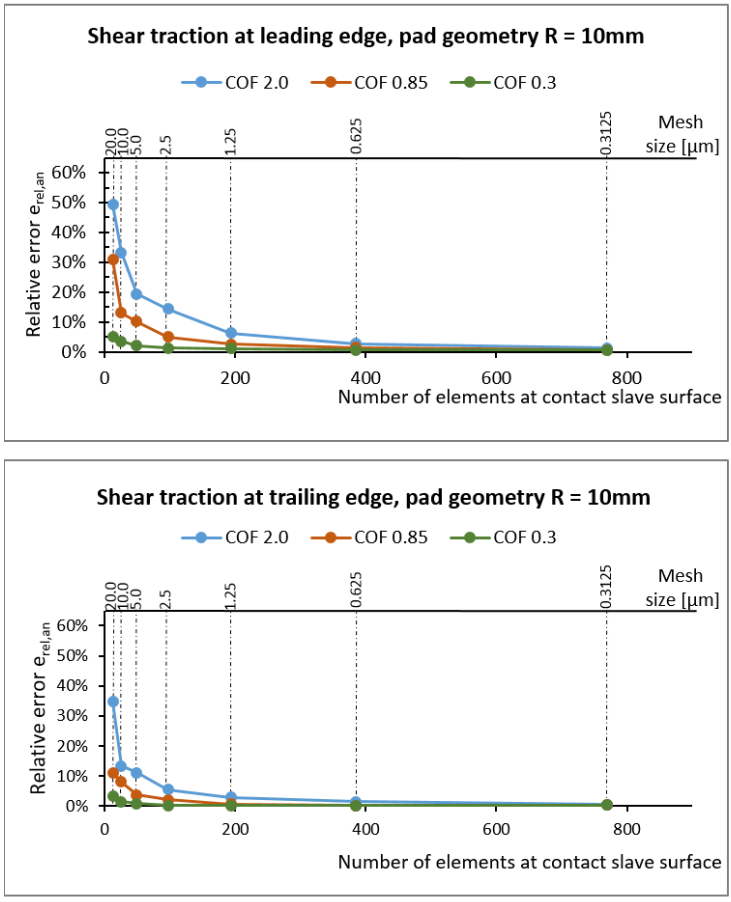

Figure 3.6: Mesh convergence curves for contact shear tractions, for different cases of coefficient of friction and pad radius equal to 10mm

The dependence of the rate of convergence on the coefficient of friction can be further investigated by analysing the contact shear traction at contact interface. As it can be seen in Figures 3.7 and 3.8, for the case of high coefficient of friction, the contact shear traction distribution has very sharp peaks at both leading and trailing edges.

This justifies the necessity of a very fine mesh to accurately capture the very steep stress gradients.

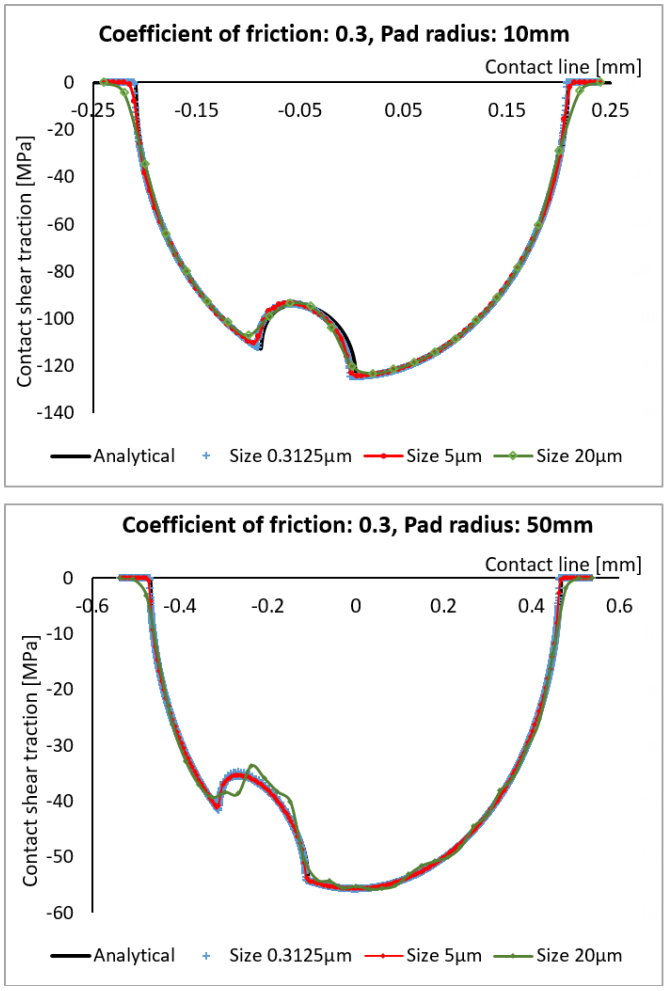

Figure 3.7: Contact shear traction at contact interface for different mesh sizes and coefficients of friction

As discussed before, the peak stress $\sigma_{xx,max}$, seems to converge to a different value than that estimated from equation (2.10). Therefore, in order to study the convergence of the results of the FEA, instead of considering the analytical solution as reference, the maximum stresses between two subsequent mesh refinements were used to calculate the

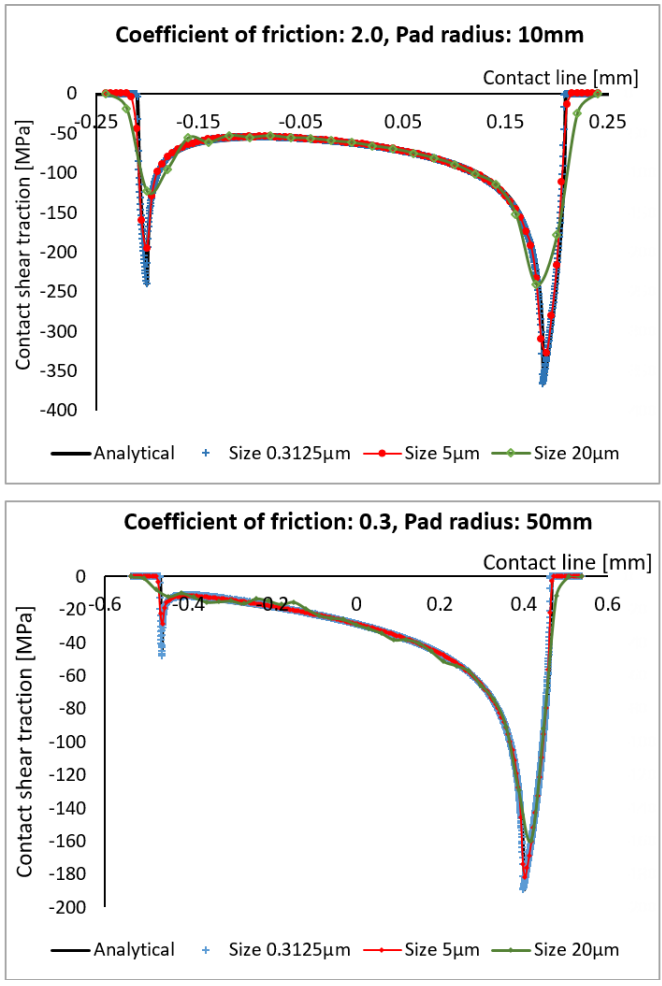

Figure 3.8: Contact shear traction at contact interface for different mesh sizes and coefficients of friction

relative error e_{rel} as:

$$e_{rel} = \left| \frac{\phi_{max}^{(i+1)} - \phi_{max}^{i}}{\phi_{max}^{(i+1)}} \right| \tag{3.3}$$

where ϕ_{max}^{i} is the maximum variable output (contact shear stress, maximum tangential stress or ratio between stick slip zone sizes) in

the ith model and $\phi_{max}^{(i+1)}$ in the $(i+1)$th model.

The results of the relative error between two consecutive mesh sizes for the maximum tangential stress are presented in Figure 3.9. For a mesh size of 0.625 μm, the relative error is around 5% for all analysed scenarios and results can be considered satisfactory (Sinclair et al., 2006). As for the shear traction component, the convergence rate of the maximum tangential stress depends upon the coefficient of friction. Again, for the smallest coefficient of friction, the convergence rate is the highest. This may also be related to the steepest gradient of the distribution of the tangential stresses at the trailing edge, as shown in Figure 3.10.

As mentioned in Lee et al. (2000), increasing the pad radius causes a reduction on the peak contact pressure and increases the contact width. Therefore, for the same loading conditions, the contact pressure distribution has a steeper gradient for pads with smaller radius. As discussed by Hills and Nowell (1994) and Johnson (1987), the analytical distribution of shear stress at contact can be seen as a superposition of contact pressure distribution and two shear tractions. Thus, it is expected that the gradient of the distribution of the tangential stresses at the trailing edge is higher for the model with smaller pad radius. The smaller contact width for smaller pad radius also implies higher peak values of tangential stresses in a smaller area (Figure 3.10). Therefore, for the same loading conditions, a finer mesh is necessary to properly capture these changes in the model with pad with smaller radius.

It can also be observed in Figure 3.10 that the peak values and, therefore, the gradient of the distribution of the tangential stresses, is

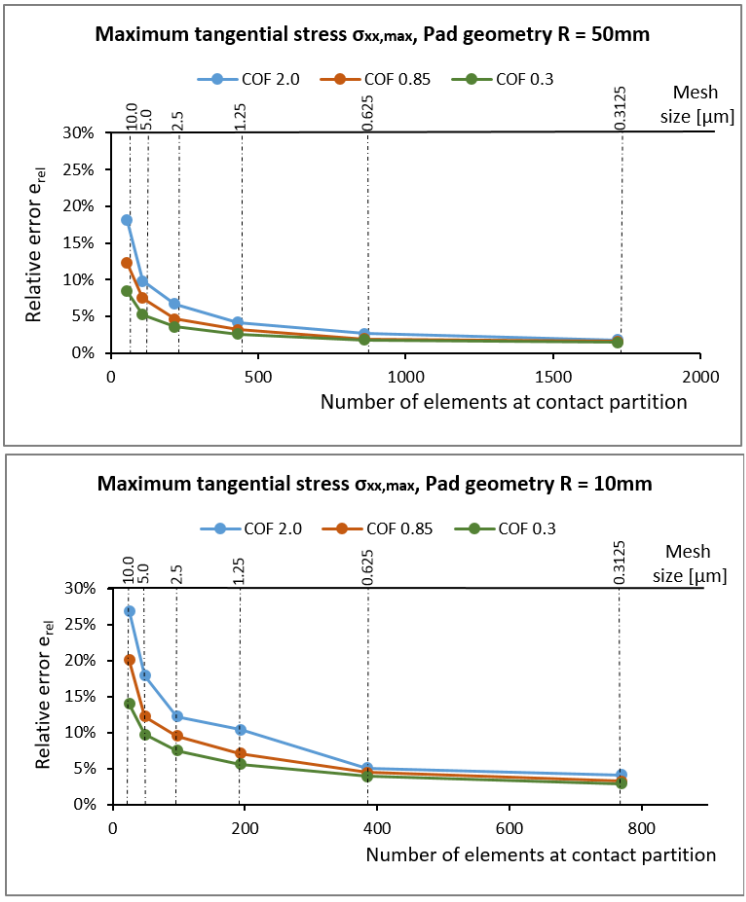

Figure 3.9: Mesh convergence curves for the maximum tangential stress, for different cases of coefficient of friction and pad radius

smaller for low coefficients of friction. Consequently, the convergence rate, for the model with 10 mm pad radius, is slower than for the model with 50 mm pad radius, as it can be seen in Figure 3.9. This impact of geometry on convergence rate is expected, as the smallest radius implies smaller contact region for the same loading condition. It also implies higher peaks of tangential stresses in a smaller area. Thus, for the same level of accuracy, a finer mesh is required in the model with pad with smaller radius.

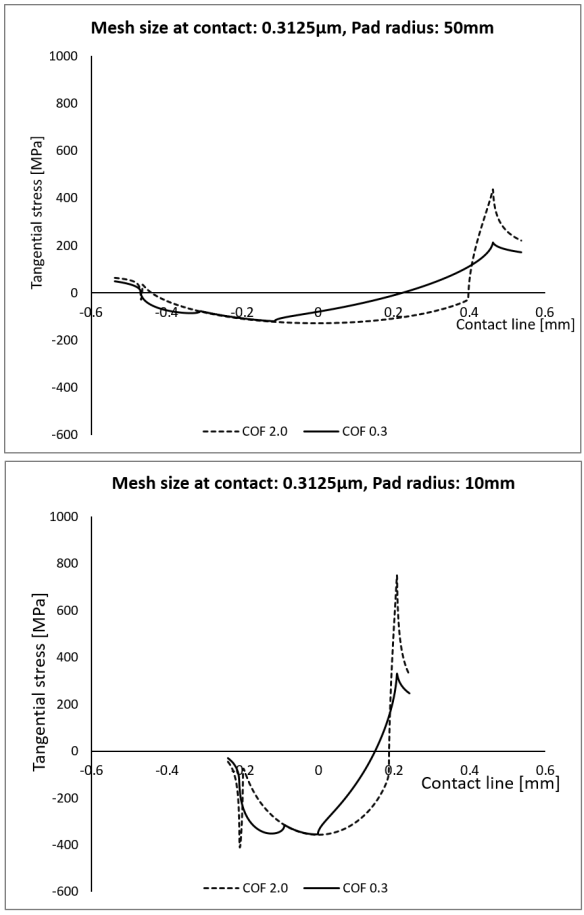

Figure 3.10: Tangential stress at contact interface, results from FEA with mesh size equal to 0.3125 µm

3.2.2 Convergence map

Aiming to help researchers to easily determine the required element size for their finite element analysis for a given stick-slip ratio and desired accuracy, we produced a "fretting fatigue convergence map", depicted in Figure 3.11. This map was constructed by plotting the stick-slip ratio (c/a) against the element size in the contact zone

for different numerical accuracies (1%, 2% and 5%) and may be used as a reference for choosing the element size in FEA of fretting fatigue (cylinder on plane configuration). This map is limited for 2D analysis of fretting fatigue considering a cylindrical pad in contact with a flat specimen.

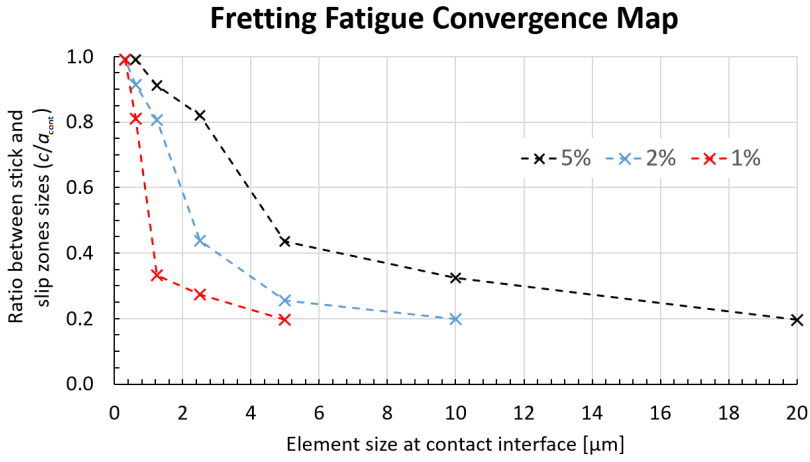

Figure 3.11: Fretting fatigue convergence map: stick-slip ratio ($^{c}/_{a_{cont}}$) as function of the element size in the contact zone for different numerical accuracies (1%, 2% and 5%)

3.2.3 Computational cost

The computational cost of the analysis increases considerably as the mesh size reduces. For instance, Figure 3.12 shows the computational time as function of the mesh size for the model with pad radius 50 mm. The computational time of the analysis of smallest mesh size model (0.3125 μm) is around 8 hours running in three cores, using the following processor: Intel Core i7-5600U CPU @ 2.60GHz with 16GB of memory RAM.

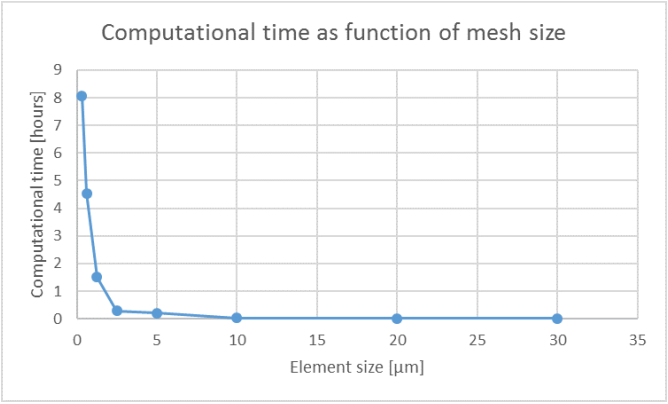

Figure 3.12: Computational time as function of the mesh size for the model with pad radius 50mm

The presented computational time is related to the analysis of only one fretting fatigue cycle. In Chapters 4 and 6, for instance, it is necessary to run the analysis of a full cycle many times, which increases the computational cost dramatically. Therefore, the accuracy of the analysis should be balanced with the computational cost.

3.3 Conclusions

In this chapter, we investigated the presence of singularity in fretting fatigue stresses distributions at contact interface. We considered different scenarios, with three distinct coefficients of friction in order to replicate different loading conditions as well as two distinct pad geometries, one with radius equal to 50 mm and another with radius equal to 10 mm.

For the considered loading conditions and coefficient of frictions, we could not find any indications of singularities as the mesh becomes

smaller; all of our results converged as the mesh size got reduced. We, in addition, discussed the convergence rate of FEM in the situations described above. We noticed that this rate also depends on the coefficient of friction, in the sense that higher coefficient of frictions led to lower rates of convergence. This means that, for a fixed element size, the level of error in the analysis depends on the loading condition. Therefore, it is recommended that the analyst performs a mesh convergence study for each of his/her loading condition of interest, as it may impact the accuracy of the corresponding results. Considering all scenarios that we have studied, a choice of element size of 0.625 μmat contact provided the smallest relative error for all variables, being around or even smaller than 2% (see convergence map above) and producing satisfactory results.

As discussed in Section 3.2.3, the main issue when considering a very small mesh size at contact interface is the computational cost of the simulation. Even though an element size of 0.625 μm provides best accuracy, for the analysis in the following chapters of this thesis, an element size of 5 μm is considered. This way a good balance between accuracy (less than 5% error, as per convergence map proposed in this chapter) and computational cost (in many situations it is necessary to run hundreds of cycles and, therefore, an analysis with really small mesh size becomes infeasible).

A "fretting fatigue convergence map" was also constructed, providing information on the required element size for a specific stick-slip ratio and different levels of accuracy.

4

LEFM approach

Fretting fatigue has commonly been modelled by linear elastic fracture mechanics (LEFM) framework (Giner et al., 2009; Noraphaiphipaksa et al., 2016; Araujo and Nowell, 2002). In LEFM, the lifetime is nor-

mally estimated by integrating an empirical crack growth law that depends on the stress intensity factors (SIF) at crack tip. The computation of those SIFs are directly affected by the crack path inside the material. The prediction of crack paths has, therefore, a major impact on the life estimates. They have been traditionally computed based on an orientation criterion at the crack tip.

Maximum tangential stress (MTS) (Erdogan and Sih, 1963) or "local symmetry" (Cotterell and Rice, 1980) are classical LEFM orientation criteria. They predict crack growth directions with good accuracy under proportional loading conditions, as presented in Boljanović and Maksimović (2011), Mageed and Pandey (1992), Miranda et al. (2003) and Richard et al. (2005). However, the applicability of those criteria for problems under non-proportional loading (for example in fretting conditions) is questionable and may lead to the prediction of erroneous crack paths, such as the ones obtained by Hojjati-Talemi et al. (2014); Giner et al. (2014) and Giner et al. (2008).

Approaches aiming to extend these classical criteria for situations of non-proportional loading have already been discussed in literature. Hourlier et al. (1985) proposed an extension of MTS in which the propagation direction is selected as the one that maximizes the amplitude of mode I stress intensity factor in a branched crack over the loading cycle. Dubourg and Lamacq (2000) proposed crack growth direction in which the effective amplitude of tangential stress at crack tip is largest. It is important to notice that, those non-proportional loading adjustments require knowledge of the stress state at the crack tip for each time in the loading cycle. Thus, the proper modelling of crack faces in-

teractions is essential, as crack closure can happen during the fatigue cycle and it directly affects the stress distribution around the crack tip.

Recently, an attempt to consider crack faces contact on the estimation of crack path under fretting conditions was done by Giner et al. (2014). They proposed an extension of the "local symmetry" criterion, in which the propagation direction is obtained as the one that minimizes the shear stress amplitude at an element ahead of the crack tip over the loading cycle. Considering a flat indenter in contact with a flat specimen, their numerical results were in agreement with experimental observations. However, they did not consider life predictions.

In this regard, the main goal of this chapter is to improve numerical estimates of fretting fatigue crack propagation path as well as life predictions, using LEFM and considering non-proportional loading condition. There has been some effort in the literature to account for non-proportional loading in life estimates (Noraphaiphipaksa et al., 2013). However, their estimates were sensible to the location where stresses around the crack tip are evaluated. To improve their results, they calibrate the numerical predictions of crack path with experimental evidence. In the approach proposed here, we use stress intensity factors that do not require any knowledge of the crack path beforehand. In fact, our results showed that the proposed methodology is capable of accurately predict crack paths, that has not been achieved before. In summary, our contributions in extending the state-of-the-art are the implementation of a orientation criterion that accounts for non-proportional loading and its use in fretting fatigue conditions, which leads not only to better life predictions by also to correct estimation of

crack paths.

The chapter is organized in the following way. Firstly, the use of a local aproach proposed by Giner et al. (2014) is discussed, implemented and reviewed for proportional and non-proportional loading conditions. Then, this analysis is extended by making use of stress intensity factors to predict the potential crack growth direction and propagation lives. For this analysis, details of the crack face interaction modelling and its effect on the SIFs calculation are presented. Later, the influence of short crack behaviour in the lives estimates is briefly explored, followed by discussion of main results and conclusions.

4.1 Minimum shear stress range criterion

The minimum shear stress range criterion was proposed by Giner et al. (2014). This criterion can be seen as a generalization, for non-proportional loading conditions, of the "criterion of local symmetry", which states that crack growth will be in the direction that causes the stress intensity factor K_{II} to vanish. In general, for non-proportional conditions, it is expected that K_{II} will not be zero in any direction and, therefore, a logical approximation would be to search for a direction that minimizes the amplitude of K_{II} over the loading cycle, named here as ΔK_{II}.

Giner et al. (2014) also mention that, in some conditions, obtaining the stress intensity factor K_{II} can be computationally expensive and also not very accurate. In order to circumvent this problem, they propose to search for the direction that minimizes the shear stress am-

plitude $\Delta\tau_{r\theta}$ at the crack tip (for an overview of the stresses at crack tip, please review Figure 2.12). From the two orthogonal planes on which $\Delta\tau_{r\theta}$ is minimized, the propagation direction is chosen as the plane with the maximum variation of the normal stress $\Delta\sigma_{\theta\theta}$. This is justified by the fact that, at this plane, less frictional energy will be dissipated (because the shear stress range is minimum) and more energy would be available for propagating the crack (selection of plane with highest normal stresses).

Giner et al. (2014) implemented the minimum shear stress range criterion in a XFEM framework. Here, an adaptation of their criterion for a conventional FE analysis is done in the following way. Firstly, a local cylindrical coordinate system (r, θ) is defined at the crack tip and the stress results from the FE analysis are transformed from the cartesian (x, y) to this local coordinate system. Then, as showed in Figure 4.1, a circular path ahead of crack tip of radius R (with $R = 0.2a_0$, where a_0 is the initial crack length) and centered at the crack tip was created, with θ varying between $-90°$ and $+90°$. The stresses at this fixed path are read and stored for each time increment in the loading cycle. These results are later used to obtain maximum and minimum envelopes as well as the variation of shear stress $\tau_{r\theta}$ and normal stress $\sigma_{\theta\theta}$ as function of θ. The propagation angle θ_P is then defined as the direction with the minimum $\Delta\tau_{r\theta}$ and with the highest value of $\Delta\sigma_{\theta\theta}$. Figure 4.2 shows a flow chart summarizing the procedure.

A python script is written to post-process the results from the analysis and to define the propagation angle as discussed above.

The performance of the minimum shear stress range criterion is

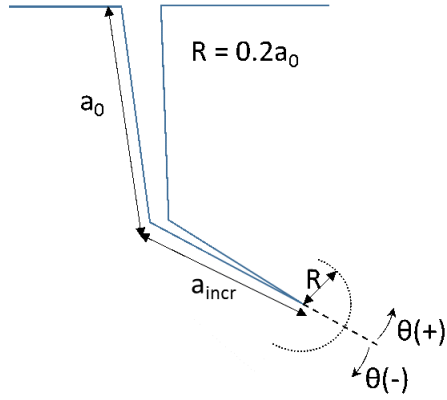

Figure 4.1: Circular path ahead of crack tip

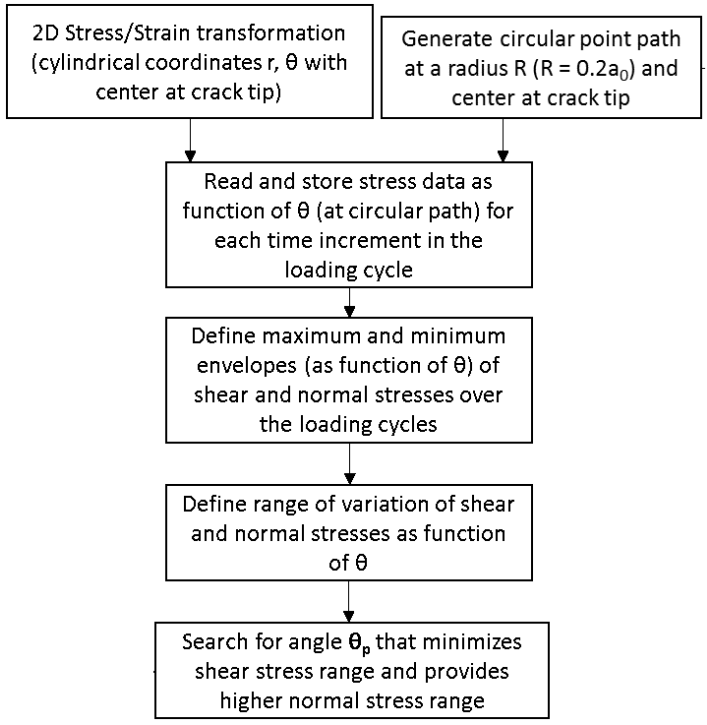

Figure 4.2: Flow chart of the implementation of minimum shear stress range criterion

checked under different conditions: proportional and non-proportional loadings. For each situation sensitivity analysis is performed to evalu-

ate how different parameters, such as the path radius R, mesh size at crack tip and propagation increment length a_{inc}, affect the propagation path.

The crack propagation is modelled using the conventional FE method with remeshing technique. The crack is simulated using a "seam" in ABAQUS, a cut in the model that can freely open during analysis. As the contact algorithm in ABAQUS provides more accurate results with linear elements, all models are meshed using a 2D quadrilateral, 4-node (bilinear) elements. Penalty formulation is used to define the tangential behaviour and a hard contact approach is used to define the normal behaviour of the contact pair. This decision was made due to convergence of the contact algorithm. The serrated fracture surfaces the analysis poses a difficult in the convergence. Penalty formulation is an unconstrained optimization problem, which is probably easier to get converged result, although it may lead to solutions that are not of interest and dependent on the penalty stiffness. Therefore, a careful selection of penalty stiffness has to be made.

In order to capture singularity, the crack tip was meshed using a ring of collapsed linear quadrilateral elements. A stepwise analysis was done and the whole model was re-meshed after advancing the crack in each increment of crack propagation.

4.1.1 Crack face interaction

The crack face contact may impact the results, especially in cases under negative cyclic loading ratio. The general contact algorithm in

ABAQUS is used to define the contact interaction between the crack faces. A python script is used to select element-based surfaces at the crack faces and to associate the general contact interaction to those surfaces. As mentioned above, penalty formulation is used to characterize the tangential behaviour of the crack faces and hard contact formulation was used for the normal behaviour of the contact pair. A fixed value of maximum elastic slip, with a 1×10^{-4} fraction of characteristic surface dimension, was used in all simulations. This value was selected considering a balance between accuracy and computation effort to compute crack face contact interaction. Ideally, a very small value should be selected, but it increases dramatically the computational cost of the simulation.

In order to verify the implementation of the crack contact interaction, a crack propagation analysis of a plate with inclined crack under compression is considered and the results are compared to literature data. As this condition falls under a proportional loading condition, the results will be presented in the following section.

4.1.2 Proportional loading

Two numerical predictions of a mixed-mode crack growth in a elastic plane plate, with a slant crack, is performed in ABAQUS. The first one considered the plate under fatigue load and is used to verify the performance of the minimum shear stress range criterion to predict crack propagation under proportional loading conditions. The second one, plate under compression, is considered in order to verify the contact interaction implementation and also the performance of the

Table 4.1: Model dimension and material properties (data from (Yan, 2010)).

Parameter	Value
Crack length, a	7 mm
Plate half-height, H	17.5 mm
Plate half-width, W	17.5 mm
Slant crack angle, α	30
Shear modulus, G	26909 MPa
Poisson's ratio, ν	0.321
Mean stress, σ_m	150 MPa
Characteristic of cyclic loading ratio, R_{cycle}	0.048

criterion to predict propagation under static compression load.

The fatigue model consisted of a plate with a center slant crack, as shown in Figure 4.3. The dimension and material properties are based on the model proposed by Yan (2010) and are summarized in Table 4.1.

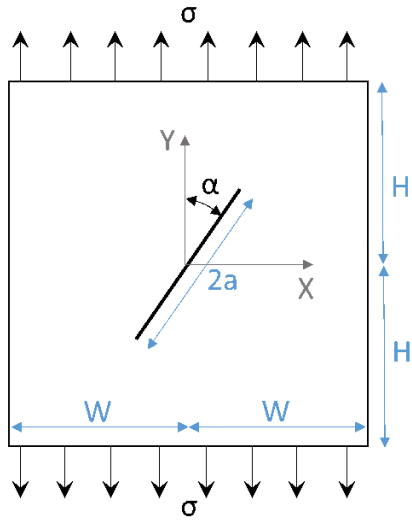

Figure 4.3: Slant centre crack model under fatigue loading

Each step of the propagation simulation consists in the analysis of a

full loading cycle, with stress σ applied in three loading steps varying from maximum, mean and minimum values (obtained from R_{cycle} and σ_m in Table 4.1). For the static analysis, each loading step is divided into 10 time increments and the solution for each of those increments is later used in the calculation of the propagation direction.

The propagation path obtained using the minimum shear stress range criterion was compared with the predicted path using MTS criterion (Yan, 2010) and it is presented in Figure 4.4. Both criteria predict the same path, implying that the minimum shear stress range criterion can also be a good choice under proportional mixed-mode conditions.

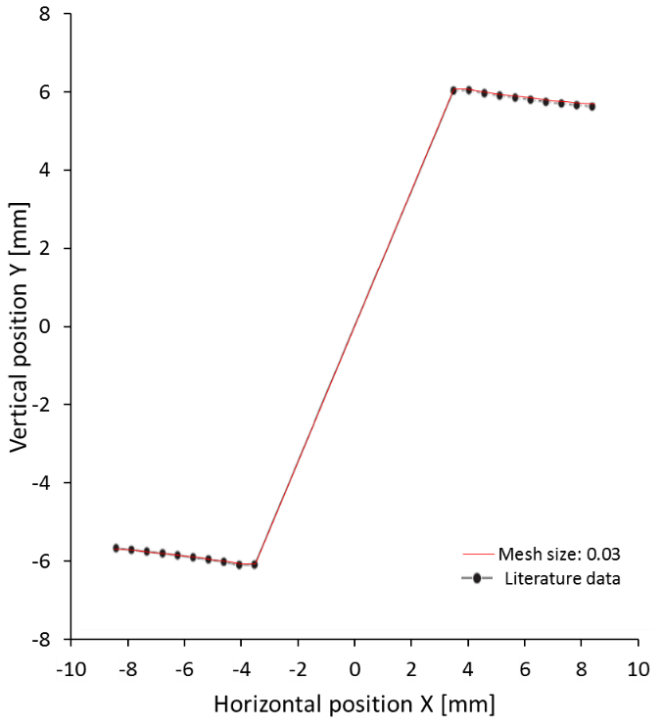

Figure 4.4: Comparison of predicted crack propagation path with literature data from (Yan, 2010)

Figure 4.5(a) and Figure 4.5(b) show results of how the mesh size influenced the results. As the element size reduces, the stress singularity at crack tip can be more accurately captured and the results tend to converge to a unique path. In addition, the propagation increment length a_{inc} has no impact on the path prediction.

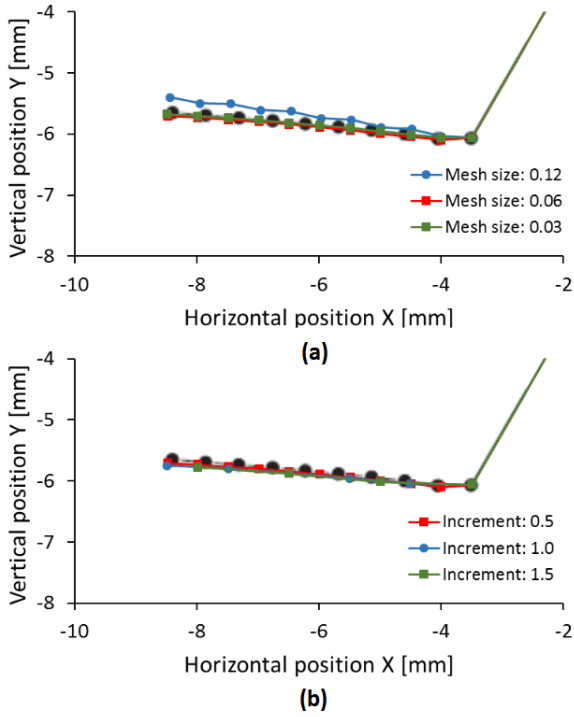

Figure 4.5: Results obtained using minimum shear stress range criterion: (a) Sensitivity check: crack tip mesh size impact on predicted propagation paths, (b) Sensitivity check: impact of propagation increment length a_{inc} on predicted propagation paths

The model with pure static compression load is shown in Figure 4.6 and it is made of a plate with a center slant crack. The dimensions are also presented in Figure 4.6, where $W = 1$ m, $a = 0.566$ m and $\theta = 45°$. For comparison and verification of our implementation, the same as the model proposed by Liu and Borja (2008) was considered

here: a plane stress condition is assumed and the following elastic material properties are adopted: Young's Modulus $E = 10000$ MPa and the Poisson's ratio $\nu = 0.30$. The crack is fully frictional with a coefficient of friction $\mu = 0.10$.

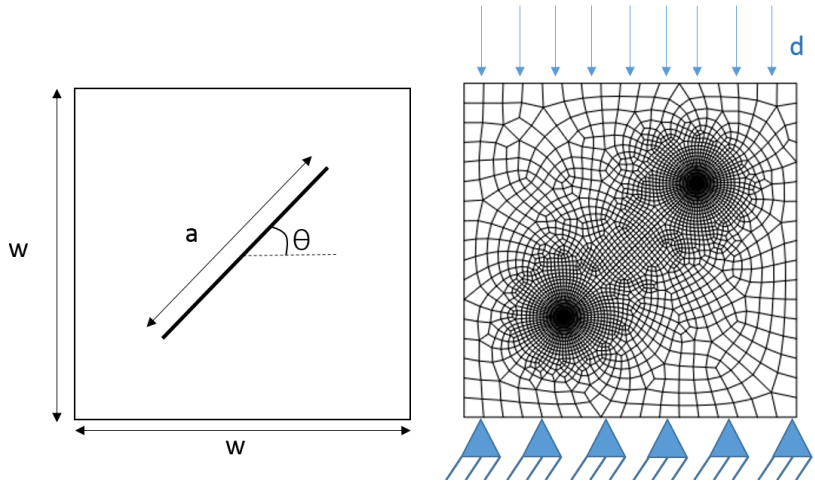

Figure 4.6: Slant centre crack model under static compression loading

Firstly, the plate is submitted to a fixed displacement at the top $d = 0.05$ m and the crack is not allowed to propagate. The results after one loading step are shown in Figure 4.7 and 4.8. It can be seen that both displacements in X and Y directions are transferred across the crack faces and also the magnitude of those displacements are in agreement with literature data.

In a later analysis, the model is again submitted to a compression displacement of 0.05 m and the crack is now allowed to grow. The analysis was preformed in six steps of crack increments of 0.04 m each and the results were compared with the ones provided by Liu and Borja (2008). As it is shown in Figure 4.9, the minimum shear stress range criterion seems to capture the crack growth behaviour similarly

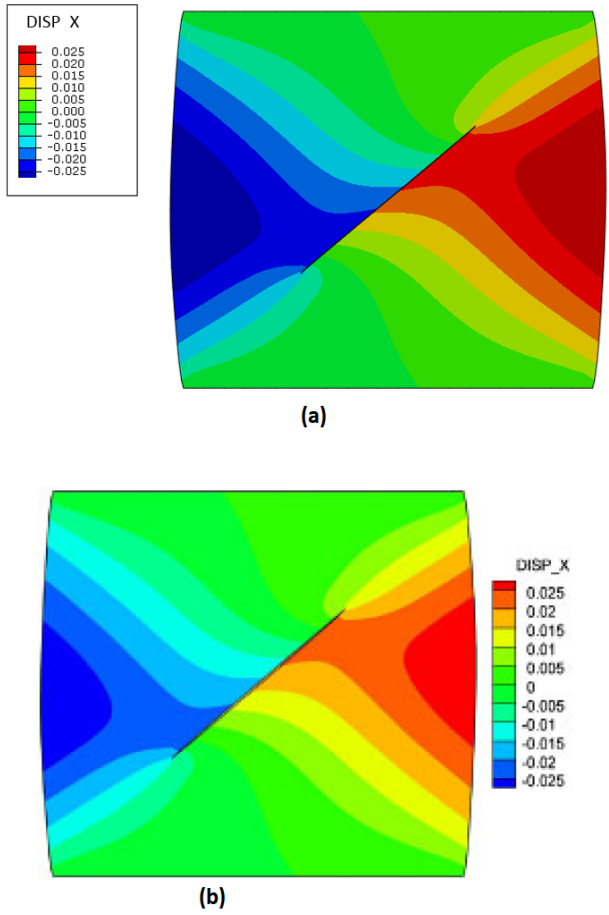

Figure 4.7: Comparison between displacements in X direction: (a) implemented model and (b) literature data from (Liu and Borja, 2008)

to the prediction from Liu and Borja (2008) with good accuracy.

The previous results imply that the minimum shear stress range criterion may be a good option to model propagation of diverse problems under proportional loading conditions. In the following section, its use under non-proportional loading will be evaluated and some brief conclusions will be drawn.

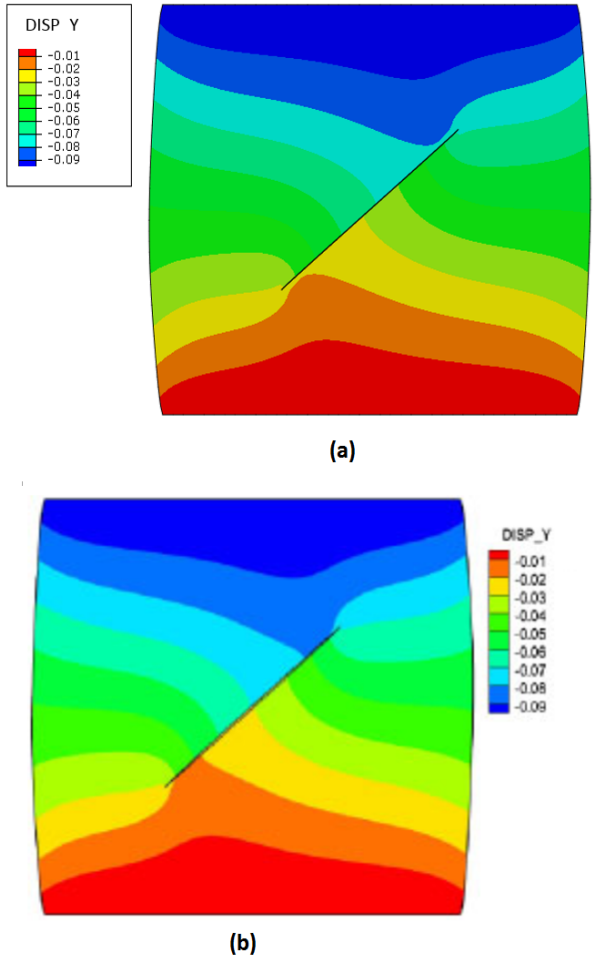

Figure 4.8: Comparison between displacements in Y direction: (a) implemented model and (b) literature data from (Liu and Borja, 2008)

4.1.3 Non-proportional loading

It is known that under fretting conditions, the stress field near the contact region is non-proportional, even if the external loads are applied in a proportional way (Tur et al., 2003; Nowell et al., 2006). In order to study the performance of the minimum shear stress range cri-

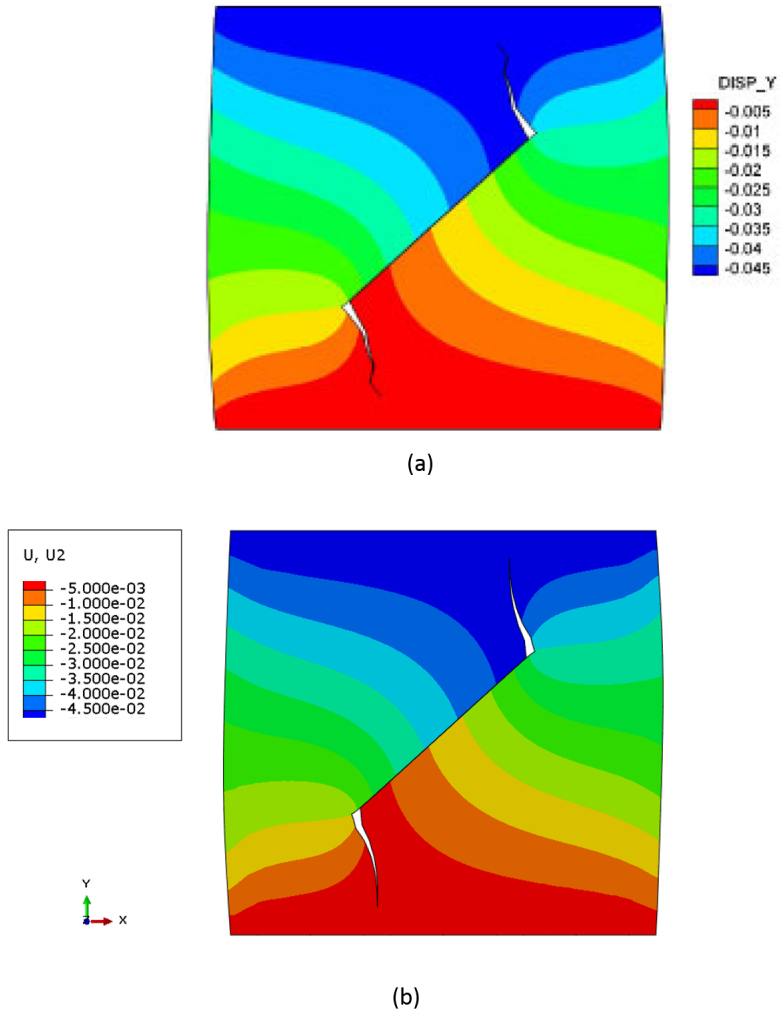

Figure 4.9: Propagation under static compression load: (a) literature data (Liu and Borja, 2008) and (b) implemented model

terion under non-proportional mixed-mode fatigue, the same elastic fretting model presented by Giner et al. (2014) is analysed using conventional FE framework. The model details such as geometry, material properties, boundary conditions and loading history are presented in Figure 4.10. The model is composed of only two parts: a pad and a

specimen, which represents a quarter of the experimental set-up, due to its symmetry. In this set-up, two flat pads are maintained in contact with a flat specimen through the application of a constant clamping or normal force F. The specimen is fixed at one end and the other end is subjected to an oscillatory bulk stress σ_{axial}.

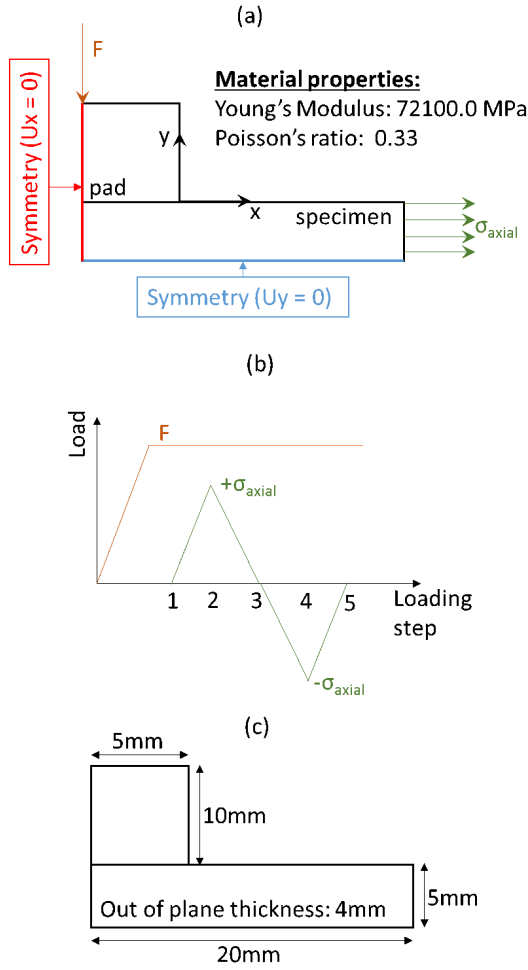

Figure 4.10: Fretting fatigue model details, based on the model from Giner et al. (2008) (a) Boundary conditions, (b) Cyclic loading steps of one full fretting cycle, (c) Model dimensions

The master-slave algorithm in ABAQUS is used to describe the con-

tact and the Lagrange multiplier formulation is used to define the tangential behaviour of the contact interface between pad and specimen, with a coefficient of friction of 0.8. The surface to surface and finite sliding options were used to define the contact interaction. A 2D quadrilateral, 4-node (bilinear), plane strain, reduced integration element (CPE4R) was used to mesh the model with a ring of collapsed elements at crack tip.

The initial crack is inserted at the contact edge in the same way as described by Giner et al. (2014), at an angle of -120° with horizontal x direction and with initial length of 50 μm. An analysis with 15 crack increments with fixed length a_{inc} equal to 50 μm is then performed. Each step of the propagation simulation consisted of the analysis of a full fretting loading cycle. This fretting cycle is divided in five loading steps (see Figure 4.10(b)). In the first loading step, the top pad was pressed against the specimen surface by a normal load $F = 100$ $\mathrm{N/mm}$ and this compressed condition was held constant until the end of the cycle. Then, an oscillatory axial stress $\sigma_{axial} = \pm 110$ MPa was applied to the side of the specimen. The contact between the crack faces was also modelled using the general contact algorithm in ABAQUS and a coefficient of friction of 0.8 was used at this interface.

Figure 4.11(a) shows experimental data from Giner et al. (2014). These are, in Figure 4.11(b), compared with the predicted path obtained when using minimum shear stress range criterion and MTS criteria. In order to extract experimental data from the picture, the software Web Plot Digitizer (Rohatgi, 2014) was used. One can conclude that the predicted path obtained by minimum shear stress range

criterion is in good agreement with the experimental observations, but that is not the case for MTS criterion. As also mentioned by Giner et al. (2014), it is important to notice that the use of MTS criterion simplifies the problem. For its computation, it is only necessary to consider the FE results at the instant of maximum σ_{axial}. Nevertheless, for computing the minimum shear stress range criterion, the entire loading cycle must be analysed and considered. Therefore, MTS criterion does not provide correct crack propagation as it neglects the effect that the rest of the fretting cycle may have on the crack propagation direction.

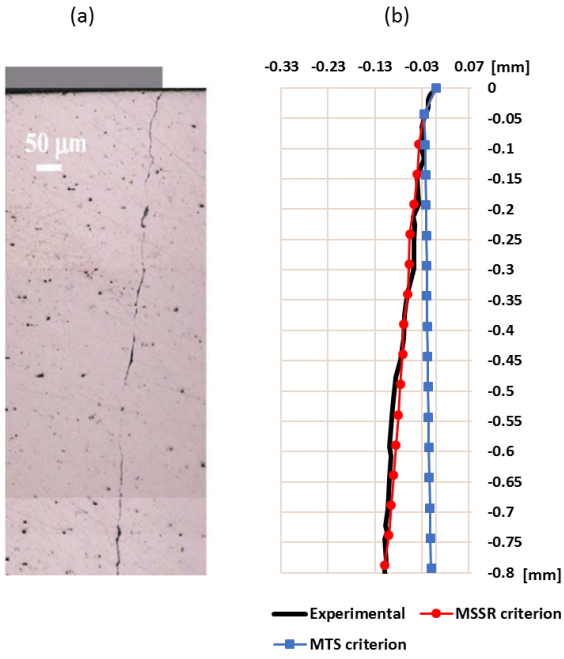

Figure 4.11: Fretting fatigue crack propagation path: (a) Experimental data from Giner et al. (2014), (b) Comparison of predicted path using different criteria and experimental data

The influence of the path radius R, mesh size at crack tip and propagation increment length a_{inc} on the crack path prediction were veri-

fied. The results are presented in Figure 4.12. It can be noticed that the path radius and the propagation increment length had no significant impact on the crack path prediction. However, as expected, the mesh size at crack tip elements can affect considerably the propagation path. In order to accurately predict the stress field ahead of the crack tip, it requires a very fine mesh size at this region. Therefore, only for very small mesh sizes, the criterion can correctly predict the crack propagation behaviour. The use of local stresses to predict orientation may not be the best option, as results may be greatly affected by the element size (Xu and Yuan, 2009a).

Under proportional loading conditions, the minimum shear stress range criterion provided the same results as MTS and both of them seem to correlate well with experimental data. In addition, the minimum shear stress range criterion seems to be a good and simple alternative to deal with fatigue problems, not only under proportional, but also under non-proportional conditions. The performance of minimum shear stress range criterion is also verified for a non-proportional loading scenario, under fretting fatigue condition. As showed by our results, this type of problem invalidates the application of conventional orientation criteria, such as MTS, but the minimum shear stress range criterion is capable of capturing the main characteristics of the crack path, providing a prediction that correlates well with experimental data.

It is also important to mention that the final results depend on the mesh size at crack tip. It requires a very fine mesh in order to accurately predict paths using minimum shear stress range criterion

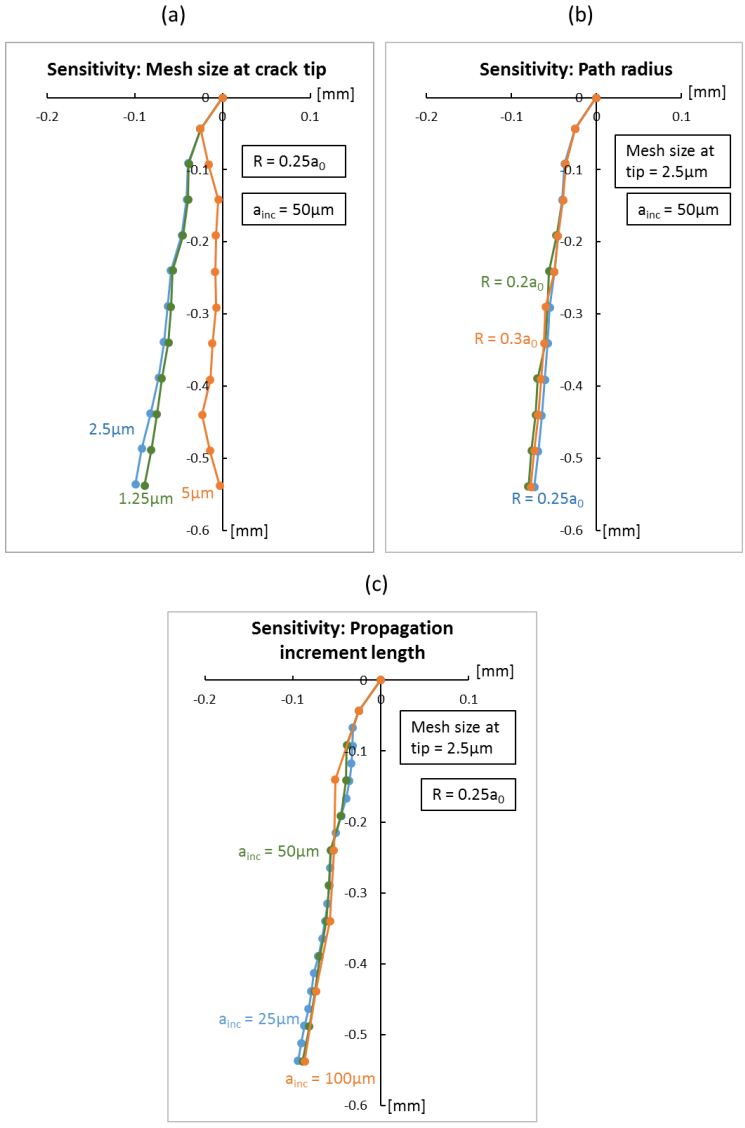

Figure 4.12: Sensitivity check: (a) crack tip mesh size impact on predicted propagation paths, (b) influence of different path radius and (c) impact of propagation increment length a_{inc} on predicted propagation paths

criteria and a mesh refinement study is therefore also recommended.

In the following sections, we will focus on a more robust way of

predicting crack paths as well as on an alternative approach to estimate life considering non-proportional loading and crack face contact for fretting cases.

4.2 Extension of MTS criterion using SIFs

We will make use of the $\Delta k^*_{I,max}$ criterion in an attempt to improve the path and life predictions for a cylindrical pad in contact with a flat plane, under fretting conditions.

Under LEFM, the FEA of a model with a crack of length a allows the calculation of stress intensity factors K_I and K_{II} at the crack tip as a function of time t. If we further assume an infinitesimally small branched crack length (δ), as represented in Figure 4.13, the stress intensity factors k^*_I and k^*_{II}, now calculated at the tip of this crack segment, can be expressed as a linear combination of K_I and K_{II} , as proposed by Ribeaucourt et al. (2007):

$$\begin{bmatrix} k^*_I(\theta,t) \\ \\ k^*_{II}(\theta,t) \end{bmatrix} = \begin{bmatrix} K_{11}(\theta) & K_{12}(\theta) \\ \\ K_{21}(\theta) & K_{22}(\theta) \end{bmatrix} \begin{bmatrix} K_I(t) \\ \\ K_{II}(t) \end{bmatrix}$$

where $K_{11}(\theta)$, $K_{12}(\theta)$, $K_{21}(\theta)$ and $K_{22}(\theta)$ are analytical functions of the branched crack orientation angle θ and can be written as (Ribeaucourt et al., 2007):

$$K_{11}(\theta) = \left(\frac{1-m}{1+m}\right)^{\frac{m}{2}} \left(\cos\theta - \frac{1}{2\pi}\sin L\theta\right)$$

$$K_{12}(\theta) = \left(\frac{1-m}{1+m}\right)^{\frac{m}{2}} \left(-\frac{3}{2}\sin\theta\right)$$

$$K_{21}(\theta) = \left(\frac{1-m}{1+m}\right)^{\frac{m}{2}} \left(\frac{1}{2}\sin\theta\right)$$

$$K_{22}(\theta) = \left(\frac{1-m}{1+m}\right)^{\frac{m}{2}} \left(\cos\theta + \frac{1}{2\pi}\sin L\theta\right)$$

where $m = {}^{\theta}/_{180}$ and $L = ln\left(\frac{1-m}{1+m}\right) - 2\left(\frac{m}{1-m^2}\right)$.

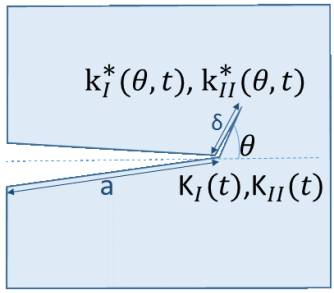

Figure 4.13: Stress intensity factors at a kinked crack from the original crack

The stress intensity factors k_I^* and k_{II}^* can be used to predict the propagation direction under different conditions. Consider first a structure subjected to mixed-model fatigue under proportional loads. Here, the ratio ${}^{K_I}/_{K_{II}}$ is kept constant during one loading cycle (Hourlier et al., 1985) and the propagation direction can be satisfactory predicted using classical LEFM orientation criteria, such as MTS criterion or "local symmetry". The growth direction obtained by MTS criterion is equivalent to the one that maximizes k_I^* (Hourlier et al., 1985) and, according to the "local symmetry" criterion, crack propagation direction can be obtained by satisfying the condition that k_{II}^* is equal to 0 (Giner et al., 2016).

For instance, Figure 4.14 shows the definition of the propagation

criteria for a mixed model proportional loading fatigue case: a block with an inclined edge crack fixed at one side and subjected to a cyclic axial load σ_{axial} at the other side. Assuming plane strain conditions, we first compute both k_I^* and k_{II}^* as function of the crack segment angle θ for different instants (1, 2, 3, 4 and 5) in the loading history. The propagation angle θ_P can be obtained by considering the position the maximizes k_I^* (solid round dots in Figure 4.14) or the the position where k_{II}^* is zero (solid square in Figure 4.14). Note that under these loading conditions, there is only one solution that satisfies the "local symmetry" criterion and there is also only one angle that maximizes k_I^* for any time.

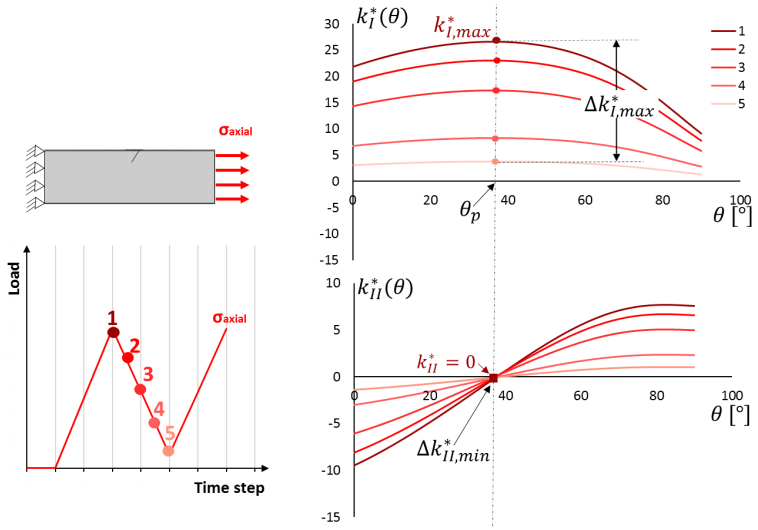

Figure 4.14: Stress intensity factor at a kinked crack from the original crack as function of time and θ, for a mixed mode proportional loading case

Under non-proportional loading, the directions of principal stresses rotate during the fatigue cycle and so the ratio between the principal stresses may be a function of time (Dahlin, 2005). Thus, the ratio between K_I and K_{II} may no longer be constant during one loading cycle

(Madge, 2009), affecting the propagation direction defined by the criteria (MTS and "local symmetry"). In order to exemplify this issue, we may take a closer look at the variation of the stress intensity factors k_I^* and k_{II}^* as function of time and θ for a fretting fatigue case. As can be seen in Figure 4.15, the ratio $^{K_I}/_{K_{II}}$ creates a time dependency in the maximum value of k_I^*, which means that there are different angles that maximizes k_I^* at different time instants in one cycle. Another noticeable point is that there is more than one value of θ such that k_{II}^* is zero. Therefore, both the "local symmetry" or MTS criterion are invalid under this loading condition.

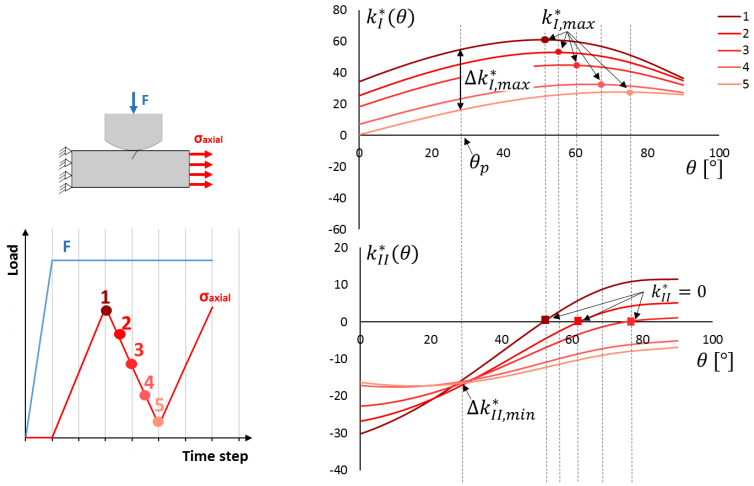

Figure 4.15: Stress intensity factor at a kinked crack from the original crack as function of time and θ, for a mixed mode non-proportional loading case

The $\Delta k_{I,max}^*$ criterion (Hourlier et al., 1985) is an extension of MTS criterion, it assumes that crack propagates in the direction that maximizes the difference between $k_I^*(\theta)$ at the instant of maximum load and at minimum load, $\Delta k_{I,max}^*$.

4.2.1 Accounting for crack face interactions

The applicability of $\Delta k^*_{I,max}$ criterion requires that the stress intensity factors at the instant of maximum and minimum load are accurately obtained. At minimum load, the crack faces might be in contact to each other, affecting the stress distribution around the crack tip, thus impacting the stress intensity factors at this instant. Therefore, the models should account for the interaction between these instances.

The crack propagation phase was analysed using the conventional FE method with re-meshing technique. The crack was simulated using a "seam" in ABAQUS and the singularity at the crack tip was captured using a ring of collapsed linear quadrilateral elements. With assistance of a python script, element-based surfaces were created at the crack faces and the general contact algorithm was used to define the contact interaction between them. Penalty formulation was used to characterize the tangential behaviour of the crack faces and hard contact formulation was used for the normal behaviour of the contact pair. A fixed value of maximum elastic slip, with a 1×10^{-4} fraction of characteristic surface dimension, was used in all simulations. The coefficient of friction between the crack faces μ faces was set to 0.8 (Giner et al., 2016).

In order to verify whether the crack face interaction was properly modelled, a simple case of a plate with an edge crack subjected to a compression load was analysed and the results compared with literature data. The model dimension and loading details were the same as the model presented by (Zheng and Luo, 2016). As shown in Fig-

ure 4.16, the stress at crack faces are in good agreement with literature data. Moreover, the vertical displacement contour presented in Figure 4.17 shows that the contact between crack faces is properly modelled as the displacement is transmitted from one crack face to another when the plate is subjected to compression.

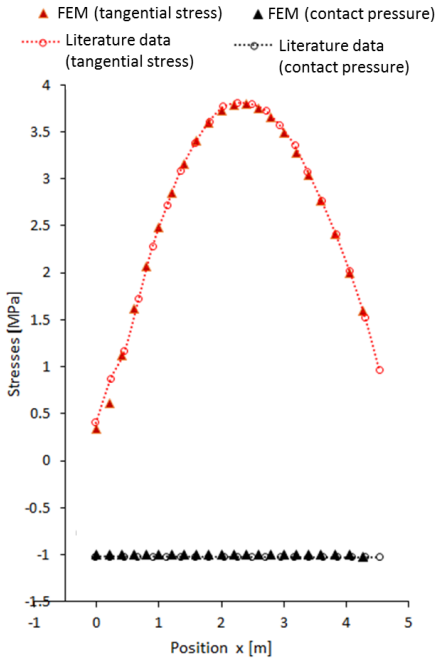

Figure 4.16: Comparison of contact stresses distribution at crack faces from literature data (Zheng and Luo, 2016) and results from simulation in ABAQUS

The presence of contact stresses at crack faces affect the calculation of the stress intensity factors. In order to take this into account, K_I and K_{II} were evaluated by the interaction integral $M(1,2)$ between

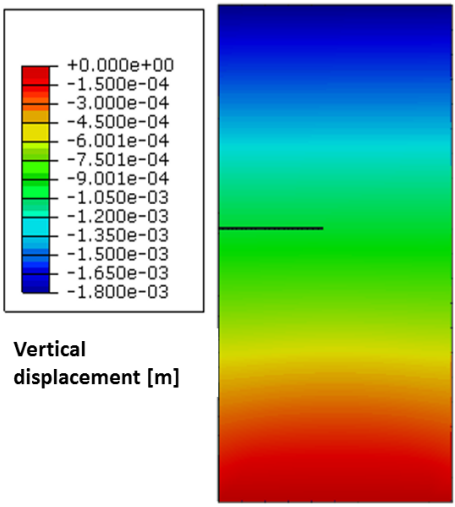

Figure 4.17: Vertical displacement distribution from simulation in ABAQUS

two states (1) and (2) of the cracked body (Kuna, 2013):

$$M^{(1,2)} = \int_{\Gamma} \left(\sigma_{ij}^{(1)} \epsilon_{ij}^{(2)} \delta_{1j} - \sigma_{ij}^{(1)} \frac{\partial u_i^{(2)}}{\partial x_1} - \sigma_{ij}^{(2)} \frac{\partial u_i^{(1)}}{\partial x_1} \right) n_j d\Gamma - \int_{\Gamma^+ + \Gamma^-} \left(\sigma_{i2}^{(1)} \frac{\partial u_i^{(2)}}{\partial x_1} - \sigma_{i2}^{(2)} \frac{\partial u_i^{(1)}}{\partial x_1} \right) n_2 d\Gamma \quad (4.1)$$

where σ_{ij}, ϵ_{ij} and u_i are stresses, strain and displacement field, respectively, and n is the outward unit normal on the contour, as illustrated in Figure 4.18. The subscripts $(i, j = 1, 2)$ refer to the two in-plane directions x_1 and x_2. The superscripts refer to the state of the body; (1) stands for a coupled state of mixed-mode (field variables obtained from FEA) and (2) is an auxiliary state with field variables defined by the asymptotic field for pure mode I or II, depending on the stress intensity factor of interest.

For K_I, the state (2) is taken as pure mode I and, in this case, this

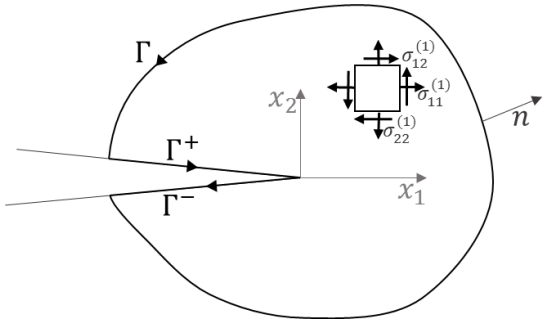

Figure 4.18: Interaction integral

stress intensity factor is related to the interaction integral as:

$$K_I = \frac{E^{'}}{2} M^{(1,modeI)}$$

where E' is the material constant related to Young's Modulus E and the Poisson's ratio ν:

$$E^{'} = \begin{cases} E \\ \frac{E}{1-\nu^2} \end{cases}$$

For K_{II}, the state (2) is taken as pure mode II:

$$K_I = \frac{E^{'}}{2} M^{(1,modeII)}$$

The first term of the interaction integral (equation (4.1)) was directly obtained by contour integral output from ABAQUS (requested for 18 contours). The second term was calculated by a numerical approximation of the line integral at crack faces considering the contact stresses at this location. Figure 4.19 shows the impact of adjusting the interaction

integral accounting for contact stress. For this analysis, a simple plane model with a slant crack, under completed reversed fatigue load is considered. Each dashed line on the graphs represents a result obtained in one of the 18 contours. The right hand side plots show results for computation of K_I and K_{II} considering only the first term on equation (4.1). As it can be seen, the values of K_I are not zero, once the axial loading is compression and crack faces are likely to be in contact (time step between 0.5 and 1). Regarding the computation of K_{II}, it can be seen that there is not a converged value of K_{II} on this condition. However, once the second term is added to equation (4.1), the results (graphs on the left hand side) showed that K_I is now contour independent for both loading conditions (traction and compression, from time step 0 to 1) and, under compression, its value is about zero, as it should. Also, for K_{II} the adjustment causes the values of K_{II} to be contour independent and converged to a unique value when the crack is under compression.

In order to verify the stress intensity factors obtained by conventional FEM, they were compared with analytical solution using weight function (Tada et al., 2000), available for the experimental configuration of a double edge notch tension (DENT) specimen. The stress intensity factor K_I for a situation under fretting condition can be estimated by the stress intensity factor in a DENT specimen, if the crack length is long enough to neglect the effect of contact stresses (Hojjati Talemi, 2014). The results presented in Figure 4.20 showed that, for long cracks, there is good agreement between analytical solutions and FEM.

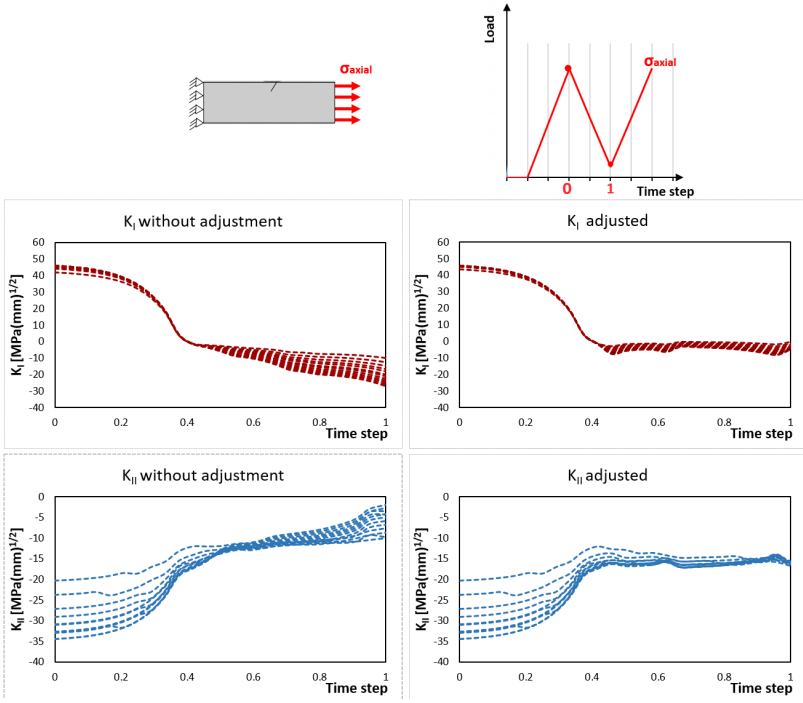

Figure 4.19: Effect of adjusting the contour integral by adding the second term due to contact stresses

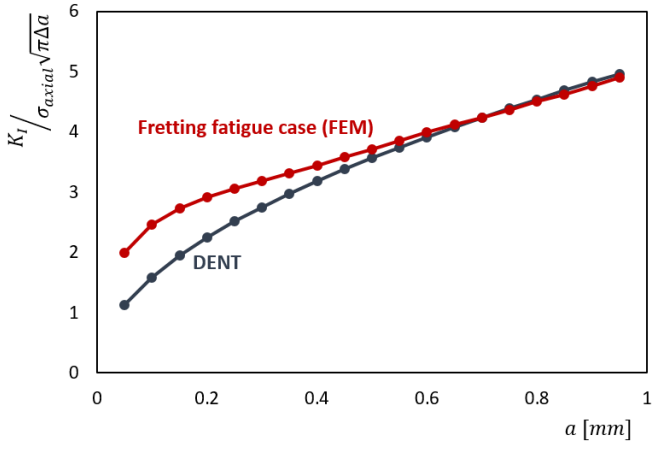

Figure 4.20: Comparison between stress intensity factor K_I obtained by analytical expression (DENT) and for fretting fatigue case (FEM)

4.2.2 Fretting Fatigue: cylindrical pad

4.2.2.1 Experimental data

Fretting fatigue tests were carried out by Hojjati Talemi (2014) using two cylindrical pads and a flat dog-bone shaped specimen. Tests are performed in a dynamic servo hydraulic machine, in which a dog bone specimen, subjected to oscillatory axial load, is maintained in contact with two cylindrical pads. These pads are kept pressed against each side of the flat specimen by a constant clamping force F while the specimen is fixed at one end and the other end is subjected to a cyclic bulk stress σ_{axial} (loading ratio 0.1). As a consequence of this set of loading, the compliance springs transmit an oscillatory tangential force $\pm Q_{max}$ at the pads. The material for both specimens and indenters is aluminium alloy 2420-T3, with a Young's modulus of 72.1GPa and a Poisson's ratio of 0.33. For further details in the experimental tests, the reader is referred to Hojjati-Talemi et al. (2014) and Hojjati Talemi (2014). Table 4.2 shows the different fretting conditions that were tested (various axial stresses and tangential loads, for the same normal load). For each condition, the test was performed until final rupture of the specimen and the total number of cycles up to failure was recorded. These values are shown in Table 4.2, column "$N_{f,exp}$" . After test, the fractured surfaces of the specimen were inspected and crack paths at mid surface of the pad (plane strain condition) were recorded.

As discussed by Hojjati-Talemi et al. (2014) and shown in Figure 4.25(a), experimental observations of crack path show that fretting fatigue crack initiates at the edge of the contact between pad and speci-

Table 4.2: Experimental conditions extracted from (R. Hojjati-Talemi et al., 2014).

Test no.	σ_{axial} [MPa]	R [mm]	F [N]	Q_{max} [N]	$N_{f,exp}$
FF1	100	50	543	155.165	1407257
FF2	115	50	543	186.25	1105245
FF3	135	50	543	223.7	358082
FF4	135	50	543	195.55	419919
FF5	160	50	543	193.7	245690
FF6	190	50	543	330.15	141890
FF7	205	50	543	322.1	114645
FF8	220	50	543	267.15	99607
FF9	220	50	543	317.845	86647

men, in a direction inwards the contact region. Then, this crack evolves under a mixed mode condition until reaching a depth from the surface of approximately the hertzian contact width $2a_{cont}$ (for the tests in Table 4.2, $a_{cont} = 0.467$ mm). After this stage, the effects of the high local stresses, generated by the contact between pad and specimen, become negligible and the crack propagates in a direction perpendicular to the applied bulk stress σ_{axial}. This typical path, growing inwards the contact region, have already been observed by various other researchers (Faanes, 1995; Navarro et al., 2006; Szolwinski and Farris, 1998) under different fretting conditions. For instance, Wharton et al. (1973) and Cardoso et al. (2016) showed the same characteristic path for samples in different materials (brass and steel).

4.2.2.2 Numerical model

A parametric 2D FE model was created in ABAQUS containing two parts. It consists of a pad and a specimen, with dimensions, boundary

conditions and mesh details shown in Figure 4.22. The model represents half of the experimental set-up, due to symmetry about the centreline of the specimen. The vertical movement in the y direction ($U_y = 0$) and rotation around z axis ($R_{xy} = 0$) were restricted at the bottom of the specimen. The sides of the pads were restrained in the x direction ($U_x = 0$). Both parts are made of aluminium 2420-T3, with material properties summarized in Table 4.3. No plasticity effect was incorporated and the material response was considered elastic. This is a reasonable assumption for high cycle fatigue, where plastic strains are very small (Ambrico and Begley, 2000).

Regarding surface deformation at the contact, the elastic surface deformation is already taken into consideration in the modelling. The plastic deformation at interface, for the fretting cases analysed here, can be neglected because of the following. The load required to cause the first yield of the specimen, assuming the phenomena is represented by a cylinder in contact with an elastic-plastic semi-infinite half space, can be predicted by Johnson (1987) and is given as:

$$P_Y = \frac{3.2\pi \left(1-\nu^2\right) R\sigma_{0.2}^2}{E}$$

where R is the pad radius (50 mm), E is the Young's Modulus (72.1 GPa) and $\sigma_{0.2}$ is the yield strength (506 MPa) of the specimen's material. For the experimental tests used here, the applied normal force per unit of thickness is 135.75 $\mathrm{N/mm}$ and the critical load P_Y is equal to 1637.25 $\mathrm{N/mm}$. Therefore, the applied normal load is only about 8% of the load necessary to cause yield at the specimen. Even for this small value of critical load, plasticity may be an important effect at

Table 4.3: Material properties for aluminium 2420-T3 (Hojjati-Talemi et al., 2014)

E	Modulus of Elasticity [GPa]	72.1
ν	Poisson's ratio	0.33
$\sigma_{0.2}$	Yield Strength [MPa]	506 ± 9

surface interface, depending on the tangential load Q. To analyse the impact of Q in the surface plasticity, the study conduct by Ambrico and Begley (2000) can be used as a reference. The idea is to verify the influence of load combinations and friction coefficient on the evolution of plastic strains. The material behaviour is broken down into three regimes: (i) cyclic plastic straining, in which the material experiences steady, reversed cyclic plastic strains, (ii) ratcheting, in which the plastic strain magnitude increases continually with load cycling, and (iii) shakedown, in which plastic strains saturate after a few cycles and subsequent material response is entirely elastic. Making use of one of the behaviour maps proposed by them and replicated here in Figure 4.21, it is possible to analyse the impact of tangential load on the surface plasticity. All the test data used in our study fall in the shakedown region and the effects of deformation hardening can be neglected.

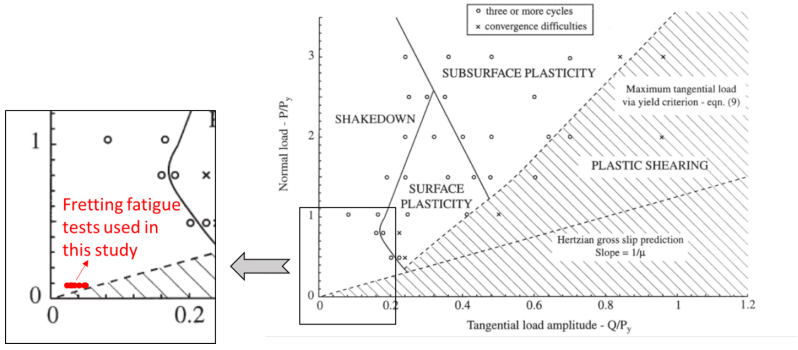

Figure 4.21: Representation of the experimental fretting fatigue tests used in this study on a plasticity behaviour map from Ambrico and Begley (2000).

The contact between pad and specimen was analysed using the master-slave algorithm with surface to surface interaction and finite sliding in ABAQUS. The cylindrical surface of the pad was considered the slave surface and the specimen flat surface was the master. The tangential behaviour was defined by Lagrange multiplier formulation and the normal behaviour was modelled by a hard contact. The coefficient of friction between the pad and specimen was kept constant and equal to 0.65.

An initial crack with length equal to 50 μm was inserted in the model at near the edge of the contact. This location was defined based on the equivalent multiaxial damage stress approach as estimated in Hojjati-Talemi et al. (2014). This crack has been orientated at $\beta = 40°$, as illustrated in Figure 4.22. The crack propagation phase was modelled using the conventional FEA with re-meshing technique, taking into consideration contact interaction between the crack faces. A stepwise procedure was performed as follows: a cyclic fretting load was applied to the model and, from a static analysis, the stress intensity factors K_I and K_{II} were calculated for each time instant of the loading cycle. Using equation (1), these stress intensity factors were expanded to k_I^* and k_{II}^* as function of time and θ. Then, the propagation direction was determined according to the $\Delta k_{I,max}^*$ criterion. The crack was advanced, during the first 25 increments, by a fixed length increment of 50 μm, then this length increment was raised to 250 μm, for the remaining propagation phase. The model was re-meshed after each increment of crack length. This procedure was repeated until final rupture of the specimen.

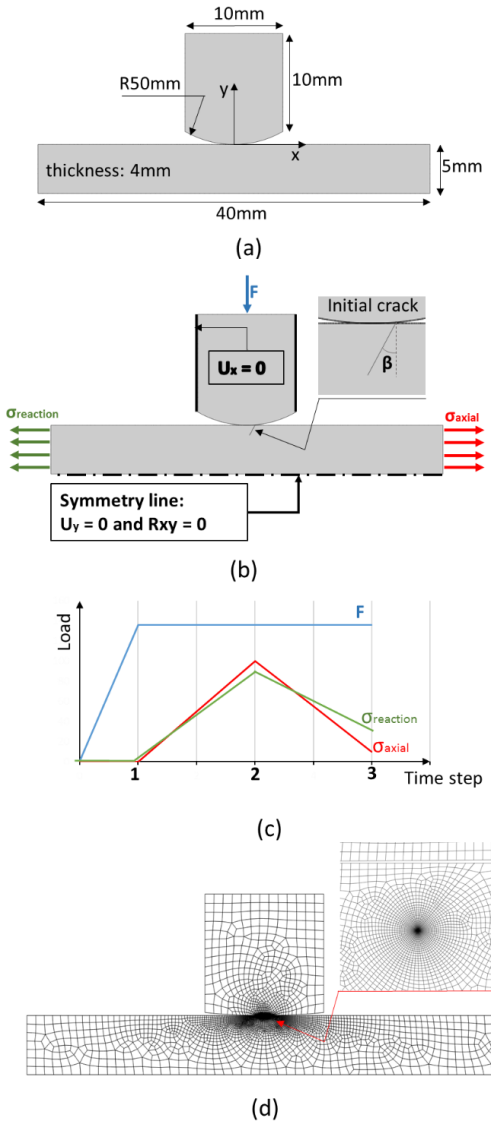

Figure 4.22: Model information: (a) dimensions of the model, details of cylinder indenter and flat specimen; (b) loading, boundary conditions and initial crack details; (c) loading history as function of time steps; (d) mesh details.

After each increment of crack length, the stress intensity factors were extracted K_I and K_{II} via the interaction integral method described in Section 4.2.1. The first term of the interaction integral (equa-

tion (4.1)) was directly obtained by contour integral output from ABAQUS (requested for 18 contours). The second term was calculated by a numerical approximation of the line integral at crack faces considering the contact stresses at this location.

The cyclic loads are applied in three steps aiming to simulate a complete fretting fatigue cycle. The effect of the tangential load Q was modelled as a cyclic reaction stress $\sigma_{reaction}$ (Hojjati-Talemi et al., 2014):

$$\sigma_{reaction} = \sigma_{axial} - \frac{2Q}{bt}$$

where b and t are the specimen width ($b = 10$ mm) and thickness ($t = 4$ mm), respectively. The maximum and minimum values of Q and σ_{axial} are obtained from experimental data. In the first loading step, the normal load F is applied at the top pad and this compressed condition is held constant until the end of the cycle. Then, the cyclic load (axial and reaction stresses) was applied to the sides of the specimen in two steps, as illustrated in Figure 4.22.

A 2D quadrilateral, 4-node (bilinear), plane strain, reduced integration element (CPE4R) was used to mesh the model with a ring of collapsed elements at crack tip. To create a fine mesh at the contact region, a small element size of about 5 μm was selected at the interface between pad and specimen. The mesh size was then gradually enlarged as the distance from the contact region was also increased.

4.2.2.3 Life prediction

The total life $N_{f,predicted}$ was obtained by adding the initiation life and the propagation life. The initiation life was predicted in Hojjati-Talemi et al. (2014), considering a continuum damage mechanics approach.

The propagation life is calculated as the number of cycles N_P necessary to cause a crack growth from an initial length (a_i) until a critical failure length (a_f). It can be estimated through a fracture mechanics approach using a crack growth law. In the present study, we integrate a Paris' Law in order to obtain the propagation life:

$$N_P = \int_{a_i}^{a_f} \frac{da}{C\Delta K^m} \tag{4.2}$$

where $C = 2.73 \times 10^{-11}$ $(\mathrm{mm/cycle})/(\mathrm{MPa}\sqrt{\mathrm{mm}})^n$ and $m = 2.6526$ are material constants, obtained from Xiang et al. (2010), ΔK is the stress intensity factor range and da is the infinitesimally small increment in crack length. For mixed-mode conditions, we assumed $\Delta K = \Delta K_{eff}$, which is given by (Liu, 2008):

$$\Delta K_{eff} = \sqrt{\Delta K_I^2 + \Delta K_{II}^2} \tag{4.3}$$

where ΔK_I and ΔK_{II} are the stress intensity range at crack tip considering maximum and minimum fatigue loading conditions.

Figure 4.23 shows a flow chart of the methodology adopted in this study and it works as follows. The stress analysis allows us to obtain stress intensity factors as well as the preferential direction of propaga-

tion θ_P. A check is then performed to evaluate if the total crack length has reached a critical value. If not, then the crack is advanced in the direction θ_P and the updated model is submitted to a new analysis. If yes, then the simulation stops, the final crack path is obtained and the total number of cycles is calculating by adding all incremental number of cycles calculated by Paris' law, considering the stored values of crack length, K_I and K_{II}.

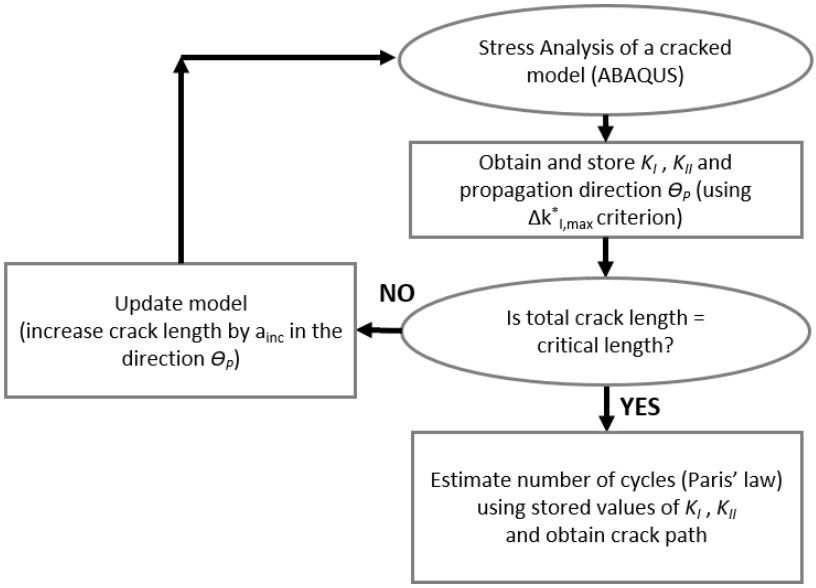

Figure 4.23: Flow chart of the methodology adopted in this study

4.2.3 Life estimates and crack path prediction

The stress intensity factors K_I and K_{II} were recorded at the loading steps 2 and 3 (at maximum and minimum fatigue load, respectively) and they were expanded in k_I^* and k_{II}^* as function of θ. Figure 4.24 shows the variation of these expanded factors for the model with an initial crack for test configuration FF4. It can be seen that $\Delta k^*_{I,max}$

criterion predicts an propagation angle θ_P approximately equal to $22°$, a direction slightly inwards the contact between pad and specimen, which is in good agreement with experimental observation. However, MTS criterion ($k^*_{I,max}$) predicts an incorrect higher angle of around $50°$, that is somewhat outwards the contact. It is interesting to notice that, to obtain the propagation direction through MTS criterion, it is only necessary to consider the maximum loading condition, disregarding the impact that the rest of the fatigue cycle might have on the problem. For proportional loading conditions, the analysis of the whole cycle leads to the same results as the analysis at maximum load. However, this is not the case for fretting fatigue and, to correctly predict the propagation direction, it is essential to consider the whole loading cycle.

Figure 4.25 shows the comparison between the experimental path and the predicted propagation path after 20 crack length increments for test configuration FF1. It can be seen that the propagation path obtained by the $\Delta k^*_{I,max}$ criterion using conventional FEA and taking into account crack face interactions is in good agreement with the experimental observations. The predicted crack evolves under the mixed-mode condition, growing inwards the contact region, up to a depth of around $1\ \mathrm{mm}$ (about two times the Hertzian semi-contact width a_{cont}) and then it propagates in a direction approximately perpendicular to the axial stress. This propagation behaviour has also been observed for the other loading cases (FF2-FF9) analysed. In addition, this path characteristic is in agreement with experimental observations. Figure 4.25 [1] also presents the prediction using MTS criterion with a propa-

[1] Reprinted from Tribology International, Vol 76, Hojjati-Talemi, R., Wahab, M. A.,

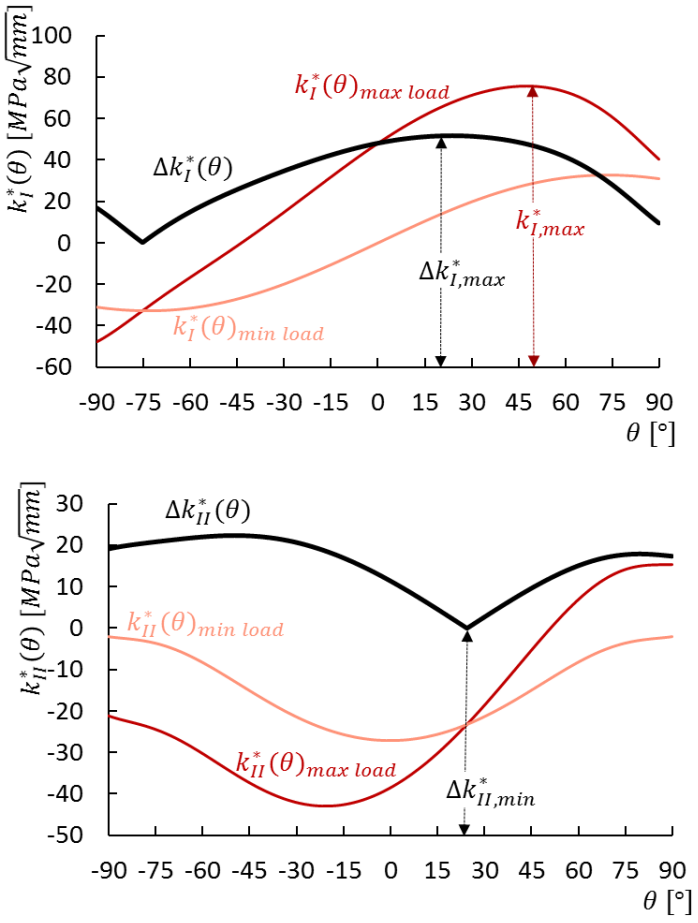

Figure 4.24: Predicted angle for initial propagation increment of test FF4 (crack length of 50 μm oriented at $\beta = 40°$ at near the edge of the contact between pad and specimen)

gation path that advances outwards the contact region, contradicting experimental data. Thus, this criterion is not recommended for fretting conditions with cylindrical pad configuration.

Mode mixity and stress intensity factors as function of time along

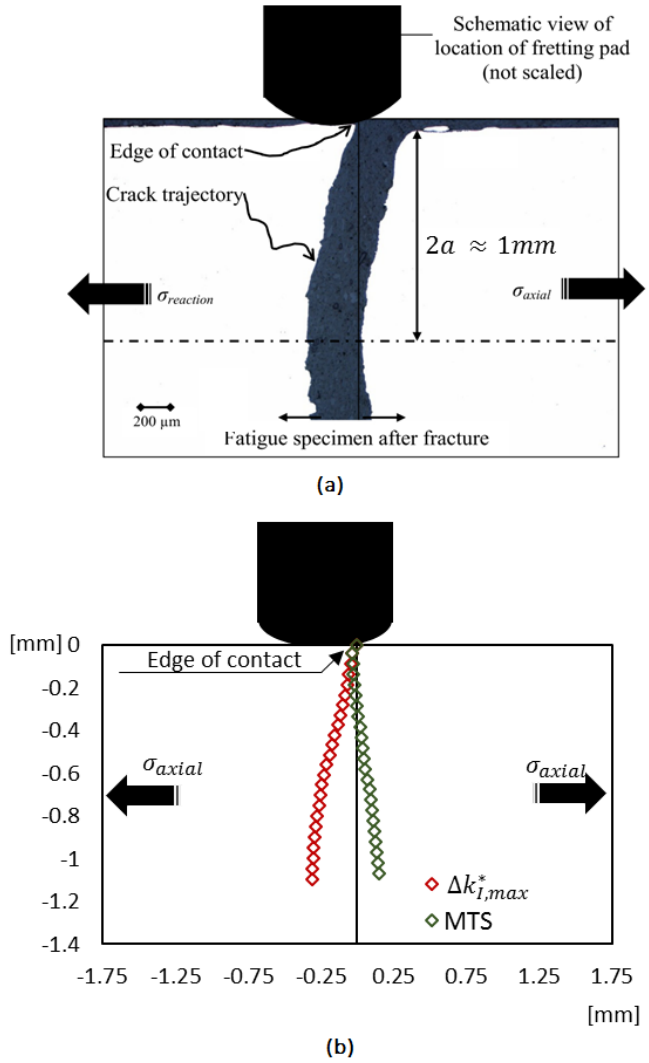

Figure 4.25: Propagation path for test FF1: (a) experimental observation , data from (R. Hojjati-Talemi et al., 2014); (b) Predicted path considering MTS and $\Delta k^*_{I,max}$ criteria

the loading cycle are shown in Figure 4.26, for test FF4 at different crack growth increments. After 1 crack length increment, it is noticeable that the mode-mixity ratio is greater than one during more than half of the loading cycle, indicating that Mode-II plays an important

role at the beginning of crack propagation. It is also clear that during the initial step of crack propagation, the crack faces are in contact for approximately half of the loading cycle ($K_I = 0$ at this condition). This is explained by the fact that, at this stage, the stress state around the crack is largely influenced by the contact between the pad and specimen, promoting crack face interaction. As the crack evolves, this impact is reduced and the crack growth is mainly promoted by the axial stresses. After 25 crack length increments, the values of mode mixity are lower than one during almost the entire loading cycle, indicating a predominant Mode-I growth. Also, it is interesting to notice that, at this stage, there is no crack faces interaction, as K_I is greater than zero during the whole cycle.

The results presented above have been obtained assuming the coefficient of friction (CoF) between crack faces is 0.8. However, to study the influence of the CoF at crack faces on the predictions, an analysis considering a much smaller value of $CoF = 0.2$ at crack faces was also performed. As it can be seen in Figure 4.27, the CoF at crack faces does not have a significant influence on the predicted paths. As expected, as the coefficient of friction between the crack faces is reduced, the influence of Mode-II on the path is also reduced and the propagation gets closer to a vertical path (pure Mode-I growth). Although we can observe this tendency on the paths, the impact of CoFs on them is still very minor, with the maximum difference in x coordinates between both paths being smaller than 5% of the heztian semi-contact with ($\Delta x_{max}/a_{cont} = 0.048$). This is because the presence of kinks along the crack faces avoids any sliding and reduces the contact between the faces. Similarly to what is discussed in Giner et al. (2014), this numer-

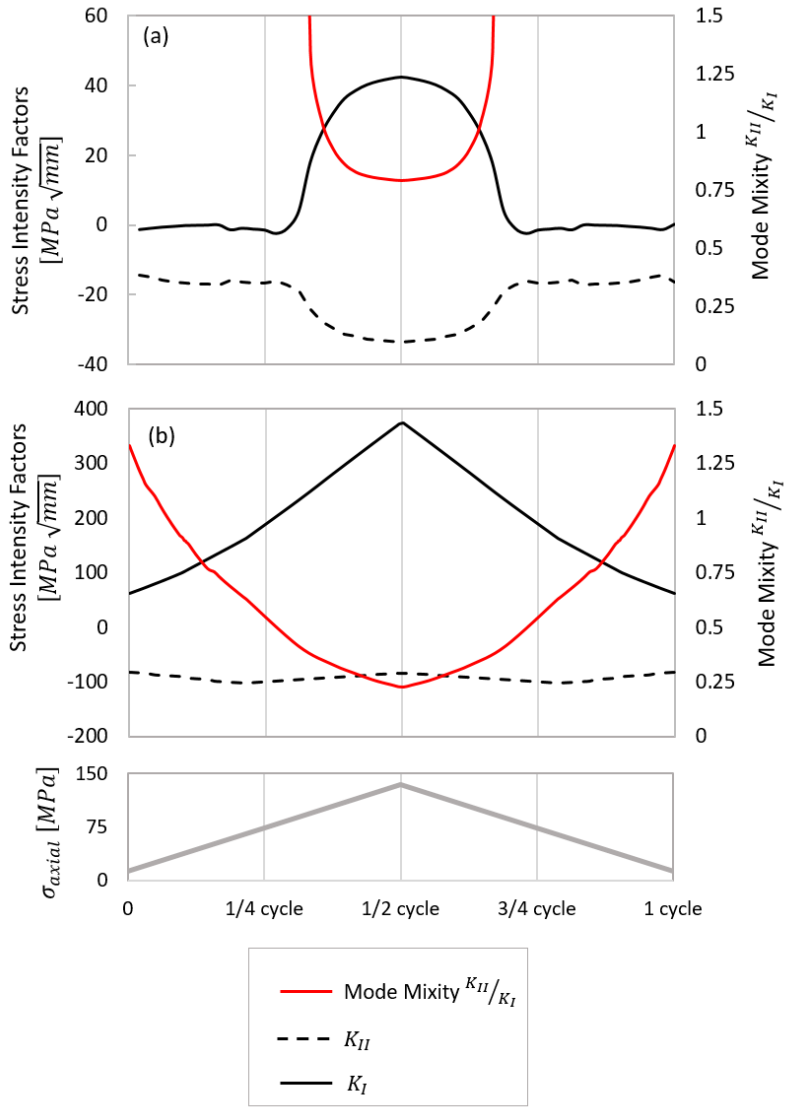

Figure 4.26: Evolution of mode mixity as function of time along the loading cycle, for test FF4: (a) after 1 crack length increment and (b) after 25 crack length increments

ical effect is believed to represent the restriction in movement caused by asperities and irregularities along the crack faces.

For all experimental tests, modelled in this study, the ratio between

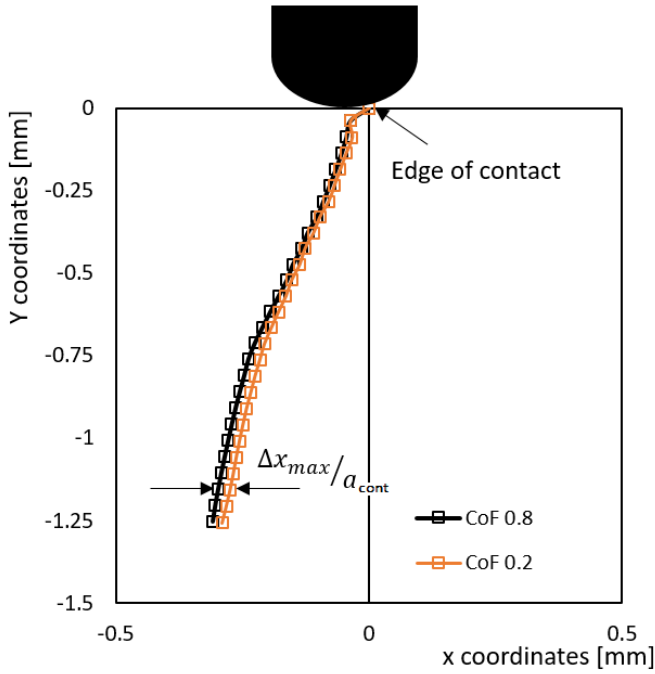

Figure 4.27: Crack propagation path for different CoF at crack faces for test FF1

stick and slip zone was about 0.8 to 0.9, creating a high stress gradient at the edge of the contact. The presence of crack greatly affects these stresses and the relative movement in the slip zones. This effect has been accounted for in our simulations and, as an illustrative example, the slip amplitude is plotted as function of the normalized contact width for test case FF2 under different crack length increments. As it can be seen in Figure 4.28, as the crack grows, the relative movement in the left side of the crack is reduced. As discussed in Giner et al. (2009), this is explained by the fact that, as the crack grows, it becomes difficult to transmit the bulk stresses to this region, due to the loss of stiffness caused by the presence of the crack.

The propagation life was estimated by inserting an initial crack near

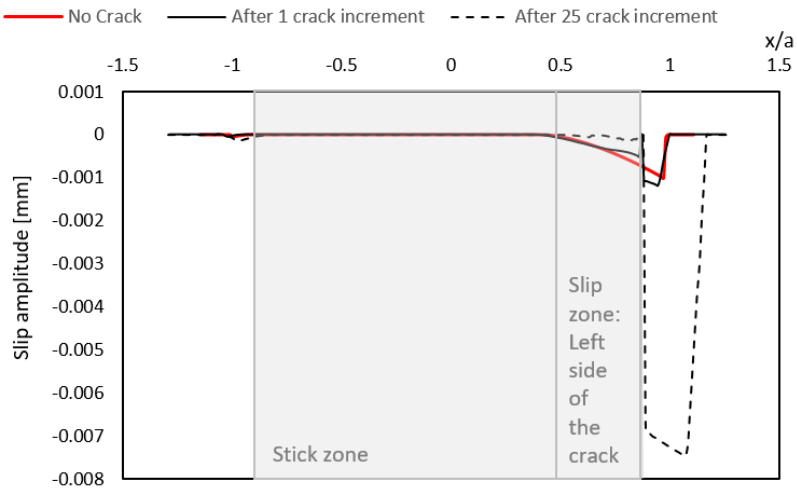

Figure 4.28: Slip distribution at contact interface as function of normalized distance x/a for different crack length increments

the contact edge and propagating it considering the $\Delta k^*_{I,max}$ criterion, as discussed above. Figure 4.29 shows the ratio between predicted propagation life and total experimental life for different test conditions. About 40% to 50% of the total life was spent in the crack propagation, illustrating the necessity of correctly predicting this phase in order to obtain a precise estimation of the total life.

Combining the initiation life (Hojjati-Talemi et al., 2014) and propagation life, the total life can be estimated. As shown in Figure 4.30, the predictions are in good agreement with observed experimental lives, being distributed around the centre line and being inside a band of $\pm 50\%$. These estimates indicated that a correct modelling of the propagation phase, considering crack face contact and using an orientation criterion that accounts for non-proportional loading, leads to, not only accurately estimation of crack path, but also decent life prediction.

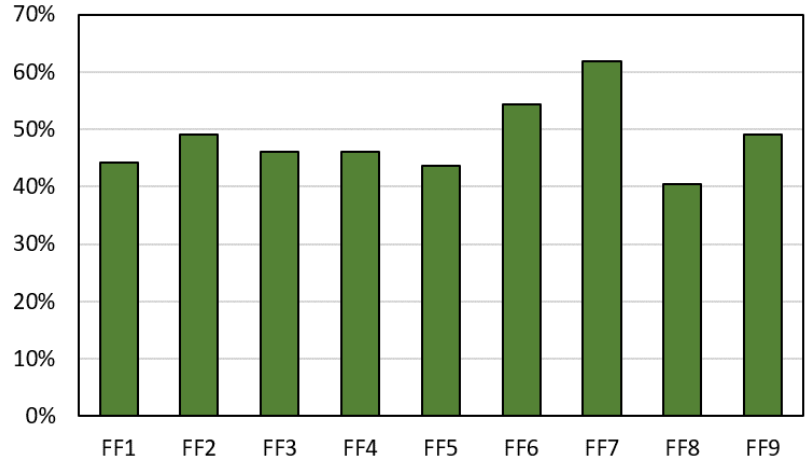

Figure 4.29: Percentage of life spent in propagation ($N_p/N_{f,experimental}$)

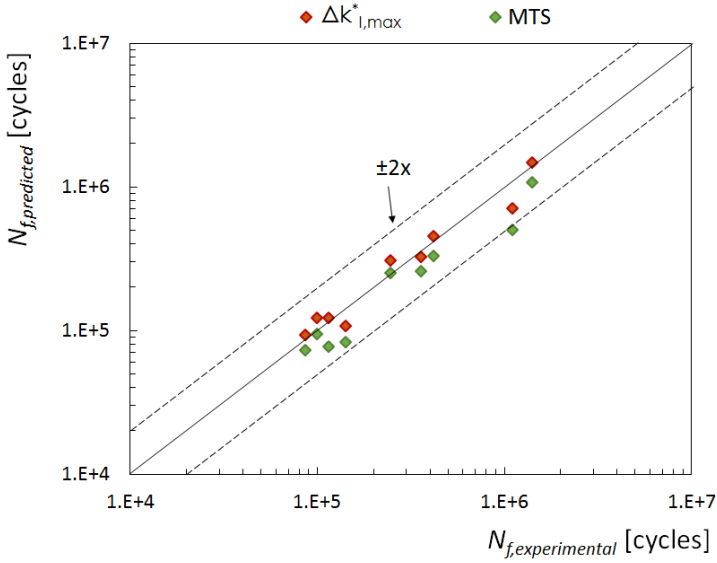

Figure 4.30: Predicted fretting fatigue total lifetime versus experimental data from the literature (Hojjati-Talemi et al., 2014)

4.2.4 Effect of short crack behaviour

Even though the results obtained in Section 4.2.3 are reasonable predictions of fretting fatigue lives, their estimates rely on a Paris crack growth law for long cracks. According to the literature (Krupp, 2007), the transition from short to long crack behaviour happens when the crack length is greater than a few grain diameters. However, for the material considered here, the grain size is considerably large and around 252 ± 118 μm (De Pauw, 2016), which invalidates the analysis assumption of long crack behaviour.

The aim of this section is to study and analyse the effect of short crack behaviour on the estimates of fretting fatigue crack propagation lives for cylindrical pad configuration. The total life, up to complete failure $N_{f,predicted}$, is computed by adding the initiation life of a crack of length 50 μm with the propagation life from this initial crack until final rupture of the specimen. For initiation life, as discussed before, we will use the predictions from Hojjati-Talemi et al. (2014), which use continuum damage mechanics.

The propagation life was predicted using a Fracture Mechanics approach, integrating a fatigue crack growth law with adjustment for short crack growth behaviour. The results in Section 4.2.3 were computed considering a simple Paris' law crack growth model (Equation 4.2). As discussed by Navarro et al. (2006), this is a simplified approach that does not take into consideration the short crack behaviour nor the crack growth threshold. In order to account for both, the model proposed by Navarro et al. (2006) will be used and will be named here as

"Paris' Law with adjustment for short cracks". It represents the fact that the fatigue threshold for short cracks is lower than for long cracks and can be written as:

$$N_P = \int_{a_i}^{a_f} \frac{da}{C\left(\Delta K_{eff}^n - \left(\Delta K_{th}\sqrt{\frac{a}{a+a_0}}\right)^n\right)} \tag{4.4}$$

where ΔK_{th} is the fatigue crack threshold, a is the crack length and a_0 is the El Haddad's parameter, given by:

$$a_0 = \frac{1}{\pi}\left(\frac{\Delta K_{eff}}{\sigma_f}\right)^2$$

and σ_f is the plain fatigue limit of the material.

For our analysis, we assumed a mixed-mode condition and we considered that the effective stress intensity factor range ΔK_{eff} is given by equation (4.3)

The total life was obtained by adding the initiation life and propagation life. As shown in Figure 4.31, the predictions for both cases (with and without short crack adjustment) are in agreement with experimental data. The predicted values well distributed around the centre line and within a band of $\pm 50\%$ of the experimental ones.

Based on the results presented in Figure 4.31, it can be observed that although the simple Paris growth law does not model the effect of short cracks, it still provides good predictions. Navarro et al. (2006) explains this behaviour as follows. It is known that for high stresses (in our case, tests FF3 to FF9), the crack growth rate for short cracks is much higher than for long cracks with the same stress intensity factor.

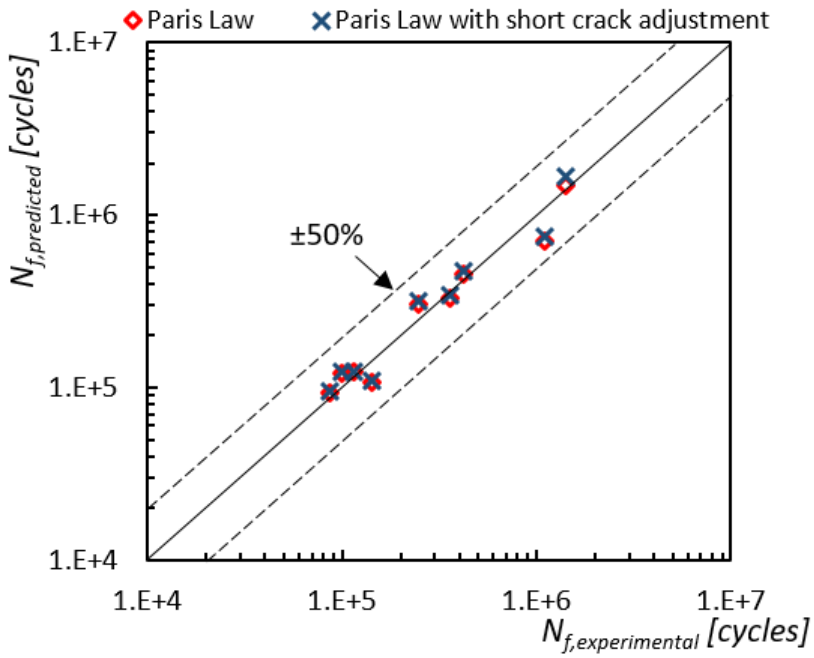

Figure 4.31: Total lifetime: prediction versus experimental data (Hojjati-Talemi et al., 2014), for crack growth laws with and without adjustment for short cracks

In this way, Paris law without short crack adjustment would provide a better estimative of the reality. However, for longer lives (tests FF1 and FF2), the short crack growth rate may reduce as crack grows and an adjustment may impact the results. Figure 4.32 shows the difference in propagation life predictions of both models and exemplify the discussion above.

In order to compare the accuracy of both life prediction techniques (with and without adjustment for short crack behaviour), the statistical method described in (Bhatti and Wahab, 2017a) and Navarro et al. (2008) is considered here. The normalized mean $\bar{x}$ and the normalized standard deviation SD_x were computed considering the experimental

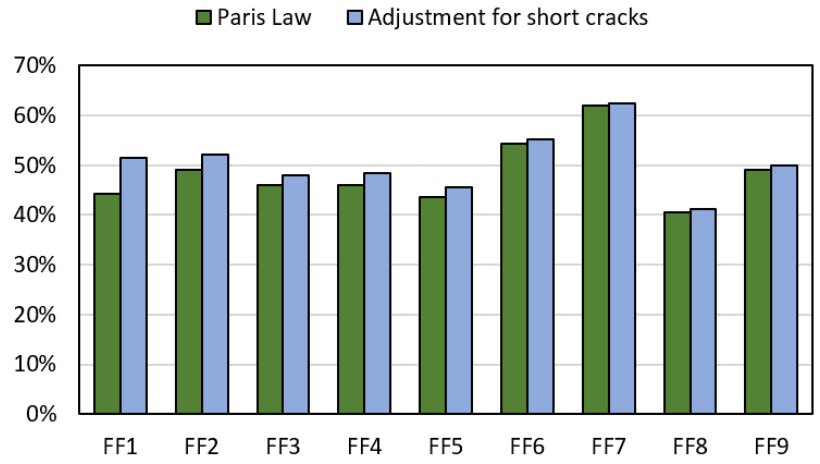

Figure 4.32: Percentage of propagation life ($N_p/N_{f,experimental}$), for both crack growth laws.

lifetime $N^i_{f,experimental}$ and the predicted one $N^i_{f,predicted}$ for each test case i. The are computed by the following equations:

$$\alpha_i = \log \frac{N^i_{f,predicted}}{N^i_{f,experimental}} \tag{4.5}$$

$$\bar{\alpha} = \frac{1}{n}\sum_{i=1}^{n} \alpha_i \tag{4.6}$$

$$SD_\alpha = \sqrt{\frac{1}{n-1}\sum_{i=1}^{n} (\alpha_i - \bar{\alpha})^2} \tag{4.7}$$

$$\bar{x} = 10^{\bar{\alpha}} \tag{4.8}$$

$$SD_x = 10^{SD_\alpha} \tag{4.9}$$

Table 4.4: Comparison of accuracy of both life predictions

Model	$\bar{x}$	SD_x
Paris Law	0.985	1.246
Adjustment for short crack behaviour	1.027	1.249

where n is the total number of test configurations. The normalized mean $\bar{x}$ and the normalized standard deviation SD_x are used as measurements to access how far the predicted results are with respect to the experimental ones. The closer to 1 those normalized values are, the better is the prediction. A comparison between both propagation laws used in this study is shown in Table 4.4. The results are very similar to each other, with the average predictions considering short crack behaviour being slightly higher than the ones without adjustment.

Although the results may imply that the effect of microstructure on the fretting fatigue predictions is small, this may not be the general conclusion. It is important to note that we only analysed the impact of short cracks on the crack growth law and some important phenomena have been ignored. For instance, those models do not take into consideration that the size of grains, their orientation and boundaries may influence the crack behaviour. In addition, the anisotropic elastic behaviour inside grain in metal alloy can affect the short crack propagation phase.

4.2.5 Computational cost

The complete analysis of crack propagation using LEFM and the extended MTS orientation criterion ($\Delta k^*_{I,max}$) takes around few hours

running in three cores, using the following processor: Intel Core i7-5600U CPU @ 2.60GHz with 16GB of memory RAM. For instance, for test case FF9, the total analysis would take 4 hours and 52 minutes in CPU time.

4.3 Conclusions

In this study, we predicted crack propagation paths for fretting fatigue specimen in contact with cylindrical pad. It is known that under this conditions, traditional LEFM orientation criteria are not valid. Thus, to obtain good predictions, the $\Delta k^*_{I,max}$ criterion was used.

For all tests considered here, the axial loading is not fully reversed. The low axial load ratio ($R = 0.1$) associated with the high stresses caused by the contact between pad and specimen is sufficient to cause crack faces to interact with each other. This interaction is of great importance at the initial stage of propagation where a Mode-II plays an important role. Therefore, a proper modelling of the contact between them is essential to predict the crack propagation path and accurately estimate the propagation life.

The path propagation predictions considered here have been performed numerically using conventional FEM including a formulation that allows for crack face contact. The numerical results are in good agreement with the experimental observations, indicating the importance of choosing an appropriate orientation criteria and considering possible crack face interactions.

5

Monotonic Cohesive Zone Model

As discussed in Chapter 4, finite element methods combined with linear elastic fracture mechanics can predict the life of components

under fretting conditions with reasonable accuracy. However, they require assumptions and simplifications that may no longer be plausible for cases where there is considerable amount of fretting. For instance, as there may be high stresses at contact interface, plasticity around the crack tip could play a significant role and linear elastic fracture mechanics theory may no longer be valid. Moreover, life estimates often rely heavily on empirical models for the crack growth law, which may not be adequate for non-proportional loading conditions, a common characteristic of fretting fatigue problems. A more robust alternative that does not rely on the assumptions above is to consider failure using cohesive zone model (CZM)

In this chapter, we focus on the crack initiation phase. At this stage, it is important to correctly predict the crack initiation location and orientation, which is often achieved by using critical plane approaches. The use of CZM as an alternative approach to accurately estimate those parameters is investigated in this chapter. CZM as well as two of its common initiation criteria, namely quadratic traction-separation criterion and maximum nominal stress criterion, are used to study crack initiation location and orientation under fretting conditions. Our results are compared with the traditional critical plane approaches and with experimental data.

The use of cohesive zones to simulate fretting phenomenon has been restricted to only few papers in the literature (Zhang et al., 2016, 2015; Kim and Yoon, 2014), discussed in detail in Section 2.4.5. To the best of our knowledge, the work presented in this thesis is the first attempt in the literature to accurately predict crack propagation

paths and estimate total fretting fatigue failure lives using cohesive zone models. The present chapter deals with the use of a CZM (bilinear traction-separation law) to predict crack initiation location and orientation. We consider two fretting experimental configurations, with flat and cylindrical pads. Here, only the initiation point of the cohesive zone is considered and the accumulation of damage during loading/unloading in a fatigue cycle is ignored. This assumption simplifies the analysis, but at the expense of inhibiting the application of CZM for life predictions. This prediction would require a cycle-by-cycle analysis, with or without a time acceleration procedure, in conjunction with a damage evolution law. This will be the focus of the next chapter.

This chapter is divided in the following sections. Firstly, a brief description of the implementation and modelling of cohesive zone damage initiation is done. In order to verify the accuracy of the results obtained using CZM, they are compared to traditional critical plane approaches. Two classical critical plane damage parameters have been used in this comparison: the Findley (FP) and Fatemi-Socie (FS) parameters. Details of the implementation required to compute those parameters is presented followed by details of the FE models used in this study and a discussion of the main results.

5.1 Initiation criteria

CZM is an alternative methodology to assess damage and failure of materials with or without cracks. In comparison with LEFM, cohesive zone models eliminate the stress singularity at crack tip and

account for non-linear material behaviour at this region. When compared with continuum damage mechanics, CZM may be understood as a damage model that considers failure only by the material separation and not by its deformation (Kuna and Roth, 2015). CZMs were developed back in the 60's with the introduction of Dugdale's strip model (Dugdale, 1960). Over the last 40 years, many models have been proposed for different materials and analysis. Brocks et al. (2003) presented a detailed literature review on the topic, discussing the most common models and presenting different applications for CZMs. Park and Paulino (2011) published another literature review, focusing on a critical discussion of the different models and their applicability.

As discussed by Kuna and Roth (2015), CZM was developed to replicate the fracture process in front of a crack tip and its basic idea is to describe the entire fracture process in a thin cohesive region. The material behaviour inside this region follows a local law, based on the traction and separations at the cohesive zone surfaces. This constitutive law creates a more realistic description of the stress at crack tip, removing the stress singularity from LEFM (Roth et al., 2014). Figure 5.1(a) shows a representation of CZM. It can be seen that damage starts once the tractions reach a cohesive strength parameter (T_{max}) or separation reaches δ_0. This defines two regimes characteristic of cohesive models: a reversible state from which there is no damage accumulated and a softening region, where the local material cohesive strength is reduced. Complete failure happens when cohesive strength reduces to zero or once separation reaches a critical value δ_f. Note that, as elucidated by Roth et al. (2014), to model failure using CZM, there is no necessity to have a predefined crack in the model. CZM allows a

unique way to model crack initiation, propagation and final failure.

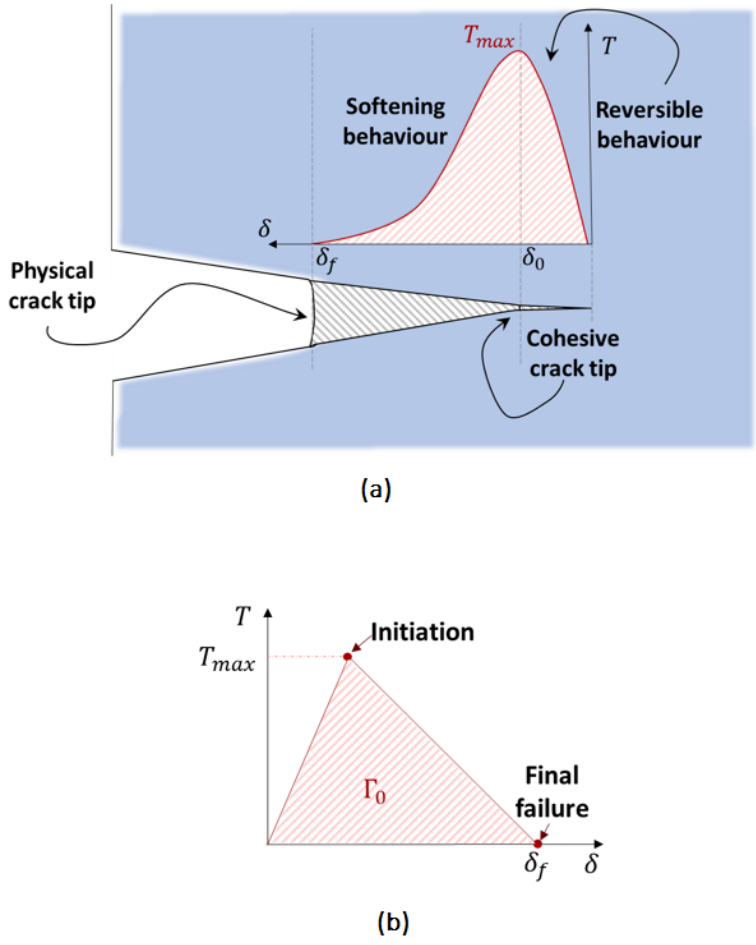

Figure 5.1: Cohesive zone model: (a) representation of its use for modelling of fracture; (b) bilinear model

Even though the cohesive strength T_{max}, the critical separation δ_f and, therefore, the area under the traction-separation law (fracture energy G) are material dependent, the shape of the traction-separation constitutive law is independent on the material. As discussed in Brocks et al. (2003), this is explained by the fact that cohesive model is a phe-

nomenological approach and, as a consequence, there is no physical evidence on which form of distribution the cohesive law should take. Many different shapes have been proposed in the literature. For instance: polynomial function (Tvergaard, 1990), exponential (Needleman, 1990), bilinear function (Geubelle and Baylor, 1998), among others. For simplicity, in this thesis, a bilinear traction-separation law is adopted and it is represented in Figure 5.1(b). The initial material response is presumed to be linear until a damage initiation criterion (initiation point) is fulfilled. After that, degradation of the material starts and damage follows a linear softening evolution law until complete failure.

The CZM was incorporated in our simulations of fretting phenomenon by using ABAQUS XFEM with cohesive segments module, as presented in Figure 5.2. Initially, a stress analysis of the undamaged material, subjected to some load and boundary conditions, is performed. The stress/strain obtained at the centroid of the XFEM elements, at each loading increment, is then used to compute a damage function. Once this damage function reaches a value of one (within some tolerance), a crack is introduced in the model, crossing one entire element. The tolerance is a parameter defined by the user. The smaller the tolerance the higher the computational cost. In our simulations, we have used the default value in Abaqus, which is ± 0.05. To check the impact of this tolerance on the results, we have also done the same analysis with a smaller tolerance of ± 0.025 and have obtained the same crack initiation locations and orientation.

The cohesive tractions and separations at the crack faces are used

to model the degradation and eventual failure of the enriched element. The initial crack location and direction can be directly formulated by the user, considering a user defined initiation criterion, programmed by the UDMGINI subroutine in ABAQUS. For further details, the reader is referred to the ABAQUS documentation Version (2013).

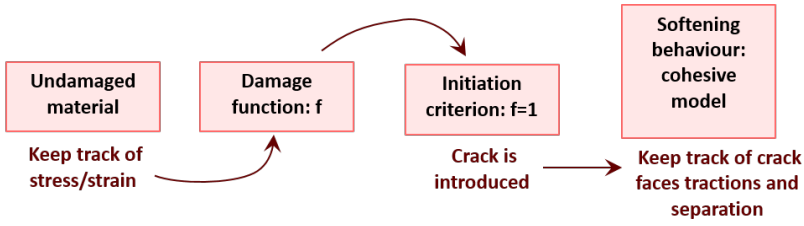

Figure 5.2: Behaviour of the XFEM with cohesive segments model in ABAQUS

The crack initiation is assumed to happen at the start of the degradation of the cohesive response of the enriched element. This process of degradation starts when the stresses and strains in the material meet a specified initiation criterion. This criterion can be written as a normalized function of the stresses and strains, with respect to the critical cohesive strength of the material (T_{max}). We denoted it as "damage initiation criterion". A crack initiates in the model when this damage criterion reaches a value of 1 with some tolerance.

For mixed mode conditions, as in the fretting fatigue case, the critical cohesive strength of the material T_{max} can be expressed as two material properties: the cohesive strength of the material under mode I condition ($t_{n,c}$) and the tangential cohesive strength of the material under pure mode II condition ($t_{s,c}$). Their values can be estimated based on laboratory tests using fracture specimens for each failure mode (I or

II) individually and correlating the fracture toughness, area under the graph Γ_0 in the traction-separation curve, and the critical separation δ_f.

A reasonable estimate of $t_{n,c}$ and $t_{s,c}$ depends on the fracture mechanism. For instance, it is known that the fracture of brittle materials involves very little plasticity. Therefore, a reasonable assumption would be that $t_{n,c}$ is roughly one order of magnitude of the Young's Modulus of the material (Mei et al., 2010). For ductile materials, such as aluminium alloys, the fracture process involves large plasticity, being characterized by the nucleation, growth and coalescence of voids ahead of crack tip. For this case, $t_{n,c}$ may be approximately equal or of the same order of magnitude of the ultimate strength of the material (Kim and Yoon, 2014; De-Andrés et al., 1999). Regarding the tangential cohesive strength of the material under pure mode II condition ($t_{s,c}$), for ductile materials, its value can be approximated considering the Tresca criterion as $t_{s,c} = 0.5t_{n,c}$, as described in Xu and Yuan (2009a). Considering this reasoning, $t_{n,c}$ was assumed equal to the ultimate tensile stress σ_u and $t_{s,c} = 0.5\sigma_u$.

As mixed mode condition is an important feature of fretting fatigue failure, it is expected that a combination of normal and shear tractions may impact the crack initiation orientation and location. Thus, two stress-based damage initiation criteria commonly used for the cohesive model (Lopresto et al., 2017) are considered: the quadratic traction-separation and the maximum nominal stress criteria. These criteria have been previously applied in fatigue and delamination problems (Mei et al., 2010; Kim et al., 2011; Xu and Yuan, 2009b).

As discussed by Mei et al. (2010), under mixed mode conditions, an approach to account for the effect of mode mixity is to consider the initiation criterion as a quadratic combination of normal and shear tractions. The quadratic traction-separation criterion, herein defined by the damage variable f_1, reflects a quadratic ratio between the maximum values in time of the normal tractions $t_{n,\theta}$ and tangential tractions $t_{s,\theta}$ acting in a potential crack plane oriented at an angle θ (see Figure 5.3). This damage variable can be written as:

$$f_1 = \sqrt{\left\{\frac{\langle t_{n,\theta}\rangle}{t_{n,c}}\right\}^2 + \left\{\frac{\langle t_{s,\theta}\rangle}{t_{s,c}}\right\}^2} \tag{5.1}$$

where, $t_{n,c}$ is the cohesive strength of the material under mode I condition and $t_{s,c}$ is the tangential cohesive strength of the material under pure mode II condition. Here, it is assumed that compressive tractions do not promote damage, therefore, $\langle t_{n,\theta}\rangle = t_{n,\theta}$ if $t_{n,\theta} > 0$ and $\langle t_{n,\theta}\rangle = 0$ otherwise.

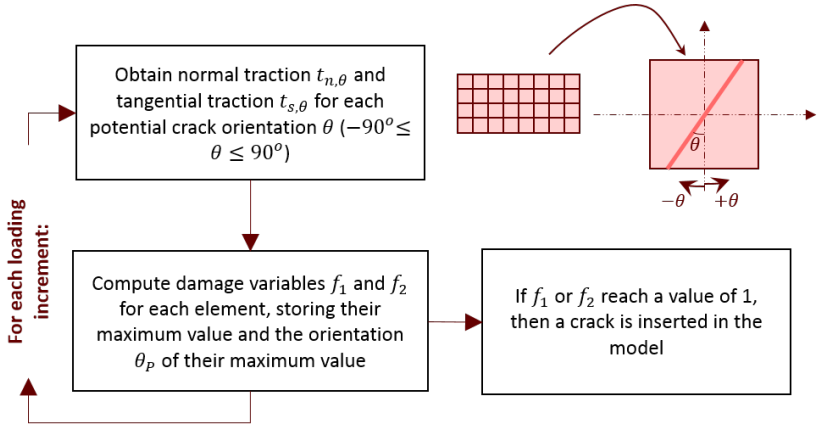

Figure 5.3: Scheme of the UDMGINI subroutine for the two implemented damage criteria for a single element

In contrast, the maximum nominal stress criterion does not con-

sider any interaction between normal and tangential tractions. Here, this damage initiation criterion is represented by the variable f_2 and can be obtained by:

$$f_2 = \max\left\{\frac{\langle t_{n,\theta}\rangle}{t_{n,c}}, \frac{\langle t_{s,\theta}\rangle}{t_{s,c}}\right\}. \tag{5.2}$$

The implementation of these two criteria was done using the user defined subroutine UDMGINI in ABAQUS. This subroutine allows the user to define not only the damage criteria, but also the crack initiation orientation. Figure 5.3 shows a scheme of the subroutine used in this study. Firstly, for each loading increment, the normal traction $t_{n,\theta}$ and tangential traction $t_{s,\theta}$ as function of the potential crack orientation θ are obtained based on the stresses at the centroid of each element. These tractions are later used to compute the damage variables f_1 and f_2 for each element as function of the angle θ. This process is repeated for all loading increments in one fretting cycle. The element in which the global maximum value of damage parameters is obtained defines the critical location for crack initiation. The angle θ_P, at which the damage is maximized, is selected as the potential crack initiation orientation.

5.2 Fretting fatigue initiation model

For this study, FE models were created in ABAQUS representing the laboratory test set-up for fretting fatigue. The models consisted of two parts: a pad and a specimen. Two pad configurations were consid-

ered, a flat indenter and a cylindrical one. Both models, with flat and cylindrical pads, replicate only half of the experimental set-up, due to symmetry of the test. This symmetry was modelled by the restriction of the vertical movement in the y direction and rotation around the z-axis at the bottom surface of the specimen. In order to avoid rigid body movement of the pads, the displacement in x direction at both sides of them were also restrained. Details of the boundary conditions are depicted in Figures 5.4 and 5.5.

The master-slave algorithm with surface to surface interaction and finite sliding was used for modelling the contact between pad and specimen. The tangential behaviour was modelled using a Lagrange multiplier formulation and the normal behaviour by a hard contact. The coefficient of friction between the cylindrical pad and specimen was kept constant and equal to 0.65, as per experimental data from Hojjati-Talemi et al. (2014), and for the case of flat indenter it was kept equal to 0.8, measured in Sabsabi et al. (2011).

For both types of pads, the specimen is subject to an oscillatory axial stress σ_{axial} and the pads are subjected to normal contact load F. The only difference between these pad configurations, in terms of loading, is the presence of compliance springs (for the case of cylindrical pads) that generates an oscillatory tangential load Q, as discussed below. The cyclic loads are applied in three steps aiming to simulate a complete fretting fatigue cycle. The normal load F is applied at the top pad in the first step and this loading condition is kept constant until the end of the fretting cycle. Then, the cyclic axial load is applied to the sides of the specimen in two steps, i.e. the maximum axial load

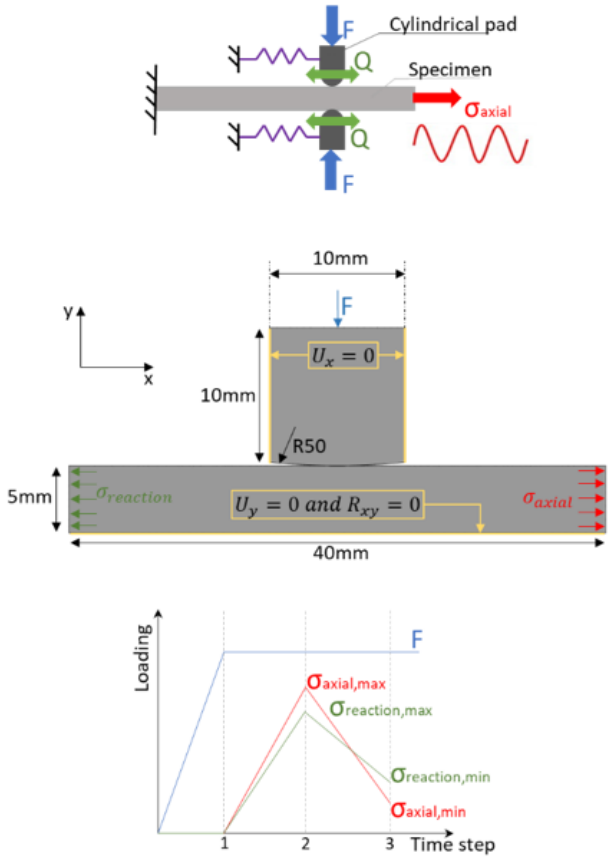

Figure 5.4: Model details for the cylindrical pad configuration: dimensions, boundary conditions, loading history

followed by the minimum one, as illustrated in Figures 5.4 and 5.5.

The cylindrical pads are secured during experiment through compliance springs that generate an oscillatory tangential load Q at the interface between pad and specimen. Its effect was considered as a cyclic reaction stress $\sigma_{reaction}$, as in Hojjati Talemi (2014).

The analyses were done considering a linear elastic material re-

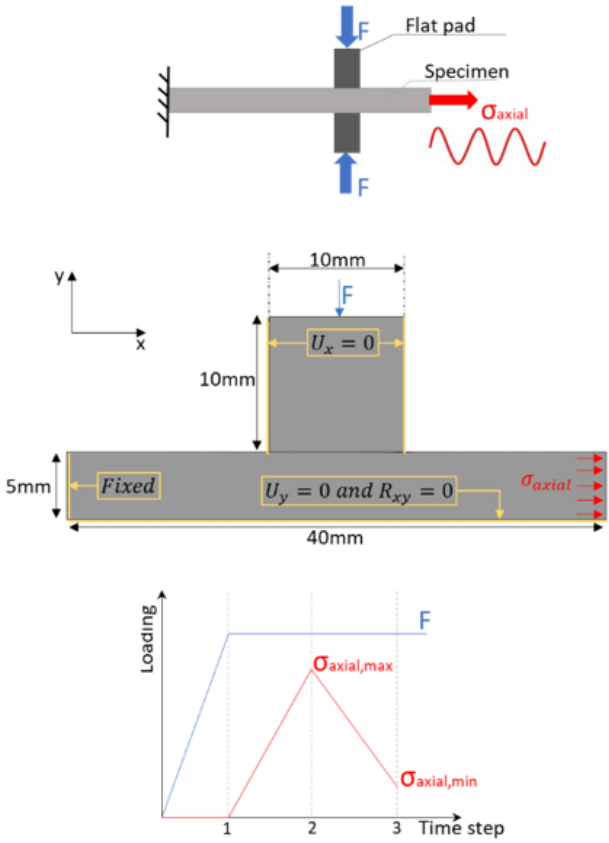

Figure 5.5: Model details for the flat pad configuration: dimensions, boundary conditions, loading history

sponse. For the flat indenter, loading conditions and material properties (aluminium 7075-T6) are the same as in the experiments conducted by Sabsabi et al. (2011). The tests were performed in a stress ratio of -1.0 for the axial load σ_{axial}. For the cylindrical pad, they replicate tests from Hojjati-Talemi et al. (2014), performed in samples from aluminium 2420-T3. During the experiments, a stress ratio of 0.1 for the axial load σ_{axial} and a -1.0 for the tangential load Q were adopted.

In both test configurations, pads and specimen are made of the

same material with the same properties. For the cohesive parameters, the cohesive strength of the material $t_{n,c}$ was assumed equal to the ultimate tensile stress σ_u, similarly to Kim and Yoon (2014).

Regarding the mesh, a 2D quadrilateral, 4-node (bilinear), plane strain, full integration element (CPE4) was used to discretize the model. For analysis considering the cohesive zone behaviour, a region of the model near the trailing edge has been meshed with a structured mesh of CPE4 enriched elements (XFEM with cohesive segments modelling). For this study, the contact interactions between crack faces are neglected as we are dealing with monotonic cohesive zone models that assume that the crack is opened during the whole fatigue cycle. Crack face interactions are indeed important and are considered in the cyclic cohesive zone model (presented in Chapter 6).

To guarantee that the model is able to correctly capture the stresses distributions at the contact between pad and specimen, a small element size at this interface (about 5 μm) was selected, based on previous convergence study detailed in Chapter 3. This element size was kept constant in the region modelled with enriched elements. The element size was then progressively increased far away from the contact and the XFEM region. Figures 5.6 and 5.7 show the mesh details for each of the models, with flat pad and cylindrical pad.

5.3 Critical plane approaches

According to critical plane approaches, the cracks nucleate and grow on specific planes, known as critical planes (Szolwinski and Far-

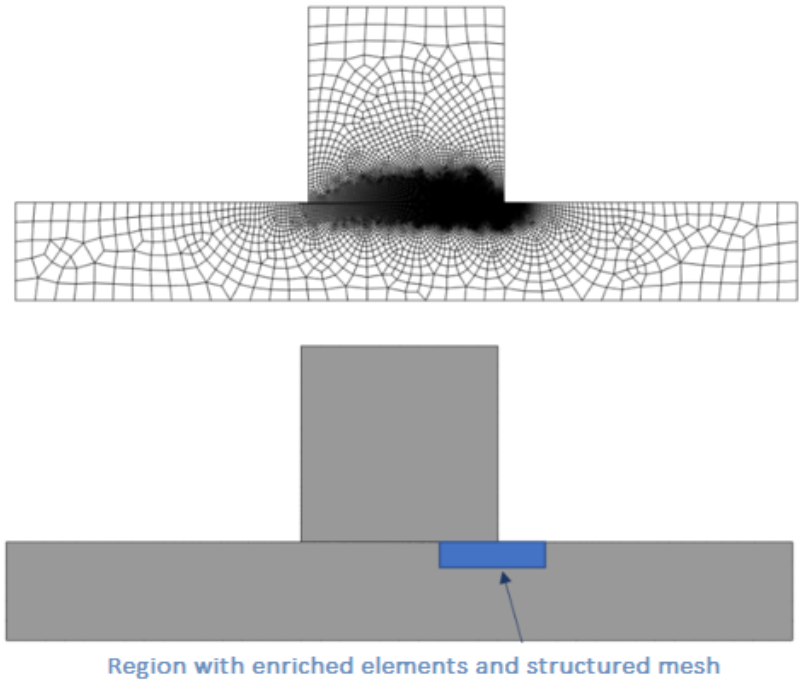

Figure 5.6: Mesh details of model with flat pad

ris, 1998; Lykins et al., 2001a; Araujo and Nowell, 2002; Bhatti and Wahab, 2017b; Bhatti et al., 2018). These planes are assumed to be maximum shear stress or strain planes, maximum tensile stress or strain planes or any combination of these, using influence factors. For our case, Findley (FP) and Fatemi-Socie (FS) parameters are employed to determine the crack initiation location and orientation. According to Findley parameter (FP), the crack initiates on a plane where the combination of maximum shear stress amplitude and maximum normal stress are maximum (Findley, 1959; Findley et al., 1956). This plane where the FP reaches its maximum value is denominated as critical

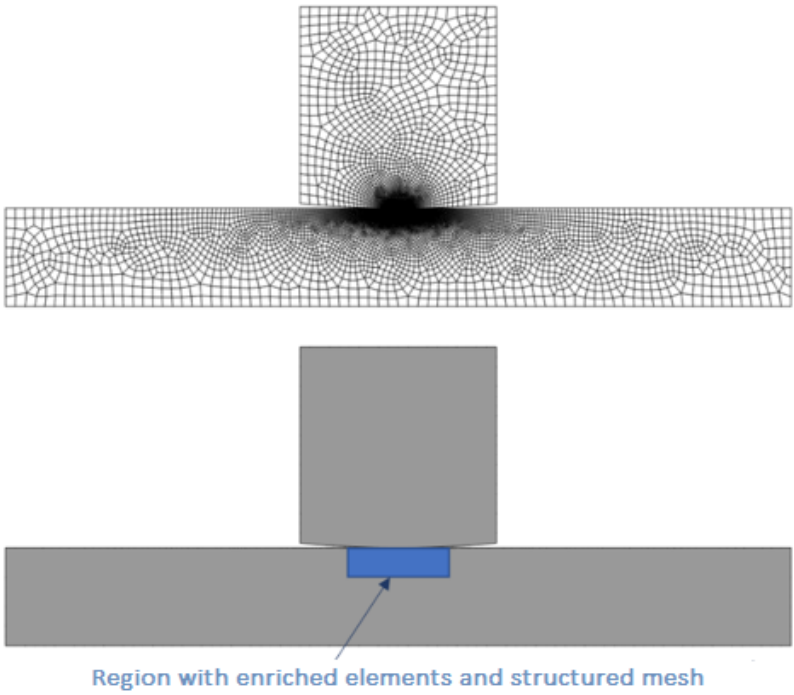

Figure 5.7: Mesh details of model with cylindrical pad

plane. Findley parameter is based on stresses and can be expressed as:

$$FP = \frac{\Delta\tau_{max}}{2} + k\sigma_n^{max}$$

where, ${}^{\Delta\tau_{max}}/_{2}$ and σ_n^{max} are the maximum shear stress amplitude and maximum normal stress on critical plane. The material constant k acts as an influence factor to the normal stress component. It can be determined using fatigue limits in tension and torsion of the material. Here, the value of k is determined as 0.16 using the experimental data from the literature (Fatemi et al., 2005; Sabsabi et al., 2011).

Fatemi and Socie performed multiaxial fatigue tests and proposed

a parameter that is suitable for material and loading conditions, which produce shear mode failure (Fatemi and Socie, 1988). They observed that, 90° phase difference induces additional cyclic hardening and can cause significant fatigue damage in low cycle fatigue. The parameter (FS) incorporates non-proportional loading and mean stress effects and is based on shear strain and normal stress. It can be written as

$$FS = \frac{\Delta\gamma_{max}}{2}\left(1 + k\frac{\sigma_n^{max}}{\sigma_y}\right)$$

where, ${}^{\Delta\gamma_{max}}/_{2}$ and σ_n^{max} are the maximum shear strain amplitude and maximum normal stress (in the plane of maximum shear strain range), respectively.

The FP and FS damage parameters include both shear and normal effects for crack initiation. The first part of these models incorporates shear effects, while the second includes normal effects with the application of influence factors. The influence factor determines the contribution of normal stress or strain in crack initiation and depends on material static and fatigue properties.

At first sight, the selection of FP and FS parameters may seem contradictory to the study and conclusions of Chapter 4, which indicated that minimum shear stress range orientation criterion should be used to predict fretting crack growth direction. However, in the present chapter we are interested in modelling crack initiation, and therefore, dealing with stage I cracks. As discussed in Section 2.4.1, empirical observation of stage I cracks showed a series of parallel ridges running in the direction of growth, indicating a shear mode propagation which is in line with the choice of parameters (FP and FS). In Chap-

ter 4, the main focus was the propagation of a long crack (hence the use of LEFM) and only stage II crack propagation has been considered. Experimental observations of stage II cracks shows that initially they grow under mixed-mode until crack reaches a depth large enough where the effect of contact stresses can be neglected and the direction of propagation becomes approximately perpendicular to the axial load. Therefore, under this condition of stage II crack growth, minimum shear stress range could be a good choice of orientation criterion. In summary, it is important to clarify that we are dealing with two different crack growth mechanisms: stage I growth, mainly dominated by shear stresses (present chapter), and stage II growth, mainly dominated by minimum shear stress range or, equivalently, maximum normal stress range (Chapter 4).

The results of the contact problem are used to compute damage parameters. The stresses and strains are stored for each load increment of the complete loading cycle. To find the highest value of the damage parameter and orientation of the critical plane, the stresses and strains are retrieved for the nodes at the contact interface from $-a$ to a, using a Matlab code. The code first reads the shear stresses and strains, for the node located at the contact edge ($x = -a$), at maximum and minimum load during the cycle. The normal stress is taken at maximum loading condition, as it gives maximum normal stress during the cycle. By applying Mohr's circle transformation, the stresses are evaluated at the rotated planes from $\theta = -90^\circ$ to 90° (using the same reference frame as shown in Figure 5.3) with increments of 1°. For each increment of plane, shear stress and strain range and normal stress are calculated to give a value of FS and FP parameters. For this node, values of com-

puted damage parameters are compared and the angle with the highest value of damage parameter is stored as local critical angle and local critical point. Using the same procedure, the local damage parameter is computed for all other nodes at the contact interface. Then all local damage parameters are compared to find the maximum value of the damage parameter. The corresponding node and angle are stored as damage initiation location and critical plane. For detailed description on determination of stress or strain ranges and flow chart, readers are referred to Bhatti and Wahab (2017a, 2018).

5.4 Verification of monotonic CZM

Generally, in fretting fatigue conditions, multiple cracks initiate at the contact interface. However, only one crack propagates to cause the failure. As discussed in the previous chapters, several researchers have found this location experimentally to be near the trailing edge of the contact.

For both flat and cylindrical pad cases, the damage initiation variables f_1 and f_2, computed via XFEM with cohesive zone models in junction with the UDMGINI subroutine, showed its maximum value near the trailing edge. Figure 5.8 shows the distribution of those damage parameters in the specimen, for the case of a flat indenter (test 1 of Sabsabi et al. (2011)). Both parameters had their maximum value in a very local region at approximately the trailing edge of the contact, due to the high stress concentration present in this configuration.

Although the maximum of both parameters is about at the same

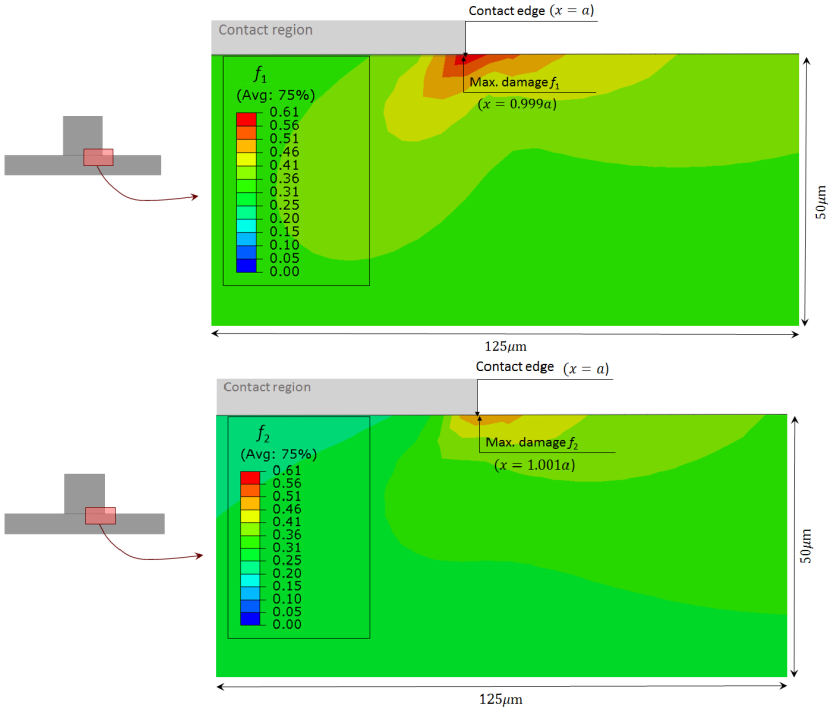

Figure 5.8: Damage initiation criteria distribution along the specimen, for test 1 of Sabsabi et al. (2011) (a) f_1 and (b) f_2 parameter.

location, their distribution with respect to the depth of the specimen is very different. For the damage initiation criterion f_1, this distribution of damage suggests that the most probable direction of crack growth is oblique and inwards the contact region, which is not the case for f_2. This difference can be justified by the influence of shear stresses in each of those parameters, as noted by equations 5.1 and 5.2. For the damage variable f_1, shear stresses play a significant role leading to a probable mixed mode condition for propagation, which is also verified in experimental tests (Szolwinski and Farris, 1998; Faanes, 1995; Navarro et al., 2006). Based on that, one may conclude that this damage variable f_1 captured better the behaviour of specimens under those

fretting conditions when compared with f_2. Therefore, the quadratic traction-separation criterion seems to be an appropriate choice of initiation criterion for fretting conditions.

Figure 5.9 shows the distribution of the damage variables for a cylindrical pad configuration. Those parameters are more smoothly distributed below the contact region, while for flat contacts, the damage is highly concentrated at the edge of the contact. This can be explained by the fact that, though there is a stress concentration on the cylindrical pad configuration, due to the geometry of the problem, it is not as significant as in the case of flat contacts. It is also important to notice that, also for the case of cylindrical pads, both parameters had their maximum value near the edge of the contact. Considering that the crack would initiate at the location of maximum damage, the results, for all tested cases with cylindrical pad (FF1 to FF9), showed initiation locations around 0.95 to 0.98 times the contact semi-width a, which is very close to the contact edge. Those predictions are in agreement with other numerical techniques, such as continuum damage mechanics (Hojjati-Talemi et al., 2014) and the experimental data mentioned above.

Regarding the crack initiation orientation, the values of the damage variables obtained in one fretting cycle are used. The element in the model with the highest damage parameters f_1 and f_2 over the loading cycle is selected and the variation of those values of damage f_1 and f_2 with the potential angle of propagation are used for the selection of the probable crack initiation orientation. Figure 5.11 shows the variation of f_1 and f_2 for the case of cylindrical pads, for test FF9.

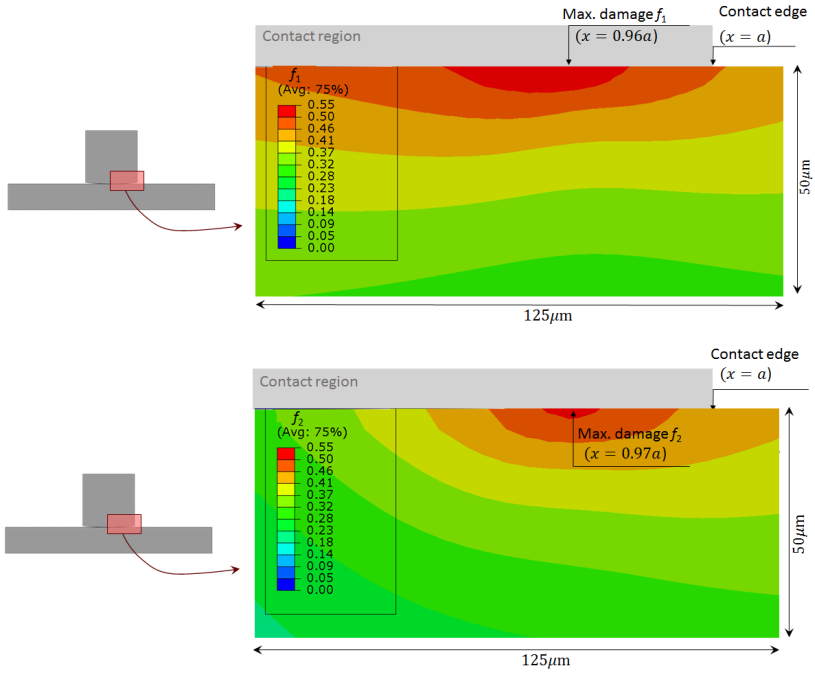

Figure 5.9: Damage initiation variables distribution along the specimen, for test FF1 from Hojjati-Talemi et al. (2014): (a) f_1 and (b) f_2 parameter.

Similar profiles were observed for other tested cases (FF1 to FF8). The damage parameter f_1 had its peak values at two shear planes, leading to two potential directions of crack growth: $+30° \pm 5°$ or $-30° \pm 5°$. The results agree well with experimental results from literature, with those angles being measured with respect to the normal to the contact surface. Lykins et al. (2001b) have shown experimentally the initiation angles to be $-40°$,$-45°$ and $-39°$ whereas Namjoshi et al. (2002) observed either at $-45°$ or $+45°$ with a variation of $\pm 15°$. Hojjati-Talemi et al. (2014) found the initiation angles between $-35°$ to $-45°$ for the aluminium alloy and Almajali (2006) found the initiation angle for Titanium alloy at $41°$. Those results are summarized in Figure 5.10. For orientation of the critical plane, researchers (Lykins et al., 2001b;

Namjoshi et al., 2002) have shown experimentally that the initiation process is mainly controlled by maximum shear stress. These maximum shear stress planes exist on both sides of the principal plane. Therefore, both the planes have potential to initiate damage in these directions. Depending upon the microstructure of the material during the experiment, the crack may take any preferred direction closer to maximum shear plane. Therefore, crack near the surface in first few grains can occur either inwards or outwards direction, with reference to the contact edge.

For the damage parameter f_2, the peak values lead to one potential propagation direction, perpendicular to the contact surface and perpendicular to the axial loading. This expected result comes from the fact that the stress state is nearly uni-axial at the contact edge. Therefore, the shear stress has minor impact on the calculation of this parameter and fracture is mainly dominated for normal stresses. For fretting fatigue, these orientation predictions ($0^\circ \pm 5^\circ$) are not accurate.

Figure 5.12 presents the variation of the damage variable f_1 and f_2 as function of the probable crack orientation angle, for the case of flat pads, for test 3. Similar to the case of cylindrical pads, the damage parameter f_1 had its peak values at two shear planes. For flat pad configuration, the two possible orientations of crack initiation are slightly higher than those for cylindrical pads: $+40^\circ \pm 5^\circ$ or $-40^\circ \pm 5^\circ$. In addition, the parameter f_2 also predicts two potential orientations: $+45^\circ \pm 5^\circ$ or $-45^\circ \pm 5^\circ$.

The previous results were also compared with critical plane approaches. Using those approaches, the initiation location and orien-

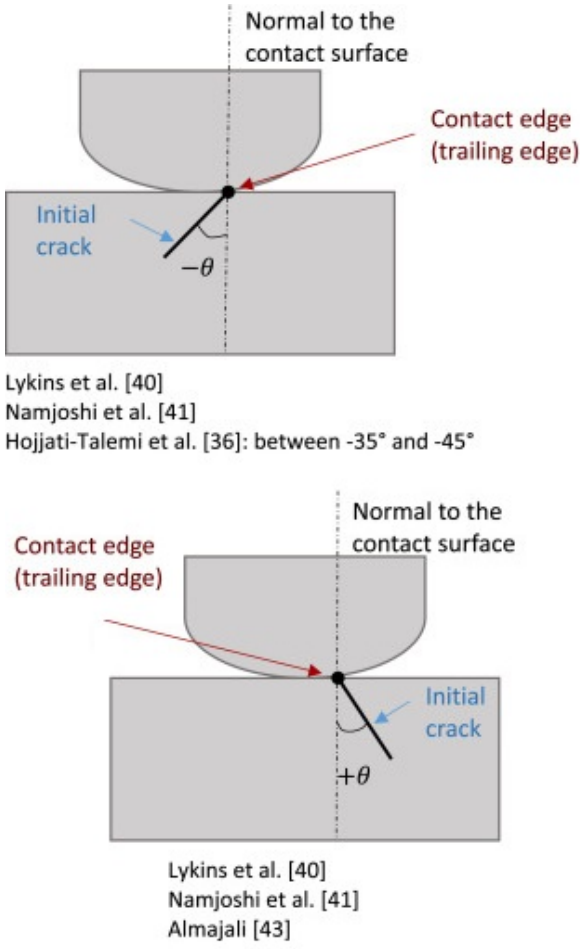

Figure 5.10: Summary of experimental data, exemplifying the crack initiation angle measured by different researchers.

tation can be predicted. Figure 5.13(a) and Figure 5.14(a) show the variation of the damage parameter at the contact interface using FP and FS parameters. The results are computed at the instant of maximum axial stress applied during the loading cycle. It is observed that regardless of the pad geometry for both cases, highest value of the parameter is achieved at $^{x}/_{a_{cont}} = 1$. Hence, good correlation is observed with experimental observations. Although both parameters showed

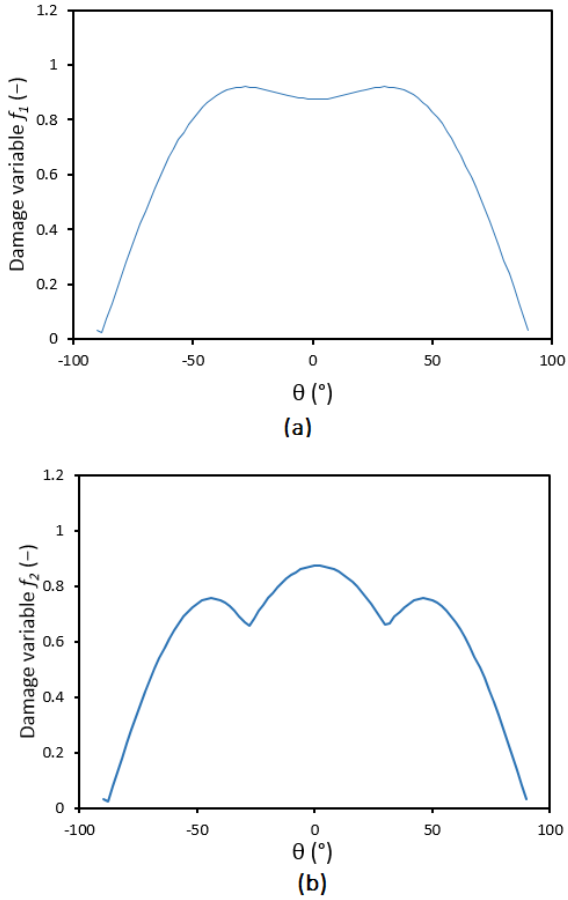

Figure 5.11: Variation of damage parameters with angles (at a point of maximum damage during a cycle): (a) f_1 and (b) f_2, for cylindrical pad (test FF9 of Hojjati-Talemi et al. (2014))

almost same initiation location, some variation in damage profile can be seen within the stick zone.

It is widely accepted that Stage I growth occurs due to reversal of shear stress to form a slip band. With the increased intensity of stress reversal, there are more chances to form a slip band (Hills and Nowell, 1994). Therefore, dislocations along persistent slip bands cause crack

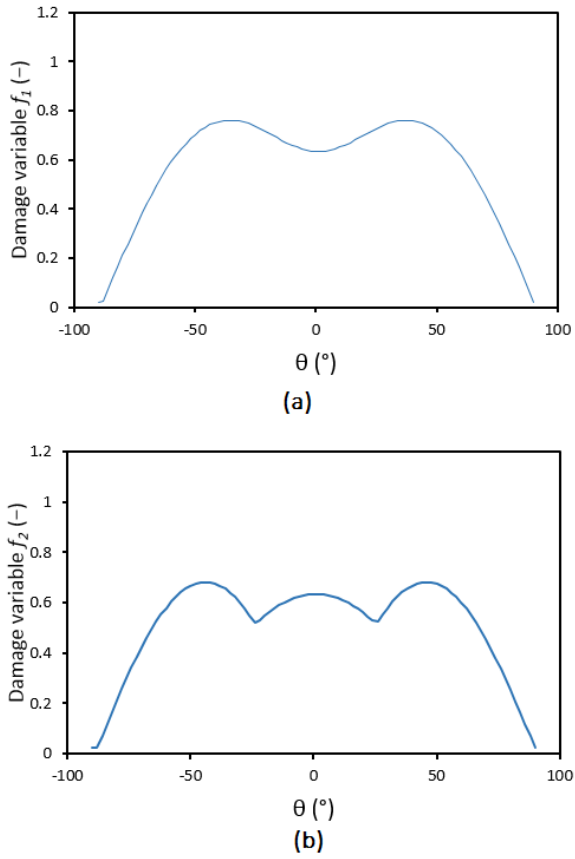

Figure 5.12: Variation of damage parameters with angles (at a point of maximum damage during a cycle): (a) f_1 and (b) f_2, for flat pad (test 3 of Sabsabi et al. (2011))

initiation along plane of maximum shear stress or close to it. Since there are, hypothetically, two possible shearing planes at $\pm 45^{\circ}$ for each element, the crack may take any preferred orientation depending upon crystallographic orientation. Figure 5.13(b) and Figure 5.14(b) shows the variation of damage parameter with different orientation angles and reinforce this hypothesis. The maximum damage parameter at the initiation site showed two peaks near the shear planes for both the cases. The numerical results showed the orientation angle is either

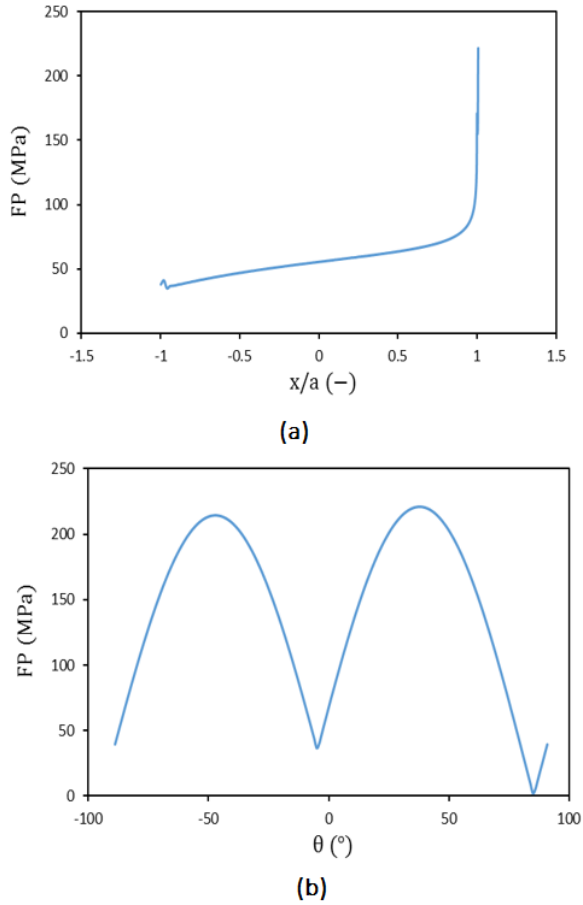

Figure 5.13: Variation of FP and FS (a) at contact interface and (b) with angles at the location of maximum damage ($x = a$), for test 1 of Sabsabi et al. (2011)

$-45° \pm 5°$ or $+35° \pm 5°$.

Analogous to the cohesive zone damage initiation criterion f_1, the critical plane approaches also predicted the critical angles for flat pad case to be slightly higher than for cylindrical pad. Findley (1959) also observed that the critical plane orientation varies with maximum stress and with combined stress state. He showed that for test with zero mean stress, critical plane varied from $45°$ to $21°$ for range of k from 0

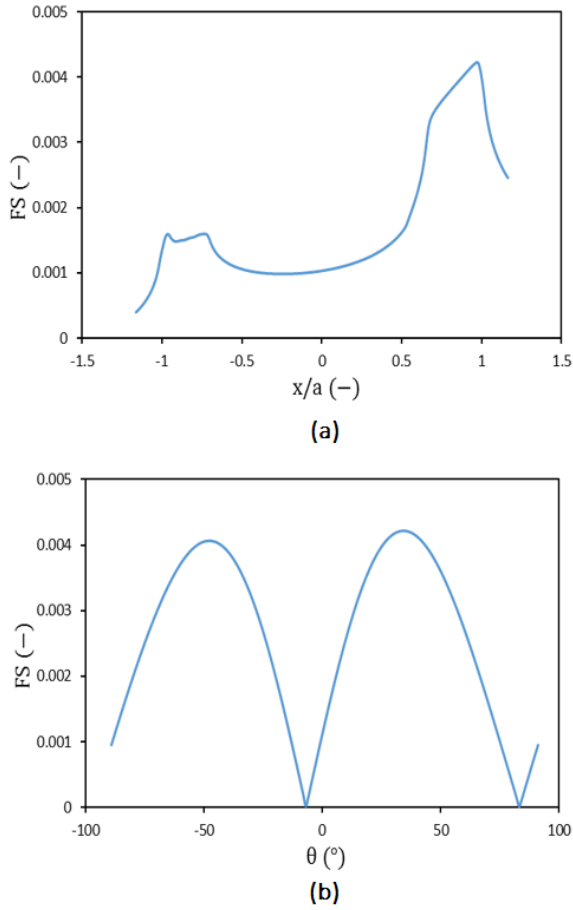

Figure 5.14: (a) Variation of FP and FS (a) at contact interface and (b) with angles at the location of maximum damage ($x = a$), for test 1 of Hojjati-Talemi et al. (2014)

to 1.1. Furthermore, its orientation was found a few degrees from the maximum shear plane for small values of k and a few degrees from the principal plane for large k. The change in material parameter k affects the initial crack orientation as it influences the contribution of normal stress to the damage parameter.

5.5 Conclusions

CZM in combination with the XFEM has been used to predict crack initiation location and orientation in fretting fatigue using cylindrical and flat pads. The predictions were made through a user subroutine UDMGINI, where two common stress based initiation criteria, namely quadratic traction-separation and maximum nominal stress, were computed. The behaviour of each of those criteria and the accuracy of their predictions were compared with experimental data and traditional critical plane approaches. For the critical plane approaches, two damage parameters FS and FP were considered. Our results showed that CZM with a quadratic traction-separation criterion (f_1 parameter) can accurately predict both the crack initiation location and the orientation for both pad conditions. The results agreed with experimental data and with traditional approaches (continuum damage mechanics and critical plane approaches). On the other hand, although the maximum nominal stress criterion (f_2 parameter) predicted correct crack initiation locations, it was not possible to obtain satisfactory results for orientation angles, especially for the cylindrical pad cases. Therefore, care should be taken while using this criterion under fretting conditions.

It is important to notice that the focus of this chapter is on the crack initiation location and orientation predictions. For life predictions, it is necessary to adjust the cohesive model, in order to account for damage accumulation, during loading and unloading, in each fretting cycle. This is the focus of the next chapter.

6

Cyclic Cohesive Zone Model

In the previous chapter, we discussed the applicability of monotonic cohesive zone models to predict crack initiation location and ori-

entation for fretting problems. One of the main drawbacks is the inability to predict lifetime. As discussed in Chapter 5, the modelling of crack propagation of fatigue scenarios using monotonic cohesive models have led to crack arrest, which is not a representation of reality. In this regard, the main goal of this chapter is to provide fretting fatigue life predictions considering a cyclic cohesive zone model, based on a traction-separation law with a bilinear form, for coupon tests with a flat pad and a flat specimen. A damage evolution law accounting for the damage accumulation due to loading and reloading in a fatigue cycle was incorporated to the cohesive model, allowing the simulation of a cycle-by-cycle failure. To minimize the computational cost of this modelling, an extrapolation of the results of the analysis is proposed.

This chapter focuses on estimating fretting fatigue life using CCZM. Firstly, the CCZM is discussed in Section 6.1 and its implementation in ABAQUS is treated in Section 6.2. Life estimation of a simple case, pure shear fatigue of a patch test, is studied and the results are compared with literature data in Section 6.2.1. In Section 6.3, the fretting fatigue case is analysed as well as model details and boundary conditions are presented. Fretting fatigue life estimates are compared with traditional approaches and experimental data in Section 6.4. Finally, conclusions are briefly explored.

6.1 Cyclic Cohesive Zone

The monotonic CZMs are mainly used to predict failure under monotonic increasing loading conditions and are not capable to model

the main features of fatigue. A characteristic of these models is that, under cyclic loading, the unloading and subsequent reloading follows the same path in a traction-separation diagram. Therefore, as discussed by Liu et al. (2013), the process zone ultimately stabilizes without additional damage, leading to crack arrest and shakedown under cyclic conditions.

As discussed by Ural et al. (2009), a cyclic degradation of the peak cohesive strength and also a distinction between the unloading and subsequent reloading paths are essential for simulating crack growth and avoid crack arrest. CCZMs are further developments of monotonic CZMs, they allow for damage accumulation during unloading and reloading conditions and are an interesting alternative to model fatigue problems. CCZMs consider the effect of a damage evolution law in the traction-separation behaviour of a cohesive model by making the cohesive strength T_{max} as a function of the current accumulated damage variable D and the initial cohesive strength $T_{max,0}$, that is,

$$T_{max} = T_{max,0}(1 - D). \tag{6.1}$$

A damage evolution law models the variation of the damage variable D as function of time. This incremental damage $\dot{D}$ (derivative of accumulated damage with respect to time) is also function of the effective tractions and separations at the cohesive surfaces, i.e., $\dot{D} = D(T, \Delta, D)$. This damage evolution law $\dot{D}$ allows the cohesive properties to evolve during the simulation. In this way, it is possible to implement degradation of those properties and capture finite lives under cyclic loading conditions.

Figure 6.1 represents the traction-separation law for a cyclic cohesive zone model. As it can be seen, the traction-separation curve is now function of damage state and the maximum value of traction that a material can resist depends upon the value of damage. In addition, the loading-reloading paths may differ, accounting for damage accumulation on this cyclic process. In addition, the loading and subsequent reloading may follow different paths in a traction-separation diagram. This difference in paths produces an irreversible damage accumulation that can be used to model interesting dissipative mechanisms for metals under fatigue conditions, such as crystallographic slip and frictional interactions between asperities (Liu et al., 2013; Nguyen et al., 2001).

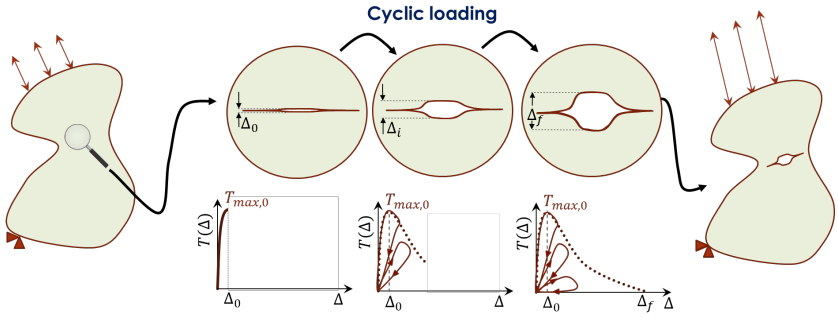

Figure 6.1: Cyclic cohesive zone model: traction-separation curve

In this thesis, the damage evolution law proposed by Roe and Siegmund (2003) is used. It is based on common damage mechanics principles:

1. the cohesive strength is inversely proportional to the accumulated damage;

2. the monotonic cohesive zone traction-separation curve delimits

an upper bound, being an envelope for all possible states;

3. the local damage endurance defines a lower bound;

4. once a deformation measure is greater than a critical value, damage starts to accumulate;

5. the increment of damage is related to the increment of deformation weighted by load level.

These requirements can be summarized in the following damage evolution equation:

$$\dot{D} = \frac{|\dot{\Delta}|}{\Delta_{\Sigma}} \left[\frac{T}{T_{max}} - \frac{\sigma_f}{T_{max,0}} \right] H(\Delta - \Delta_0) \tag{6.2}$$

where $\dot{D}$ is the derivative of the damage D with respect to time t, σ_f is the fatigue endurance limit, Δ_{Σ} is the accumulated cohesive length and T and Δ are the effective tractions and effective separation, respectively. Note that to be able to compute damage accumulation in a cycle, two new parameters are required: σ_f and Δ_{Σ}. Moreover, the Heaviside step function $H(\Delta - \Delta_0)$ is used to delimit the reversible and irreversible regimes of the constitutive law. If separation is smaller than the critical value Δ_0, then the Heaviside function is zero, there is no accumulation of damage and the model behaves elasticly. Otherwise, the Heaviside function is equal to one, damage is accumulated and the material starts to degrade.

Winter (2009) proposed an implementation of the model developed by Roe and Siegmund (2003), he considers the behaviour of the material being a combination of two parts: (1) an undamaged continuum

with an arbitrary material law connected by (2) a cohesive interface with its own cohesive properties and traction-separation curve (cohesive stiffness K of the reversible part of the traction-separation curve, cohesive strength and critical separation). In this implementation, the accumulated cohesive length Δ_Σ is adopted as five times the critical separation Δ_0.

A different approach is adopted in our study. The cohesive elements are considered embedded in the description of the extended finite elements, which contain not only the damage of the cohesive surfaces but also its continuum properties. To be able to incorporate a damage evolution law in ABAQUS, instead of effective tractions and effective separation, element stresses and strains obtained from XFEM are used. In ABAQUS XFEM with cohesive segments methodology, the elastic material behaviour characterizes the reversible region of the cohesive law. Therefore, there is no need to explicitly use a Heaviside function to describe both regimes. Consequently, equation (6.2) may been re-written as:

$$\dot{D} = \frac{|\dot{\varepsilon}|}{\varepsilon_\Sigma} \left[\frac{\sigma_{eff}}{T_{max}} - \frac{\sigma_f}{T_{max,0}} \right] \tag{6.3}$$

where $\dot{\varepsilon}$ is the incremental strain at the cohesive surfaces, σ_{eff} is the effective stress acting on the cohesive surface and ε_Σ is the accumulated cyclic strain. The incremental strain is:

$$\dot{\varepsilon} = \varepsilon_t - \varepsilon_{t-1} \tag{6.4}$$

where ε_t is the element effective strain at a time t and ε_{t-1} is the

effective strain at a previous time increment $t-1$.

As pointed out by Liu et al. (2013), mixed mode conditions may be incorporated to the cohesive model by considering an effective separation, given by a combination of the normal and tangential separation at the cohesive surface. In this case, unloading occurs when this effective separation decreases, even if separation in one direction (tangential or normal) increases. The effective separation can be translated in the effective strain for a XFEM with cohesive segments approach. The effective strain ε is given by a composition of normal ε_n and tangential ε_t strains obtained at the cohesive surface:

$$\varepsilon = \sqrt{\varepsilon_n^2 + \varepsilon_t^2} \tag{6.5}$$

The effective traction σ_{eff} is a combination of the normal and tangential traction at the cohesive surface and may also be translated by the effective stresses acting on the cohesive surface. It is given as:

$$\sigma_{eff} = \sqrt{\sigma_n^2 + \sigma_t^2} \tag{6.6}$$

where σ_n is the normal stress and σ_t is the tangential stress acting on the cohesive surfaces.

The accumulated cyclic strain ε_Σ can be correlated with the accumulated cohesive length Δ_Σ, considering the cohesive parameters of the cohesive interface proposed by Winter (2009):

$$\varepsilon_\Sigma = \frac{K}{E}\Delta_\Sigma \tag{6.7}$$

where K is the cohesive stiffness, E is the Young's Modulus and Δ_Σ is accumulated cohesive length, typically adopted as five times the critical separation Δ_0.

The cyclic damage law developed by Roe and Siegmund (2003) has been used successfully to predict fatigue failure at interface of different materials (Roe and Siegmund, 2003; Wang and Siegmund, 2005). Their methodology has been used to study fatigue failure in metals, in special for fretting cases.Zhang et al. (2015, 2016) have used it in their fretting fatigue analysis, however they have not validated their results with any experimental data. To the best of our knowledge, our work is the first attempt to accurately predict fretting fatigue total lifetime using cyclic cohesive zone models with an extrapolation procedure.

6.2 ABAQUS implementation

The damage evolution law is implemented in the ABAQUS model, by using the user subroutine USDFLD to interpolate the material properties (that is, cohesive strength T_{max} and the fracture energy G) according to the damage parameter obtained through equation (6.3). Figure 6.2 shows the flow chart summarizing the procedure adopted in this work. Firstly, the undamaged material properties, initial cohesive strength $T_{max,0}$ and fracture energy G, are stored. During the first increment of loading, the damage D, instantaneous maximum cohesive strength T_{max} and incremental strain $\dot{\varepsilon}$ are initialized. Then, the effective stresses and strain are computed (equations (6.5) and (6.6)) at the potential crack propagation angle. This angle is obtained via

UDMGINI subroutine as described below.

Once the effective stresses and strains are calculated, the effective incremental $\dot{\varepsilon}$ strain is obtained considering the effective strains at a previous time increment (equation (6.4)). Next, the increment of damage is computed by equation (6.3) and the accumulated damage D at the end of the loading increment is obtained by integrating equation (6.3) over time. This value of damage D is used to interpolate the material properties T_{max} and G during the analysis. In this way, for the next loading increment, the material properties are going to be reduced according to the level of damage in the structure.

This procedure is repeated for all loading increments of the analysis. Firstly, a check is performed to verify if the current loading increment is the first loading increment or not. If it is the first one, the variables D, T_{max} and $\dot{\varepsilon}$ are initialized, as described above. If it is not, then a second check is performed to verify if the accumulated damage D has reached 1. If yes, no further damage is allowed to happen and the instantaneous maximum cohesive strength in the element is set to zero. If damage D has not reached 1, the values of effective stresses and strains, incremental strain and accumulated damage are computed for the current loading increment. Again, this damage variable is used to reduce the instantaneous material properties through equation (6.1) before the calculation of stresses and strains in a next loading increment.

An user subroutine UDMGINI was written to compute the potential propagation angle. This angle is defined as the one that provides the absolute maximum normal stress σ_n over the time. For each time

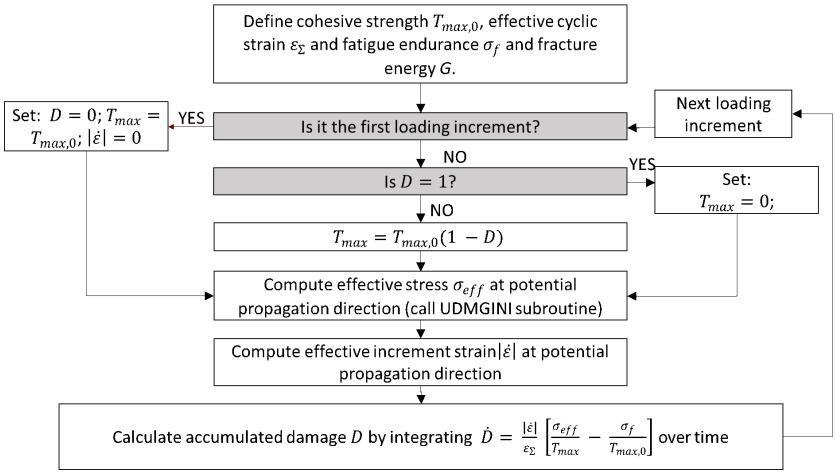

Figure 6.2: Flow chart: USDFLD user subroutine implementation

increment, the normal stress σ_n is calculated for a series of angles θ, varying from $-90°$ to $+90°$ with $1°$ increment at the element ahead of the crack tip. If there is no crack in the model, this angle is calculated at the element in which the damage variable D is maximum. The maximum value of σ_n and its respective angle θ is stored for each loading increment. Once the damage variable D reaches 1 at the element, a crack is created and its oriented in the direction in which the value of σ_n is maximum.

Figure 6.3 shows a representation of the python code written to read the model input file of one complete cycle loading. It contains details of geometry, mesh details and material properties, using RESTART option. The flow chart of such implementation is represented in Figure 6.3. Firstly, the input files of one loading cycle is generated and submitted together with the two subroutines USDFLD and UDMGINI for analysis in ABAQUS. After simulation of one cycle is complete, the python code extract the results and analyses of the crack length and

damage in the model. If there is a crack and its length is greater than a critical value a_c, the simulation stops. Otherwise, if no crack has initiated or an existent crack has not grown, another input file containing loading conditions for the next 100 cycles is created and submitted for analysis. If a crack has initiated in the model (first element has been cracked) or an existent crack has increased in size by one element, then the number of cycles and crack length are stored in a text file, before running the next 100 cycles. The simulation is terminated once the crack length reaches $a_c = 150\ \mu\text{m}$. The analysis was performed cycle-by-cycle, with each input file considering the loading of 100 cycles. The selection of 100 cycles was made to reduce the size of odb files while keeping the time increment of the analysis sufficient small.

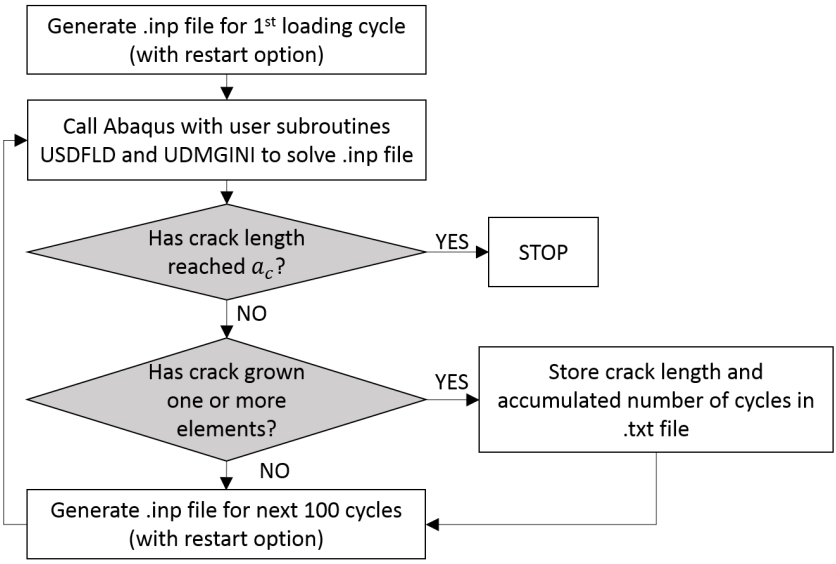

Figure 6.3: Flow chart: python script

6.2.1 Verification: Pure reversible shear fatigue

In order to verify the implementation of the cyclic cohesive model, the results of damage evolution of an element subjected to purely reversible shear stress is compared with literature data from Winter (2009). The model consisted of one XFEM element of unit size dimensions. Plane stress conditions were assumed. Loading and boundary conditions are summarized in Figure 6.4.

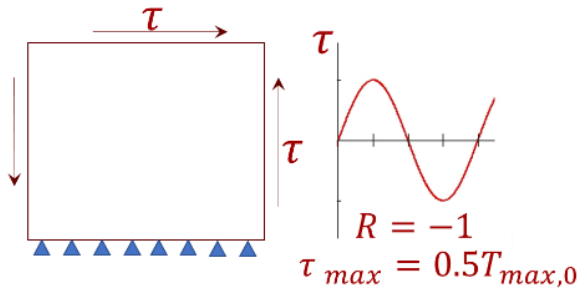

Figure 6.4: Low cycle fatigue model: pure reversible shear stress condition

In this model, the material properties used in the ABAQUS model (XFEM with cohesive segments in junction with a damage evolution law) were: $T_{max,0} = 20000$ MPa, Elastic modulus $E = 10^6$ MPa, Fatigue endurance $\sigma_f = 0.0$, strain at failure $\varepsilon_f = 0.1$, effective cyclic strain $\varepsilon_\Sigma = 2\varepsilon_f$. A bilinear shaped cohesive law is assumed between tractions and separations on the potential cohesive zone.

Firstly, a complete six loading cycles analysis was done using the already available implementation in ABAQUS (XFEM with cohesive elements). It is important to notice that this implementation considers a monotonic CZM in junction with a XFEM methodology, details in ABAQUS documentation Version (2013). As previously discussed, it

is expected that monotonic cohesive models are not able to predict damage accumulation under cyclic conditions and, therefore, are not a good option to model fatigue. We also used our implementation of a cyclic cohesive zone and ran the same analysis.

The results comparing these two methodologies are presented in Figure 6.5. The monotonic cohesive law is indeed unable to capture the cyclic damage accumulation, and the behaviour simulated is purely elastic. In our CCZM implementation, the cohesive strength of the material reduced as the damage variable increased, and the model was able to predict damage accumulation due to a cyclic loading condition.

The results of damage accumulation as function of number of cycles were compared with literature data from Winter (2009) and are shown in Figure 6.6. Our implementation agrees well with literature data, showing that it is able to correctly predict the evolution of damage in the element and the total number of cycles to failure.

6.3 Fretting fatigue crack propagation

The same experimental set-up presented by Sabsabi et al. (2011) and Hojjati-Talemi et al. (2013) is considered in this section. In this coupon configuration, two flat pads are kept in contact to a flat specimen due to a normal load F. The specimen is, then, subjected to fatigue load completely reversible ($R = -1$) fatigue loading σ_{axial}, as represented in Figure 6.7(a). The pad dimensions are: $H = 10$ mm, $J = 10$ mmand out of plane thickness equal to 5 mm. The symmetry of the problem allow us to model only half of the set-up, as shown in Figure 6.7(b).

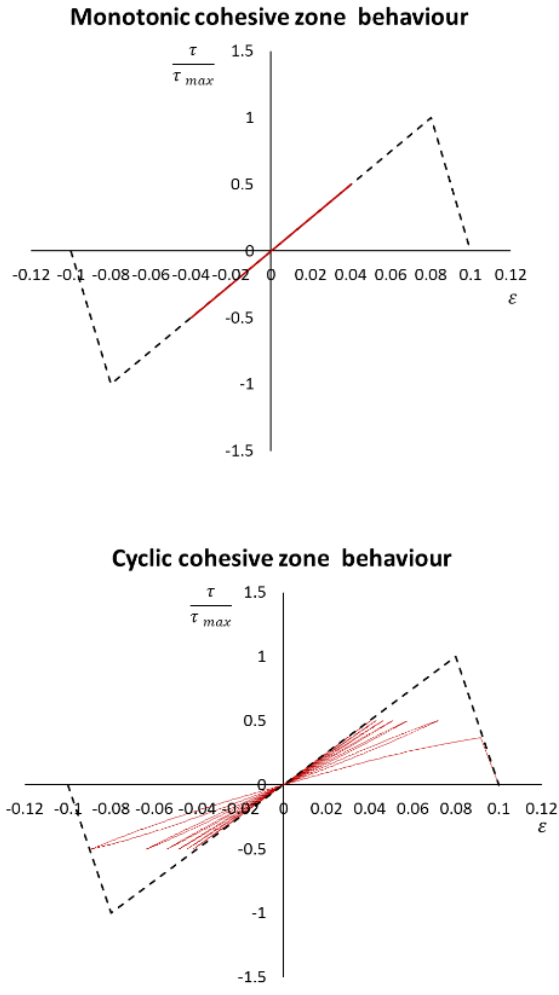

Figure 6.5: Comparison between responses of a monotonic and cyclic cohesive zone model

This has been modelled by restricting the half-width surface of the specimen to move in the x direction and also to rotate around the z-axis. The following boundary conditions at the pad were applied: both sides were restricted to move in y direction and contact interaction between pad and specimen was established. Regarding dimensions,

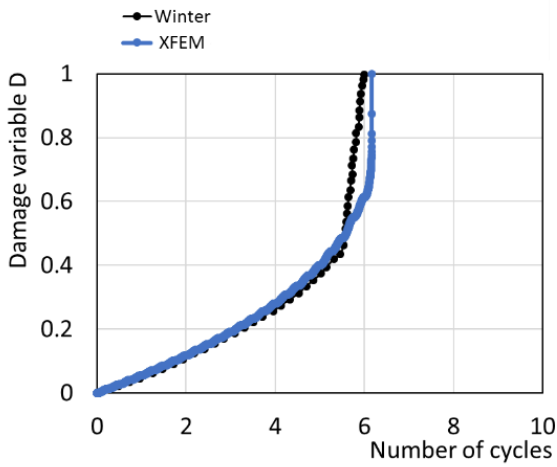

Figure 6.6: Comparison between our implementation and literature data

the specimen model had length $L = 20$ mm, half width $B = 5$ mm and out of plane thickness equal to 5 mm.

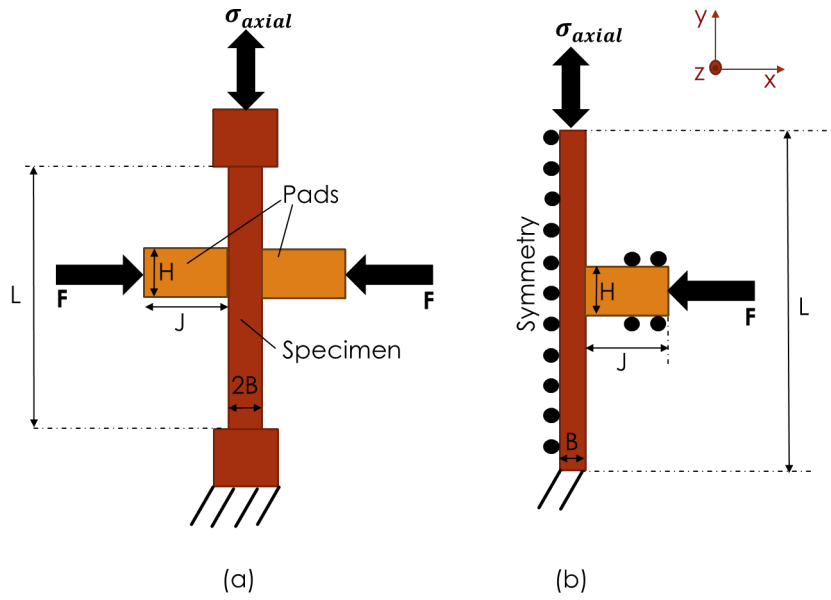

Figure 6.7: Model details: (a) experimental test set-up; (b) loading and boundary conditions

The contact between both parts (pad and specimen) was defined using finite sliding with a surface to surface interaction. The contact between crack faces was also modelled using a surface to surface interaction. For both cases, the master-slave algorithm was used with tangential behaviour modelled using a Penalty method with slip tolerance equal to 0.01 and the default hard contact was chosen to define the normal behaviour. A constant value of 0.8 (Sabsabi et al., 2011) was selected as the coefficient of friction between crack faces and also between pad and specimen.

Firstly, a normal load F was applied and kept constant throughout the analysis. Then, the cyclic axial loading condition was applied in N loading steps of 100 sinusoidal cycles each, as shown in Figure 6.8. If no element in the model was cracked during the first 100 cycles, another input file containing loading conditions for the next 100 cycles was created and submitted for analysis. However, if one element was cracked, then the number of cycles and accumulated crack length were stored in a text file, before running the next 100 cycles. This procedure was repeated until total crack length is equal to 150 $\mu\mathrm{m}$.

A linear elastic material response with material properties of aluminium 7075-T6 were the same as in the experiments conducted by Sabsabi et al. (2011), with Young's Modulus equal to 72 GPa and Poisson's ratio equal to 0.33. The fretting tests were performed in a stress ratio of -1.0 for the axial load (σ_{axial}). For completeness, the loading conditions and number of cycles to failure of the tests analysed in this study are summarized in Table 6.1.

For the cohesive parameters, a bilinear traction-separation curve is

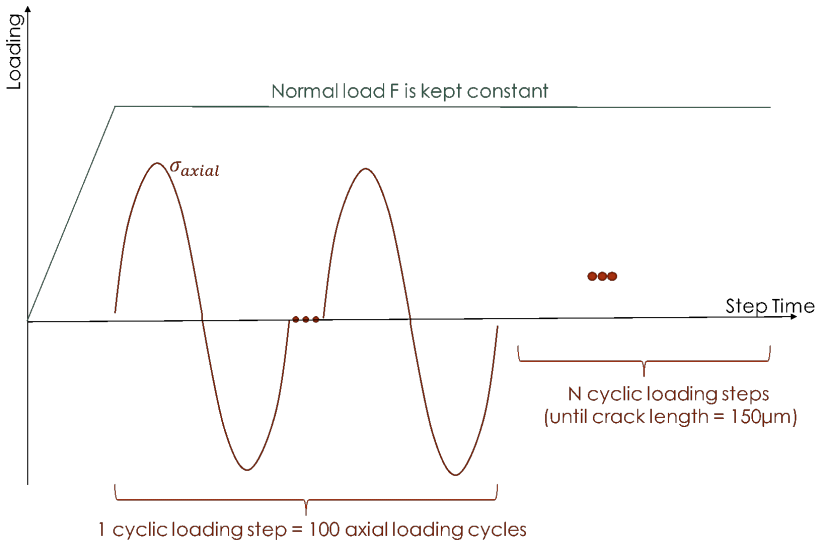

Figure 6.8: Loading conditions

assumed. The material initial cohesive strength $T_{max,0}$ is considered equal to material's ultimate tensile stress σ_u (572 MPa in Sabsabi et al. (2011)), as used by Kim and Yoon (2014). The fracture energy, area below the traction-separation curve, is estimated based on the fracture toughness (20 $\mathrm{MPa\,m^{1/2}}$ (Committee, 1990)). As the area underneath the traction-separation curve is given by the fracture energy G, the critical separation can be estimated as $\Delta_f = 0.018$ mm.

The cyclic behaviour requires the definition of two additional parameters σ_f and ε_Σ. The value of σ_f is taken to be equal to 166 MPa (Sabsabi et al., 2011). The cohesive stiffness is estimated based on the length of the XFEM elements ($l = 5$ $\mu\mathrm{m}$, the number of possible crack paths $n = 20$ (number of interface cohesive elements among continuum elements in a discrete approach, such as the one in Winter (2009)) and material Young's modulus E, with $K = {}^{nE}/_{l} = 28.8 \times 10^6$

Table 6.1: Loading conditions from experiment

Test	F [N]	σ_{axial} [MPa]	N_f [cycles]
5	2000	190	12,509
6	4000	110	92,259
7	4000	130	47,714
8	4000	150	32,905
9	4000	170	27,391
10	4000	190	9,590
11	8000	110	82,549
12	8000	130	43,567
13	8000	150	25,872
14	8000	170	23,046
15	8000	190	8,760

$\mathrm{MPa/mm}$ (Winter, 2009). The accumulated cohesive length is taken as $\Delta_\Sigma = 2\Delta_f = 0.036\ \mathrm{mm}$ (Winter, 2009). Therefore, as per equation (6.7), the accumulated cyclic strain ε_Σ is taken as approximately 14.4.

Regarding the mesh, a 2D quadrilateral, 4-node (bilinear), plane strain, reduced integration element (CPE4R) was considered. To model the cohesive behaviour, a structured mesh of CPE4R enriched elements (XFEM with cohesive segments) has been used to discretize a small area of the model, close by the trailing edge of the contact. In addition, the fillet of radius equal to 10 $\mu\mathrm{m}$, as per pad experimental dimensions in Sabsabi et al. (2011), is added to the pad to avoid unrealistic stress concentrations at this region. To guarantee accuracy of the model, we selected an element size of about 5 $\mu\mathrm{m}$ at the contact interface (Hojjati-Talemi et al., 2013). This element size was maintained constant throughout the area discretized with XFEM enriched elements. This size of elements was then gradually raised remote from

the trailing edge and the enriched region, as it can be seen in Figure 6.9.

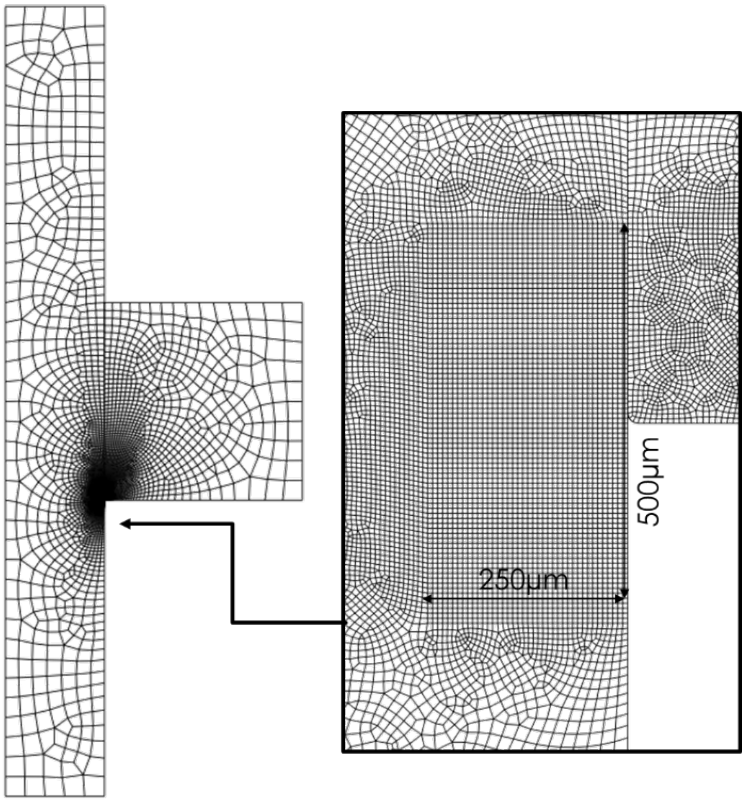

Figure 6.9: Mesh details and dimensions of the region meshed with XFEM with cohesive segments

6.4 Verification of CCZM

A cycle by cycle procedure is extremely computationally demanding. To reduce this computational burden and be able to get reasonable estimates for total fretting fatigue lives, an extrapolation procedure has been adopted. Firstly, a cycle-by-cycle analysis until the crack length is

equal to 150 μm (equal to several times the grain size of this material, which is between 10 to 30 μm (Sabsabi, 2010)) is performed. Once this analysis is completed, the crack length as function of number cycles is stored in a text file. Then, for values of crack length greater than 75 μm, the relationship between crack length and number of cycles is assumed to follow a power law. This assumption is based on fitting of experimental data of crack growth law of longer cracks (Carpinteri and Paggi, 2009), whose length is relatively larger than the microstructural dimension of the grain size (Lankford, 1985). By fitting the data already obtained from the cycle-by-cycle analysis, an extrapolation is performed and the number of cycles up to complete failure is estimated.

The following power law is used:

$$a = AN^m \tag{6.8}$$

where a is the crack length, N the number of cycles and A and m constants of the regression model.

Taking the natural logarithm from both sides of equation (6.8), the power law regression is simplified by a simple linear regression as the relation between crack length and number of cycles becomes linearised:

$$ln(a) = ln(A) + mln(N) \tag{6.9}$$

Therefore, it is only necessary to fit a linear model to the stored data, reducing the necessity of excessively many points to accurately estimate the parameters A and m. To reduce the computational bur-

den of the simulations, crack growth was simulated until crack length reached a critical value and six data points (crack length versus number of cycles) were used to fit the linear model.

Figure 6.10 presents the relation between crack length and number of cycles for the fretting fatigue analysis using XFEM with cyclic cohesive models. Two distinct regimes can be observed. The first regime deals with short cracks, where the relationship is definitely not linear in a natural logarithm scale. The second regime is related to longer cracks, with length greater than than 75 μm, and it presents a linear relationship between crack length and number of cycles in a natural-log scale. This evidences the robustness of cyclic cohesive zones to predict both crack growth regimes (initiation and propagation) in a unified way, as there is no necessity of separating those regimes prior to the start of the analysis.

It is known that the crack growth rate is influenced by many factors, such as microstructures of materials, components size and geometry, loading conditions, environments, and temperatures, as discussed in Tanaka (1974). Therefore, the clear definition of a short crack and long crack regime is not straightforward. A threshold of 75 μm was chosen to guarantee that all analysed cases were in long crack regime.

The coefficients m (slope), $ln(A)$ (intercept) and coefficient of determination R^2 (which measures how close the data are to the fitted regression line) of the linear regression are presented in Table 6.2. As it can be verified by the coefficient of determination R^2, the linear relationship is very reasonable. These parameters A and m are used in an extrapolation of the linear model for crack length equal to half of the

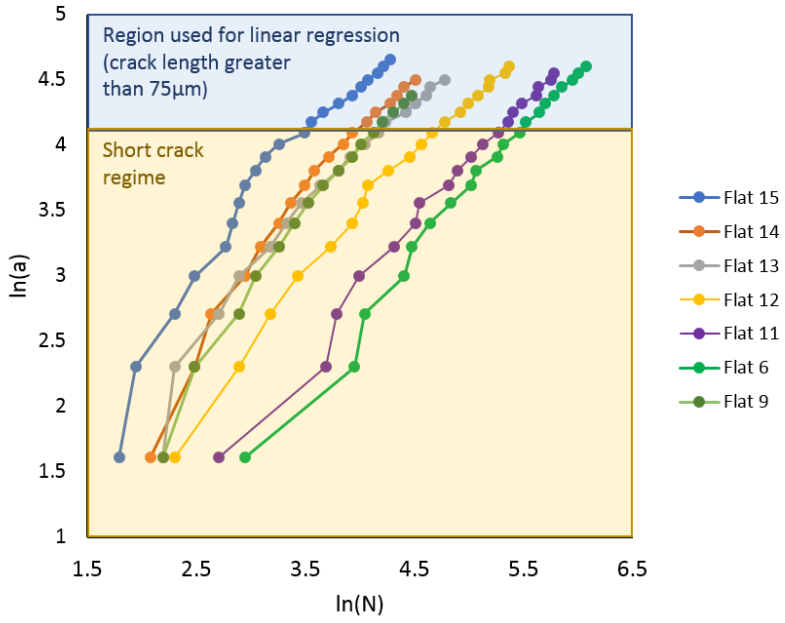

Figure 6.10: Logarithm of crack length as function of logarithm of number of cycles for different test cases

specimen's length B (until total failure of the specimen). Therefore, these extrapolations are used to estimate the total lifetime.

The estimated total life is obtained by extrapolating the linear relationship presented in equation (6.9) for the complete failure of the specimen. The estimated lifetime values are compared with observed experimental lives and the results are presented in Figure 6.11. It can be observed that the estimates are well distributed around the centre line and are within a scatter band of $\times 1.5$. These estimates indicates accuracy of CCZMs to predict fretting fatigue lives.

Crack propagation paths were obtained by considering the crack orientation criteria described in Section 6.2. The direction of propa-

Table 6.2: Parameters of the regression models

	m	$ln(A)$	R^2
Flat15	0.777466	1.326006	0.9989
Flat14	0.724829	1.23443	0.9915
Flat13	0.756474	0.906993	0.9795
Flat12	0.732927	0.661731	0.9715
Flat11	0.754247	0.174267	0.9691
Flat9	0.748441	1.026225	0.9969
Flat6	0.751541	0.037798	0.9959

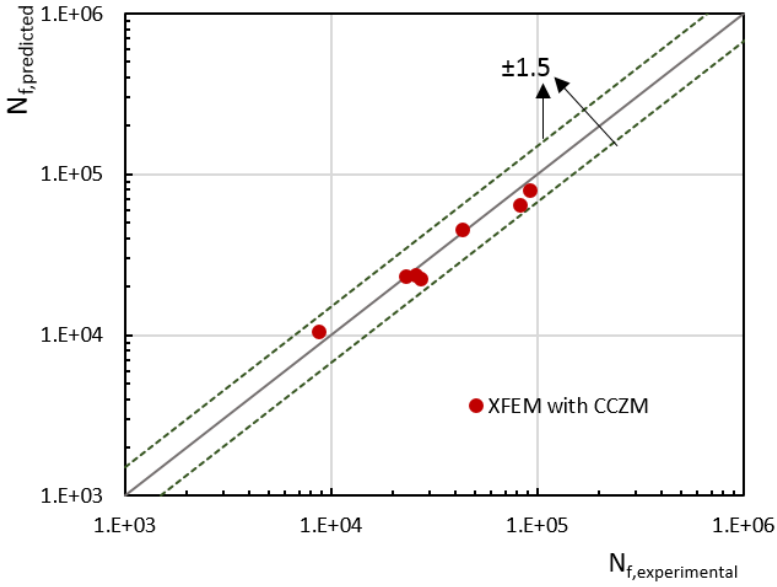

Figure 6.11: Fretting fatigue predicted life versus experimental total lifetime

gation was selected as the one that maximizes the normal stress σ_n. For all analysed cases, paths were approximately perpendicular to the applied bulk stress. This is a reasonable path and has also been considered in previous numerical analysis (Hojjati-Talemi et al., 2013). Fig-

ure 6.12 shows contours of von Mises stress for test No. 15 at different number of cycles, for maximum loading condition (crack is fully opened).

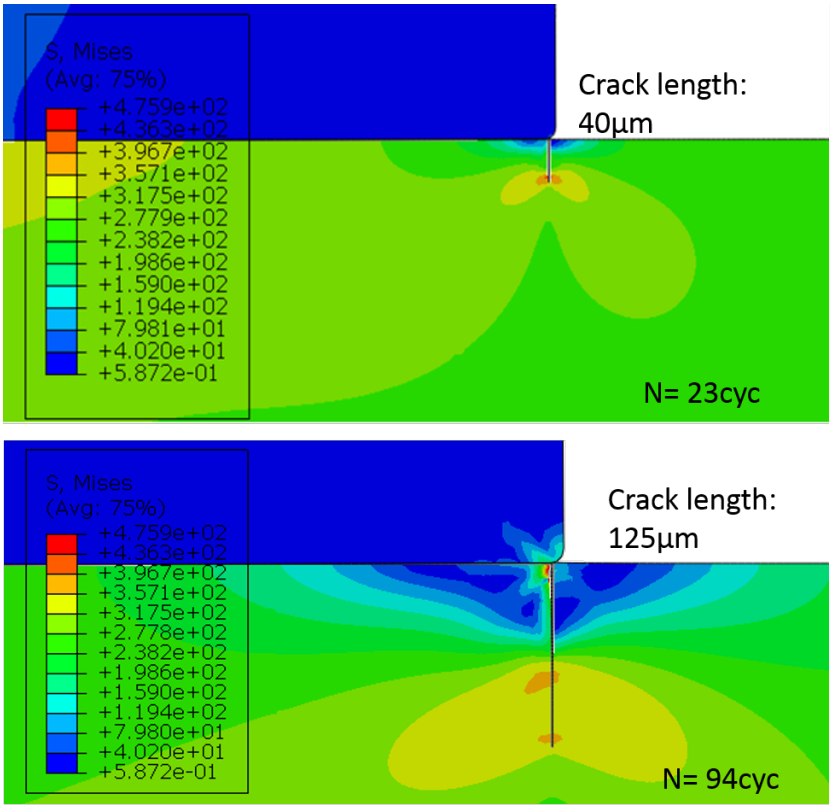

Figure 6.12: Crack path for test No. 15 at different number of cycles.

Results of lifetime are also compared with a traditional approach. The initiation lifetime is estimated using the continuum damage mechanics (CDM) methodology proposed in Hojjati-Talemi et al. (2013) and the propagation lifetime is estimated considering classical fracture mechanics. The total lifetime for this traditional approach (CDM + fracture mechanics) is obtained by adding the initiation and propagation lives.

Table 6.3: Propagation lifetime estimated from fracture mechanics approach

Test No.	N_P
Test 15	8627
Test 14	11536
Test 13	16000
Test 12	23254
Test 11	35981
Test 9	11536
Test 6	35981

Calibration tests	
Test No.	N_P
Test 5	8627
Test 8	16000
Test 10	8627
Test 7	23254

For the propagation life, the crack is assumed to propagate perpendicularly to the bulk stress and analytical expressions for a double notch DENT specimen from Tada et al. (2000) is used to estimate the stress intensity factor of the long crack. For these calculations, the effect of contact stresses are neglected, and the cracked specimen is assumed to be represented by a double notched specimen under alternated bulk stress loading condition. Propagation phase is considered to happen when crack length is between 75 μm to complete failure (crack length equal to 5 mm). The lifetime is obtained by integrating the Paris' Law, with constants described in Hojjati-Talemi et al. (2013). Table 6.3 shows the estimated propagation lives for all analysed test scenarios.

For details of the implementation of CDM methodology to predict initiation lifetime, the reader is refer to Hojjati Talemi (2014), Hojjati-Talemi et al. (2014) and Hojjati-Talemi et al. (2013). As described in Hojjati-Talemi et al. (2014), the damage parameters A and β are estimated using a set of calibration tests (here we used tests numbers 5, 7, 8 and 10). A non-linear minimization procedure is performed in order to minimize the root mean square error between the calibration tests and the experimental initiation lifetime of those set of tests. The initiation lifetime N_i is obtained from the integral of the damage equation, replicated here for completeness:

$$N_i = \frac{R_v^{-\beta}\left(\sigma_{eq,max}^{-(m+2\beta)} - \sigma_{eq,min}^{-(m+2\beta)}\right)}{A(m+2\beta+2)}$$

where m is the hardening exponent ($m = 10$, as in Hojjati-Talemi et al. (2013)), A and β are the damage parameters, R_v, $\sigma_{eq,min}$ and $\sigma_{eq,max}$ are the mean triaxiality function, the mean equivalent stress at minimum load and the mean equivalent stress at maximum load, respectively. The values of R_v, $\sigma_{eq,min}$ and $\sigma_{eq,max}$ are calculated from the finite element analysis of a full fretting cycle. They are obtained from averaging the stresses in the specimen, around the contact edge in a semi-circular region of radius 56 μm (Hojjati-Talemi et al., 2013). From the non-linear procedure described above, we obtained $ln(A) = -63.09$ and $\beta = 0.015$.

Table 6.4 shows the estimated initiation lifetime N_i for all analysed cases and the values of R_v, $\sigma_{eq,min}$ and $\sigma_{eq,max}$ obtained from finite element.

Table 6.4: Initiation lifetime estimated from continuum damage mechanics approach

	$\sigma_{eq,min}$	$\sigma_{eq,max}$	R_v	N_i
Test15	1684.7	291.8	1.056	133
Test14	1538.0	282.0	1.057	11510
Test13	1365.2	274.2	1.058	9872
Test12	1175.0	268.5	1.057	20313
Test11	934.1	259.2	1.058	46568
Test9	1504.4	199.3	1.045	15855
Test6	979.2	155.1	1.057	56278

Figure 6.13 shows a comparison between the estimates of each method. It can be noted that the estimates of XFEM in junction with cyclic cohesive zone models have smaller error when compared with experimental data than estimates from CDM with classical fracture mechanics.

Even though a visual improvement is already noticeable, in order to compare the accuracy of both life prediction techniques, the statistical parameter proposed in Hojjati-Talemi et al. (2013) is considered. The root relative squared error (RRSE) is a normalized measurement that allows to quantify how far the predicted results are with respect to the experimental ones. RRSE is a measure of the overall error of the estimated values and its computed as:

$$RRSE = \sqrt{\frac{\sum_{i=1}^{n} \left(N_e^i - N_o^i\right)^2}{\sum_{i=1}^{n} \left(N_e^i - \frac{1}{n}\sum_{j=1}^{n} N_o^j\right)^2}}$$

where N_e^i is the estimated total lifetime for each test i, N_o^i is the observed experimental lifetime for each test i, and n is the total number of analysed tests. The closer to 0 this normalized error is, the better is the

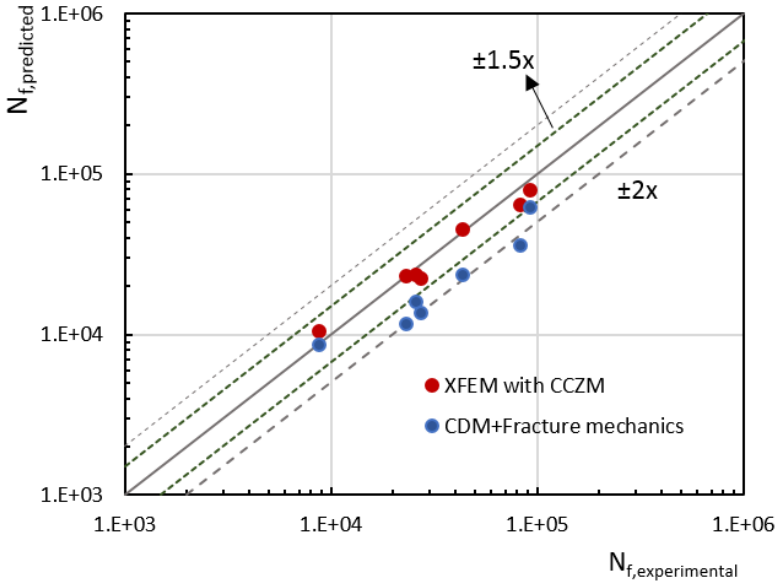

Figure 6.13: Comparison between estimated lifetime obtained by XFEM with CCZM methodology and CDM with fracture mechanics approach

Table 6.5: Root relative squared error

	XFEM with CCZM	CDM with LEFM [27]
RRSE	0.32	0.92

prediction. A comparison between both approaches, CDM+fracture mechanics and XFEM+CCZM, is shown in Table 6.5. The XFEM+CCZM seems to be a good approach for dealing with prediction of lives under fretting fatigue for a flat on flat test configuration.

6.5 Input parameters and their influence on results

As per equation 6.3, the damage law is basically defined by the folowing input parametes: $T_{max,0}$, σ_f and ε_Σ. Assuming an isotropic material, the cohesive strength $T_{max,0}$ is defined by the ultimate tensile strength of the material, that can be easily measured in laboratory. The higher the fatigue endurance σ_f, the longer the predict life (as per equation 6.3), as an increase in σ_f causes a decrease on the incremental damage. A correct prediction of this parameter is, therefore, of great importance for the model.

The incremental cyclic damage is inversely proportional to The accumulated cyclic strain ε_Σ. This parameter is estimated based on the fracture energy. Therefore, it is expected that the fracture energy would play a strong hole on the prediction. The analysis was performed estimating the fracture energy (area below the traction-separation curve) based on the fracture toughness K_{Ic} (20 $\mathrm{MPa\,m^{1/2}}$). To check the impact of the he fracture energy on the analysis, the a value of fracture toughness K_{Ic} equal to 40 $\mathrm{MPa\,m^{1/2}}$ has been also simulated.

Figure 6.14 shows the results of both analysis. Based on a extrapolation of the linear curve, the total failure was computed for both cases. For the case with K_{Ic} equal to 20 $\mathrm{MPa\,m^{1/2}}$, the total life was 10395 cycles. In addition, for K_{Ic} equal to 40 $\mathrm{MPa\,m^{1/2}}$, the total lifetime was 32291 cycles. Therefore, a double on the fracture energy would result in life predictions that are 3.5 times longer. This shows the necessity of

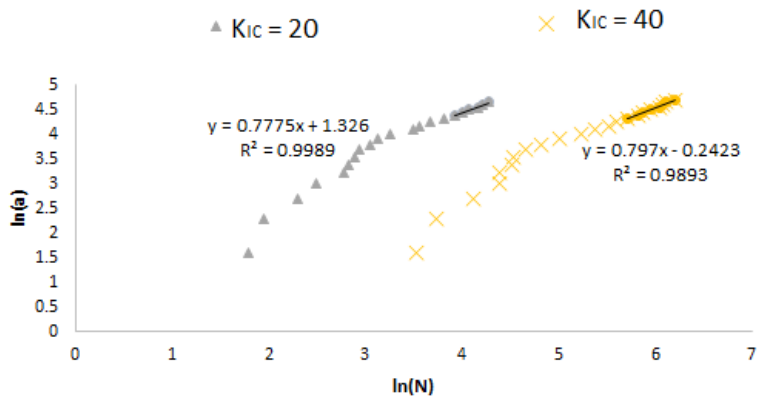

Figure 6.14: Crack length versus number of cycles, in log scale, for different fracture energies.

correctly specifying the ε_Σ parameter of the cohesive model in order to guarantee the accuracy of the predictions. It is important to notice, however, that the experimental determination of fracture energy is not straightforward, especially for mixed mode conditions.

6.6 Computational cost

The complete analysis of crack initiation and propagation up to a crack length of 150 μm using XFEM with cyclic cohesive zone models takes about 30 hours, using the following processor: Intel Core i7-5600U CPU @ 2.60GHz with 16GB of memory RAM. For instance, for test case number 15, the total analysis would take 27 hours and 33 minutes in CPU time.

It is interesting to make a comparison between the computational time considering LEFM to model propagation and the failure analy-

sis using XFEM with CCZM. As discussed in Section 4.2.5, the total failure analysis (crack growth until complete rupture of the specimen) considering LEFM would take only a few hours, while, as described above, the CCZM analysis of crack growth up to only 150 μmwould take more than a day, using the same computer. This enormous difference is expected, as LEFM is dealing with a linear analysis problem, while CCZM threat the process zone ahead of the crack tip in a non-linear way.

To analyse a crack growth until complete rupture of the specimen (crack length of about 5 mm) in a cycle-by-cycle procedure, it would take an infeasible amount of time. Therefore, we emphasise the necessity of an extrapolation of the results in order to predict total lifetime.

6.7 Conclusions

Estimates of fretting fatigue lives have been computed by considering CCZMs. The lifetime predictions were obtained through an extrapolation of the results obtained from this XFEM with cohesive segments analysis. In order to accurately model the damage accumulation due to cyclic loading, a user subroutine USDFLD has been proposed. This allowed the material properties to change during the analysis, accordingly to the level of damage computed based on stress and strains in the XFEM element. Once the damage level reached one, the element was cracked. The number of cycles and the crack length were stored in a text file for further post-processing.

Two regimes have been observed when analysing the curves of

crack length as function of the number of cycles. For short cracks, the growth is non-linear in a natural-log scale, whereas for longer cracks (longer than 75 μm) the behaviour is linear. Therefore, linear curves have been fitted using the longer crack growth data from the analysis. An extrapolation of this linear relationship has been performed in order to predict life to complete failure.

Results of the simulations have been compared with traditional approaches and with experimental data. Scatter plots of lifetime estimates versus experimental data showed that predictions from CCZM were in a narrower error band than predictions obtained by traditional approaches. The root relative squared error of CCZM approach was also considerably smaller than the one from traditional approaches. This implies that CCZM provides an accurate alternative for predicting fretting lives, for flat on flat coupon tests configuration.

To the best of our knowledge, there has no effort in the literature to accurately predict fretting fatigue lives and crack propagation path using cyclic cohesive zone. Our work is the first one that provides a methodology with an extrapolation procedure that allows computation of fretting lives under high cycle fatigue. Our results have been validated with experimental data, which has not been done previously in the literature.

7

Conclusion and Future Work

In this thesis we have evaluated alternatives for numerical modelling of failure from fretting fatigue. This phenomenon brings extra

complexity to modelling due to its non-proportional loading characteristic and the high stresses at contact interface, causing material non-linearities to play a significant role on failure. Throughout this thesis we have tackled those difficulties, providing solutions to incorporate their effects on the numerical model.

7.1 Conclusions

Firstly, the traditional numerical model of fretting coupon tests is presented for a cylindrical pad in contact with a flat specimen. Chapter 3 provides a study of the impact of numerical errors on the estimate of stresses at contact interface. This is of main importance once those stresses are normally used to predict crack initiation lives and location. A map is proposed to guide researches on the adequate choice of finite element size in their models. Additionally, a study of stress singularities is performed, showing that no crack singularity is found for this fretting test configuration. This implies that the use of fracture mechanics analogies to study the stress around the contact may not be suitable for this configuration.

Fretting fatigue lives are normally estimated as a sum of crack initiation life and a crack propagation up to total failure. Initiation lives are commonly estimated using continuum damage mechanics and crack propagation lives are obtained considering a crack propagation law in combination with classical linear elastic fracture mechanics. However, traditional crack orientation criteria from LEFM (such as maximum tangential stress criterion) were developed for proportional loading

conditions, which is not the case in fretting scenarios. In order to circumvent this issue, in Chapter 4, we implemented an extension of MTS criterion that accounts for non-proportional loading conditions. To correctly use this criterion, stresses at crack tip needed to be computed for every instant of the loading cycle. This poses another issue on the modelling, as crack faces may be in contact during the loading cycle and this interaction affects directly the stress at crack tip. Therefore, we have created an python script that allowed as to consider the effect of crack face contact in our 2D simulations using conventional finite element. The results of Chapter 4 showed that the extension of MTS criterion was able to accurately predict crack propagation paths and propagation lives.

A major limitation of LEFM to predict fretting fatigue lives is that it requires a very small plasticity zone around the crack tip, which may not be the case, specially in fretting cases due to the high stresses at contact interface. Additionally, live predictions often rely on classical crack growth empirical laws (such as Paris' Law) that may not be applicable to non-proportional loading scenarios. Cohesive zone models come as an alternative to deal with failure without these assumptions.

In Chapter 5, we have used monotonic cohesive zone models to predict crack initiation location and orientation. The results have been compared with experimental data and classical critical plane approaches. Monotonic cohesive zone models seems to be a good alternative for modelling the phenomenon, however it can not be used to predict lives in a cyclic loading condition. To solve this issue, in Chapter 6, we have implemented cyclic cohesive zone models in Abaqus and used it to

predict lives of fretting fatigue coupon tests (flat pad in contact with a flat specimen). Initiation and propagation phases are modelled together and there is no need to separate these two regimes, as in most traditional approaches. Our results showed a very good agreement with experiments, being well centred around experimental data and in a narrower error band that traditional predictions tools (continuum damage mechanics in junction with LEFM).

7.2 Recommendations for future work

Our focus in this thesis was the modelling and estimation of fretting fatigue lives, considering complex aspects of this phenomenon. Even though the results obtained in Chapter 6 showed a good advance in comparison with traditional approaches, there is still room for improvement.

In Chapter 4, the numerical predictions of fretting fatigue lives considering the behaviour of short cracks on the crack growth law were briefly explored. Based on the results obtained, there was no significant difference between predictions ignoring the effect of short cracks and the ones accounting for it. Although the results may imply that the effect of microstructure on the fretting fatigue predictions is small, this may not be the general conclusion. It is important to note that we only analysed the impact of short cracks on the crack growth law and some important phenomena have been ignored. For instance, those models do not take into consideration that the size of grains, their orientation and boundaries may influence the crack behaviour. In addition, the

anisotropic elastic behaviour inside grain in metal alloy can affect the short crack propagation phase. These points need to be considered, as they might greatly affect the numerical predictions.

Although numerical results obtained in Chapter 4 matched well with empirical observations, the effect of mean stresses had been neglected and it may impact on the results.

As showed in Chapter 4, the use of crack orientation criterion that accounts for non-proportional loading condition allows for correct path predictions. In Chapter 6, a simple maximum tangential stress criterion crack orientation has been used and a better approach should be developed.

Additionally, in order to predict fretting lives using cohesive zone models, an extrapolation procedure was necessary due to the computational burden of this methodology. Would be interesting to actually model a cycle-by-cycle analysis of a full fracture under fretting conditions. In this way, we could gather information of when Paris' Law is a good alternative and in what conditions it should be avoided. Moreover, a significant insight of the non-proportional loading impact in the lives could also be verified.

Finally, we have considered only laboratory configurations and further studies dealing with real scale structures are needed in order to improve the prediction capability of the proposed approaches in this thesis.

Appendix A

List of publications

Journal Publications

1. Resende Pereira, K. de F., Bordas, S., Tomar, S., Trobec, R., Depolli, M., Kosec, G., & Abdel Wahab, M. (2016). On the convergence of stresses in fretting fatigue. *MATERIALS*, 9(8).

2. Resende Pereira, K. de F., Yue, T., & Abdel Wahab, M. (2017).

Multiscale analysis of the effect of roughness on fretting wear. *TRIBOLOGY INTERNATIONAL*, 110, 222-231.

3. Resende Pereira, K. de F., & Abdel Wahab, M. (2017). Fretting fatigue crack propagation lifetime prediction in cylindrical contact using an extended MTS criterion for non-proportional loading. *TRIBOLOGY INTERNATIONAL*, 115, 525-534.

4. Bhatti, N. A., Resende Pereira, K. de F., & Abdel Wahab, M. (2018). A continuum damage mechanics approach for fretting fatigue under out of phase loading. *TRIBOLOGY INTERNATIONAL*, 117, 39-51.

5. Resende Pereira, K. de F., Bhatti, N. A., & Abdel Wahab, M. (2018). Prediction of fretting fatigue crack initiation location and direction using cohesive zone model. *TRIBOLOGY INTERNATIONAL*, 127, 245-254.

6. Kosec, G., Slak, J., Depolli, M., Trobec, R., Resende Pereira, K. de F., Tomar, S., Jacquemin, T., et al. (2019). Weak and strong from meshless methods for linear elastic problem under fretting contact conditions. *TRIBOLOGY INTERNATIONAL*, 138, 392-402.

7. Bhatti, N. A., Resende Pereira, K. de F., & Abdel Wahab, M. (2019). Effect of stress gradient and quadrant averaging on fret-

ting fatigue crack initiation angle and life. *TRIBOLOGY INTERNATIONAL*, 131, 212-221.

8. Resende Pereira, K. de F., & Abdel Wahab, M. (in press). Fretting fatigue lifetime estimation using a cyclic cohesive zone model. *TRIBOLOGY INTERNATIONAL*.

Conference proceedings

1. Resende Pereira, K. de F., Bordas, S., Tomar, S., Trobec, R., Depolli, M., Kosec, G., & Abdel Wahab, M. (2016). Cyclic cohesive zone models and its applicability to fretting fatigue crack propagation. In M. Abdel Wahab (Ed.), *International Journal of Fracture Fatigue and Wear* (Vol. 4, pp. 228-233). Presented at the 5th International Conference on Fracture Fatigue and Wear, Ghent, Belgium: Labo Soete, Universiteit Gent.

2. Trobec, R., Depolli, M., Kosec, G., Bordas, S., Tomar, S., Resende Pereira, K. de F., & Abdel Wahab, M. (2016). Parallelization approaches for fretting fatigue simulation. In M. Abdel Wahab (Ed.), *International Journal of Fracture Fatigue and Wear* (Vol. 4, pp. 204-208). Presented at the 5th International Conference on Fracture Fatigue and Wear, Ghent, Belgium: Labo Soete, Universiteit Gent.

3. Resende Pereira, K. de F., Yue, T., & Abdel Wahab, M. (2015). Multiscale modelling of roughness effect in fretting wear. In M. Abdel Wahab (Ed.), *International Journal of Fracture Fatigue and Wear, Proceedings* (Vol. 3, pp. 272-278). Presented at the 4th International Conference on Fracture Fatigue and Wear.

4. Resende Pereira, K. de F., & Abdel Wahab, M. (2017). Minimum shear stress range: a criterion for crack path determination. In M. Abdel Wahab (Ed.), *6th International Conference on Fracture Fatigue and Wear (FFW)* (Vol. 843). Presented at the 6th International Conference on Fracture Fatigue and Wear (FFW), UK: IOP Publishing.

5. Bhatti, N. A., Resende Pereira, K. de F., & Abdel Wahab, M. (2019). A comparison between critical-plane and stress-invariant approaches for the prediction of fretting fatigue crack nucleation. In M. Abdel Wahab (Ed.), *Proceedings of the 7th International Conference on Fracture Fatigue and Wear* (pp. 530-538). Presented at the 7th International Conference on Fracture Fatigue and Wear, Springer Singapore.

6. Resende Pereira, K. de F., & Abdel Wahab, M. (2019). Effect of short crack behavior on the propagation life prediction for a fretting cylindrical pad configuration. In M. Abdel Wahab (Ed.), *Proceedings of the 7th International Conference on Fracture Fatigue and Wear* (pp. 539-546). Presented at the 7th International Confer-

ence on Fracture Fatigue and Wear, Springer Singapore.

7. Resende Pereira, K. de F., & Abdel Wahab, M. (2020). An Implementation of Cyclic Cohesive Zone Models in ABAQUS and Its Applicability to Predict Fatigue Lives. In M. Abdel Wahab (Ed.), *Lecture Notes in Mechanical Engineering* (pp. 684-691). Singapore.

Bibliography

Olof Vingsbo and Staffan Söderberg. On fretting maps. *Wear*, 126(2): 131–147, 1988a. ix, 10, 12

Kenneth Langstreth Johnson. *Contact mechanics*. Cambridge university press, 1987. ix, 14, 16, 17, 23, 25, 71, 109

X Yan. Fatigue growth prediction of center slant crack in rectangular plate. *Fatigue & fracture of engineering materials & structures*, 33(6): 365–377, 2010. xi, xv, 85, 86

Fushen Liu and Ronaldo I Borja. A contact algorithm for frictional crack propagation with the extended finite element method. *Inter-*

national Journal for Numerical methods in engineering, 76(10):1489–1512, 2008. xi, 87, 88, 89, 90, 91

E Giner, N Sukumar, FD Denia, and FJ Fuenmayor. Extended finite element method for fretting fatigue crack propagation. *International Journal of Solids and Structures*, 45(22):5675–5687, 2008. xi, 2, 42, 78, 92

Eugenio Giner, Mohamad Sabsabi, Juan José Ródenas, and F Javier Fuenmayor. Direction of crack propagation in a complete contact fretting-fatigue problem. *International Journal of Fatigue*, 58:172–180, 2014. xi, 32, 38, 42, 45, 78, 79, 80, 81, 91, 93, 94, 119

Anxing Zheng and Xianqi Luo. A mathematical programming approach for frictional contact problems with the extended finite element method. *Archive of Applied Mechanics*, 86(4):599–616, 2016. xii, 101, 102

JM Ambrico and MR Begley. Plasticity in fretting contact. *Journal of the Mechanics and Physics of Solids*, 48(11):2391–2417, 2000. xii, 109, 110

Reza Hojjati-Talemi, Magd Abdel Wahab, Jan De Pauw, and Patrick De Baets. Prediction of fretting fatigue crack initiation and propagation lifetime for cylindrical contact configuration. *Tribology International*, 76:73–91, 2014. xiii, xiv, xv, 3, 10, 31, 32, 42, 49, 60, 62, 78, 107, 110, 111, 113, 114, 122, 123, 124, 126, 141, 143, 151, 152, 155, 158, 186

M Sabsabi, E Giner, and FJ Fuenmayor. Experimental fatigue testing of a fretting complete contact and numerical life correlation using x-fem. *International Journal of Fatigue*, 33(6):811–822, 2011. xiii, xiv, 141, 143, 146, 149, 150, 156, 157, 173, 176, 177, 178

Reza Hojjati Talemi. *Numerical modelling techniques for fretting fatigue crack initiation and propagation*. PhD thesis, Ghent University, 2014. xv, 3, 33, 49, 60, 105, 107, 142, 186

J. Ding, S. B. Leen, and I. R. McColl. The effect of slip regime on fretting wear-induced stress evolution. *International Journal of Fatigue*, 26:521–531, 2004. 2

O. Vingsbo and S. Söderberg. On fretting maps. *Wear*, 126:131–147, 1988b. 2

Han-Kyu Jeung, Jae-Do Kwon, and Choon Yeol Lee. Crack initiation and propagation under fretting fatigue of inconel 600 alloy. *Journal of Mechanical Science and Technology*, 29(12):5241–5244, dec 2015. ISSN 1738-494X. doi: 10.1007/s12206-015-1124-8. URL `http://link.springer.com/10.1007/s12206-015-1124-8`. 2

D.A. Hills and D. Nowell. *Mechanics of Fretting Fatigue*. Solid Mechanics and Its Applications. Springer Netherlands, 1994. ISBN 9780792328667. URL `https://books.google.be/books?id=t9Q60-N-13MC`. 2, 23, 24, 25, 71, 155

JJ Madge, SB Leen, and PH Shipway. A combined wear and crack nucleation–propagation methodology for fretting fatigue prediction. *International Journal of Fatigue*, 30(9):1509–1528, 2008. 3, 39, 49, 50

C Navarro, M Garcia, and J Dominguez. A procedure for estimating the total life in fretting fatigue. *Fatigue & Fracture of Engineering Materials & Structures*, 26(5):459–468, 2003. 3, 36, 39, 48, 49, 50

E Giner, C Navarro, M Sabsabi, M Tur, J Domínguez, and FJ Fuenmayor. Fretting fatigue life prediction using the extended finite ele-

ment method. *International Journal of Mechanical Sciences*, 53(3):217–225, 2011a. 3, 37, 48

Robert L Johnson and Robert C Bill. Fretting in aircraft turbine engines. *NASA reports*, 1974. 10

Cyrus B Meher-Homji, George Gabriles, et al. Gas turbine blade failures-causes, avoidance, and troubleshooting. In *Proceedings of the 27th turbomachinery symposium*. Texas A&M University. Turbomachinery Laboratories, 1998. 10

J Ding, IR McColl, SB Leen, and PH Shipway. A finite element based approach to simulating the effects of debris on fretting wear. *Wear*, 263(1-6):481–491, 2007. 10

G Harish, MP Szolwinski, TN Farris, and T Sakagami. Evaluation of fretting stresses through full-field temperature measurements. In *Fretting Fatigue: Current Technology and Practices*. ASTM International, 2000. 11

J Dobromirski. Variables of fretting process: are there 50 of them? *ASTM Special Technical Publication*, 1159:60–60, 1992. 12

BP Conner and T Nicholas. Using a dovetail fixture to study fretting fatigue and fretting palliatives. *Journal of Engineering Materials and Technology*, 128(2):133–141, 2006. 12

PJ Golden and T Nicholas. The effect of angle on dovetail fretting experiments in ti-6al-4v. *Fatigue & fracture of engineering materials & structures*, 28(12):1169–1175, 2005. 12

Patrick J Golden. Development of a dovetail fretting fatigue fixture for turbine engine materials. *International Journal of Fatigue*, 31(4): 620–628, 2009. 12

Abdelwaheb Ferjaoui, Tongyan Yue, M Abdel Wahab, and Reza Hojjati-Talemi. Prediction of fretting fatigue crack initiation in double lap bolted joint using continuum damage mechanics. *International Journal of Fatigue*, 73:66–76, 2015. 13

M Eriten, AA Polycarpou, and LA Bergman. Development of a lap joint fretting apparatus. *Experimental mechanics*, 51(8):1405–1419, 2011. 13

Reza Hashemi Oskouei and Raafat Nasr Ibrahim. Improving fretting fatigue behaviour of al 7075-t6 bolted plates using electroless ni–p coatings. *International Journal of Fatigue*, 44:157–167, 2012. 13

TN Chakherlou, M Mirzajanzadeh, and Jeffrey Vogwell. Effect of hole lubrication on the fretting fatigue life of double shear lap joints: An experimental and numerical study. *Engineering Failure Analysis*, 16 (7):2388–2399, 2009. 13, 29

H Hertz. Über die berührung fester elastische körper und über die harte. *Verhandlungen des Vereins zur Beförderung des Gewerbefleisses*, 1882. 14

Rupert Stevenson Bradley. Lxxix. the cohesive force between solid surfaces and the surface energy of solids. *The London, Edinburgh, and Dublin Philosophical Magazine and Journal of Science*, 13(86):853–862, 1932. 16

KL Johnson, K Kendall, and AD Roberts. Surface energy and the contact of elastic solids. In *Proceedings of the Royal Society of London A:*

Mathematical, Physical and Engineering Sciences, volume 324, pages 301–313. The Royal Society, 1971. 16

Yoshiharu Mutoh. Mechanisms of Fretting Fatigue. *JSME international journal. Ser. A, Mechanics and material engineering*, 38(4):405–415, 1995. ISSN 09148809. 24

S. a. Namjoshi, S. Mall, V. K. Jain, and O. Jin. Fretting fatigue crack initiation mechanism in Ti-6Al-4V. *Fatigue & Fracture of Engineering Materials & Structures*, 25(10):955–964, oct 2002. ISSN 8756-758X. doi: 10.1046/j.1460-2695.2002.00549.x. URL `http://doi.wiley.com/10.1046/j.1460-2695.2002.00549.xhttp://www.scopus.com/inward/record.url?eid=2-s2.0-0036792846{&}partnerID=tZOtx3y1`. 24, 152, 153

Christopher D Lykins, Shankar Mall, and Vinod Jain. An evaluation of parameters for predicting fretting fatigue crack initiation. *International Journal of Fatigue*, 22(8):703–716, 2000. ISSN 01421123. doi: 10.1016/S0142-1123(00)00036-0. 24, 27

Matthew P Szolwinski and Thomas N Farris. Mechanics of fretting fatigue crack formation. *Wear*, 198(1-2):93–107, 1996. 24, 36

Matthew P Szolwinski and Thomas N Farris. Observation, analysis and prediction of fretting fatigue in 2024-t351 aluminum alloy. *Wear*, 221(1):24–36, 1998. 25, 31, 36, 48, 108, 144, 150

P. a. McVeigh and Thomas N. Farris. Finite Element Analysis of Fretting Stresses. *Journal of Tribology*, 119(4):797, 1997. ISSN 07424787. doi: 10.1115/1.2833887. 25, 27, 56

M. Tur, J. Fuenmayor, J.J. Ródenas, and E. Giner. 3D analysis of the influence of specimen dimensions on fretting stresses. *Finite Elements in Analysis and Design*, 39(10):933–949, 2003. ISSN 0168874X. doi: 10.1016/S0168-874X(02)00139-7. 26, 90

C Petiot, L Vincent, K Dang Van, N Maouche, J Foulquier, and B Journet. An analysis of fretting-fatigue failure combined with numerical calculations to predict crack nucleation. *Wear*, 181:101–111, 1995. 27

K Iyer and S Mall. Analyses of contact pressure and stress amplitude effects on fretting fatigue life. *Journal of engineering materials and technology*, 123(1):85–93, 2001. 27, 56

IR McColl, J Ding, and SB Leen. Finite element simulation and experimental validation of fretting wear. *Wear*, 256(11-12):1114–1127, 2004. 27

Heung Soo Kim, Shankar Mall, and Anindya Ghoshal. Two-dimensional and three-dimensional finite element analysis of finite contact width on fretting fatigue. *Materials transactions*, pages 1012201243–1012201243, 2011. 27, 138

Fei Shen, Weiping Hu, and Qingchun Meng. A damage mechanics approach to fretting fatigue life prediction with consideration of elastic–plastic damage model and wear. *Tribology International*, 82: 176–190, 2015. 27

Peter J Blau. The significance and use of the friction coefficient. *Tribology International*, 34(9):585–591, 2001. 28

Arnab Ghosh, Weiyi Wang, and Farshid Sadeghi. An elastic–plastic

investigation of third body effects on fretting contact in partial slip. *International Journal of Solids and Structures*, 81:95–109, 2016. 29

Arto Lehtovaara and Roger Rabb. A numerical model for the evaluation of fretting fatigue crack initiation in rough point contact. *Wear*, 264(9-10):750–756, 2008. 29

George Gavrilă and Spiridon Cretu. Influence of roughness and friction coefficient on the contact wear in partial slip conditions. *Transaction on control and mechanical systems*, 2012. 29

Tongyan Yue and Magd Abdel Wahab. Finite element analysis of fretting wear under variable coefficient of friction and different contact regimes. *Tribology International*, 107:274–282, 2017. 29

Sam Naboulsi and Ted Nicholas. Limitations of the coulomb friction assumption in fretting fatigue analysis. *International Journal of Solids and Structures*, 40(23):6497–6512, 2003. 29

MH Wharton, DE Taylor, and RB Waterhouse. Metallurgical factors in the fretting-fatigue behaviour of 70/30 brass and 0.7% carbon steel. *Wear*, 23(2):251–260, 1973. 30, 37, 108

K Endo and H Goto. Initiation and propagation of fretting fatigue cracks. *Wear*, 38(2):311–324, 1976. 30, 37

JA Alic and AL Hawley. On the early growth of fretting fatigue cracks. *Wear*, 56(2):377–389, 1979. 31

Wieslaw Switek. Early stage crack propagation in fretting fatigue. *Mechanics of Materials*, 3(3):257–267, 1984. 31

S Faanes. Inclined cracks in fretting fatigue. *Engineering fracture mechanics*, 52(1):71–82, 1995. 31, 38, 108, 150

Carlos Navarro, Sergio Muñoz, and Jaime Domínguez. Propagation in fretting fatigue from a surface defect. *Tribology international*, 39(10): 1149–1157, 2006. 31, 108, 124, 125, 150

RA Cardoso, JA Araújo, JLA Ferreira, and FC Castro. Crack path simulation for cylindrical contact under fretting conditions. *Frattura ed IntegritaÌĄ Strutturale*, 35:405, 2016. 31, 39, 108

BP Conner, AL Hutson, and L Chambon. Observations of fretting fatigue micro-damage of ti–6al–4v. *Wear*, 255(1):259–268, 2003. 31, 37

1 KJ Nix and TC Lindley. The influence of relative slip range and contact material on the fretting fatigue properties of 3.5 nicrmov rotor steel. *Wear*, 125(1-2):147–162, 1988. 31, 37

K Sato, H Fujii, and S Kodama. Crack propagation behaviour in fretting fatigue. *Wear*, 107(3):245–262, 1986. 31

Nitikorn Noraphaiphipaksa, Anchalee Manonukul, Chaosuan Kanchanomai, and Yoshiharu Mutoh. Fretting-contact-induced crack opening/closure behaviour in fretting fatigue. *International Journal of Fatigue*, 88:185–196, 2016. 32, 33, 42, 45, 77

A De Pannemaecker, S Fouvry, M Brochu, and JY Buffiere. Identification of the fatigue stress intensity factor threshold for different load ratios r: From fretting fatigue to c (t) fatigue experiments. *International Journal of Fatigue*, 82:211–225, 2016. 32

Yoshiharu Mutoh and Jin-Quan Xu. Fracture mechanics approach to fretting fatigue and problems to be solved. *Tribology International*, 36 (2):99–107, 2003. 32, 38, 48

Reza Hojjati-Talemi and Magd Abdel Wahab. Fretting fatigue crack initiation lifetime predictor tool: using damage mechanics approach. *Tribology International*, 60:176–186, 2013. 32

Nitikorn Noraphaiphipaksa, Anchalee Manonukul, and Chaosuan Kanchanomai. Fretting fatigue with cylindrical-on-flat contact: Crack nucleation, crack path and fatigue life. *Materials*, 10(2):155, 2017. 33, 46

E Giner, M Tur, A Vercher, and FJ Fuenmayor. Numerical modelling of crack–contact interaction in 2d incomplete fretting contacts using x-fem. *Tribology International*, 42(9):1269–1275, 2009. 33, 77, 121

JA Araujo and D Nowell. The effect of rapidly varying contact stress fields on fretting fatigue. *International Journal of Fatigue*, 24(7):763–775, 2002. 33, 48, 77, 145

Toshio Hattori, Masayuki Nakamura, Hiroshi Sakata, and Takashi Watanabe. Fretting fatigue analysis using fracture mechanics. *JSME international journal. Ser. 1, Solid mechanics, strength of materials*, 31(1): 100–107, 1988. 36

DA Hills, D Nowell, and JJ O'Connor. On the mechanics of fretting fatigue. *Wear*, 125(1-2):129–146, 1988. 36

Sergio Munoz, Carlos Navarro, and Jaime Dominguez. Application of fracture mechanics to estimate fretting fatigue endurance curves. *Engineering Fracture Mechanics*, 74(14):2168–2186, 2007. 37, 50

PJ Golden and AF Grandt. Fracture mechanics based fretting fatigue life predictions in ti–6al–4v. *Engineering fracture mechanics*, 71(15): 2229–2243, 2004. 37

V Lamacq, MC Dubourg, and L Vincent. Crack path prediction under fretting fatigueâĂŤa theoretical and experimental approach. *Journal of Tribology*, 118(4):711–720, 1996. 38, 42

MH El Haddad, KN Smith, and TH Topper. Fatigue crack propagation of short cracks. *Journal of Engineering Materials and Technology*, 101(1): 42–46, 1979. 39

Nitikorn Noraphaiphipaksa, Chaosuan Kanchanomai, and Y Mutoh. Numerical and experimental investigations on fretting fatigue: Relative slip, crack path, and fatigue life. *Engineering Fracture Mechanics*, 112:58–71, 2013. 39, 42, 43, 79

D Rozumek and E Macha. A survey of failure criteria and parameters in mixed-mode fatigue crack growth. *Materials science*, 45(2):190, 2009. 40

Fazil Erdogan and GC Sih. On the crack extension in plates under plane loading and transverse shear. *Journal of basic engineering*, 85(4): 519–525, 1963. 40, 78

MA Hussain, SL Pu, and J Underwood. Strain energy release rate for a crack under combined mode i and mode ii. In *Fracture analysis: Proceedings of the 1973 national symposium on fracture mechanics, part II*. ASTM International, 1974. 41

KKWG Palaniswamy. On the problem of crack extension in brittle solids under general loading. *Mechanics today*, 4:30, 1978. 41

Marie-Christine Dubourg and Valerie Lamacq. Stage ii crack propagation direction determination under fretting fatigue loading: a new approach in accordance with experimental observations. In *Fretting fatigue: current technology and practices*. ASTM International, 2000. 42, 78

Francois Hourlier, Hubert d'Hondt, Michel Truchon, and Andre Pineau. Fatigue crack path behavior under polymodal fatigue. In *Multiaxial Fatigue*. ASTM International, 1985. 43, 44, 78, 98, 100

Rachelle Ribeaucourt, M-C Baietto-Dubourg, and Anthony Gravouil. A new fatigue frictional contact crack propagation model with the coupled x-fem/latin method. *Computer Methods in Applied Mechanics and Engineering*, 196(33):3230–3247, 2007. 44, 97

Marie-Christine Baietto, Emilien Pierres, Anthony Gravouil, Bruno Berthel, Siegfried Fouvry, and Benoit Trolle. Fretting fatigue crack growth simulation based on a combined experimental and xfem strategy. *International Journal of Fatigue*, 47:31–43, 2013. 44, 48

Marie-Christine Baietto, Emilien Pierres, and Anthony Gravouil. A multi-model x-fem strategy dedicated to frictional crack growth under cyclic fretting fatigue loadings. *International Journal of Solids and Structures*, 47(10):1405–1423, 2010. 44

E Giner, M Sabsabi, and FJ Fuenmayor. Calculation of k ii in crack face contacts using x-fem. application to fretting fatigue. *Engineering Fracture Mechanics*, 78(2):428–445, 2011b. 45

Eugenio Giner, José Díaz-Álvarez, Miguel Marco, and Mª Henar Miguélez. Orientation of propagating crack paths emanating from

fretting-fatigue contact problems. *Frattura ed IntegritàĮ Strutturale*, page 285, 2016. 45, 98, 101

Juan Carlos Martínez, Libardo Vicente Vanegas Useche, and Magd Abdel Wahab. Numerical prediction of fretting fatigue crack trajectory in a railway axle using xfem. *International Journal of Fatigue*, 100: 32–49, 2017. 45

N Noraphaiphipaksa, Anchalee Manonukul, Chaosuan Kanchanomai, and Yoshiharu Mutoh. Fretting fatigue life prediction of 316l stainless steel based on elastic–plastic fracture mechanics approach. *Tribology International*, 78:84–93, 2014. 45

Yoshiharu Mutoh, Jin-Quan Xu, and Kazunori Kondoh. Observations and analysis of fretting fatigue crack initiation and propagation. In *Fretting Fatigue: Advances in Basic Understanding and Applications*. ASTM International, 2003. 48

Carlos Navarro, Sergio Muñoz, and Jaime Dominguez. On the use of multiaxial fatigue criteria for fretting fatigue life assessment. *International Journal of fatigue*, 30(1):32–44, 2008. 48, 126

So Suresh and RO Ritchie. Propagation of short fatigue cracks. *International Metals Reviews*, 29(1):445–475, 1984. 50

Kyungmok Kim and Myung-Jin Yoon. Fretting fatigue simulation for aluminium alloy using cohesive zone law approach. *International Journal of Mechanical Sciences*, 85:30–37, 2014. 51, 132, 138, 144, 177

Huayang Zhang, Jinxiang Liu, and Zhengxing Zuo. Numerical study of the effects of residual stress on fretting fatigue using xfem. *Materials*, 8(10):7094–7105, 2015. 51, 132, 168

Huayang Zhang, Jinxiang Liu, and Zhengxing Zuo. Investigation into the effects of tangential force on fretting fatigue based on xfem. *Tribology International*, 99:23–28, 2016. 52, 132, 168

C.T Tsai and Shankar Mall. Elasto-plastic finite element analysis of fretting stresses in pre-stressed strip in contact with cylindrical pad. *Finite Elements in Analysis and Design*, 36(2):171–187, 2000. ISSN 0168874X. doi: 10.1016/S0168-874X(00)00016-0. 56

Mark Ainsworth and J.Tinsley Oden. A posteriori error estimation in finite element analysis. *Computer Methods in Applied Mechanics and Engineering*, 142(1):1–88, 1997. ISSN 00457825. doi: 10.1016/S0045-7825(96)01107-3. 56

M Massingham and PE Irving. The effect of variable amplitude loading on stress distribution within a cylindrical contact subjected to fretting fatigue. *Tribology international*, 39(10):1084–1091, 2006. 56

Glenn B Sinclair. Stress singularities in classical elasticity–i: Removal, interpretation, and analysis. *Applied Mechanics Reviews*, 57(4):251–298, 2004. 58, 63

Martin Bäker. How to get meaningful and correct results from your finite element model. *arXiv preprint arXiv:1811.05753*, 2018. 61

G B Sinclair, J R Beisheim, and S Sezer. Practical convergence-divergence checks for stresses from FEA. *Proceedings of the 2006 International ANSYS Conference*, 50(Reference 1), 2006. 71

Sung-Keun Lee, Kozo Nakazawa, Masae Sumita, and Norio Maruyama. Effects of contact load and contact curvature radius of cylinder pad on fretting fatigue in high strength steel. In *Fretting*

Fatigue: Current Technology and Practices. ASTM International, 2000. 71

Brian Cotterell and JRf Rice. Slightly curved or kinked cracks. *International journal of fracture*, 16(2):155–169, 1980. 78

Slobodanka Boljanović and Stevan Maksimović. Analysis of the crack growth propagation process under mixed-mode loading. *Engineering fracture mechanics*, 78(8):1565–1576, 2011. 78

AM Abdel Mageed and RK Pandey. Studies on cyclic crack path and the mixed-mode crack closure behaviour in al alloy. *International Journal of Fatigue*, 14(1):21–29, 1992. 78

ACO Miranda, MA Meggiolaro, JTP Castro, LF Martha, and TN Bittencourt. Fatigue life and crack path predictions in generic 2d structural components. *Engineering Fracture Mechanics*, 70(10):1259–1279, 2003. 78

Hans A Richard, M Fulland, and M Sander. Theoretical crack path prediction. *Fatigue & fracture of engineering materials & structures*, 28 (1-2):3–12, 2005. 78

D Nowell, D Dini, and DA Hills. Recent developments in the understanding of fretting fatigue. *Engineering fracture mechanics*, 73(2): 207–222, 2006. 90

A Rohatgi. Web plot digitizer. ht tp. *arohatgi. info/WebPlotDigitizer/(accessed Aug 2014)*, 2014. 93

Yangjian Xu and Huang Yuan. Computational modeling of mixed-mode fatigue crack growth using extended finite element methods. *International Journal of Fracture*, 159(2):151, 2009a. 95, 138

Peter Dahlin. *Growth of fatigue cracks subjected to non-proportional Mode I and II*. PhD thesis, KTH, 2005. 99

Jason John Madge. *Numerical modelling of the effect of fretting wear on fretting fatigue*. PhD thesis, University of Nottingham, 2009. 100

Meinhard Kuna. *Finite elements in fracture mechanics*, volume 10. Springer, 2013. 103

Hiroshi Tada, P Paris, and G Irwin. The analysis of cracks handbook. *New York: ASME Press*, 2:1, 2000. 105, 185

Yibing Xiang, Zizi Lu, and Yongming Liu. Crack growth-based fatigue life prediction using an equivalent initial flaw model. part i: Uniaxial loading. *International Journal of Fatigue*, 32(2):341–349, 2010. 114

Liming Liu. *Modeling of mixed-mode fatigue crack propagation*. PhD thesis, Graduate School of Vanderbilt University, 2008. 114

Ulrich Krupp. *Fatigue crack propagation in metals and alloys: microstructural aspects and modelling concepts*. John Wiley & Sons, 2007. 124

Jan De Pauw. *Experimental research on the influence of palliatives in fretting fatigue*. PhD thesis, Ghent University, 2016. 124

Nadeem Ali Bhatti and Magd Abdel Wahab. A numerical investigation on critical plane orientation and initiation lifetimes in fretting fatigue under out of phase loading conditions. *Tribology International*, 115: 307–318, 2017a. 126, 149

Meinhard Kuna and Stephan Roth. General remarks on cyclic cohesive zone models. *International Journal of Fracture*, 196(1-2):147–167, 2015. 134

Donald S Dugdale. Yielding of steel sheets containing slits. *Journal of the Mechanics and Physics of Solids*, 8(2):100–104, 1960. 134

Wolfgang Brocks, Alfred Cornec, and Ingo Scheider. Computational aspects of nonlinear fracture mechanics. *GKSS FORSCHUNGSZENTRUM GEESTHACHT GMBH-PUBLICATIONS-GKSS*, 30, 2003. 134, 135

Kyoungsoo Park and Glaucio H Paulino. Cohesive zone models: a critical review of traction-separation relationships across fracture surfaces. *Applied Mechanics Reviews*, 64(6):060802, 2011. 134

Stephan Roth, Geralf Hütter, and Meinhard Kuna. Simulation of fatigue crack growth with a cyclic cohesive zone model. *International Journal of Fracture*, 188(1):23–45, 2014. 134

Viggo Tvergaard. Effect of fibre debonding in a whisker-reinforced metal. *Materials science and engineering: A*, 125(2):203–213, 1990. 136

A Needleman. An analysis of decohesion along an imperfect interface. In *Non-Linear Fracture*, pages 21–40. Springer, 1990. 136

Philippe H Geubelle and Jeffrey S Baylor. Impact-induced delamination of composites: a 2d simulation. *Composites Part B: Engineering*, 29(5):589–602, 1998. 136

ABAQUS Version. 6.13, analysis user's manual. *Dassault Systemes Simulia Corp., Providence, RI*, 2013. 137, 172

Haixia Mei, Shravan Gowrishankar, Kenneth M Liechti, and Rui Huang. Initiation and propagation of interfacial delamination in

integrated thin-film structures. In *2010 12th IEEE Intersociety Conference on Thermal and Thermomechanical Phenomena in Electronic Systems*, pages 1–8. IEEE, 2010. 138, 139

A De-Andrés, JL Pérez, and M Ortiz. Elastoplastic finite element analysis of three-dimensional fatigue crack growth in aluminum shafts subjected to axial loading. *International Journal of Solids and Structures*, 36(15):2231–2258, 1999. 138

Valentina Lopresto, Langella Antonio, and Abrate Serge. *Dynamic response and failure of composite materials and structures*. Woodhead Publishing, 2017. 138

Yangjian Xu and Huang Yuan. Computational analysis of mixed-mode fatigue crack growth in quasi-brittle materials using extended finite element methods. *Engineering Fracture Mechanics*, 76(2):165–181, 2009b. 138

CD Lykins, S Mall, and V Jain. A shear stress-based parameter for fretting fatigue crack initiation. *Fatigue & Fracture of Engineering Materials & Structures*, 24(7):461–473, 2001a. 145

Nadeem Ali Bhatti and Magd Abdel Wahab. Finite element analysis of fretting fatigue under out of phase loading conditions. *Tribology International*, 109:552–562, 2017b. 145

Nadeem Ali Bhatti, Kyvia Pereira, and Magd Abdel Wahab. A continuum damage mechanics approach for fretting fatigue under out of phase loading. *Tribology International*, 117:39–51, 2018. 145

William Nichols Findley. A theory for the effect of mean stress on

fatigue of metals under combined torsion and axial load or bending. *Journal of Engineering for Industry*, 81(4):301–305, 1959. 145, 157

William Nichols Findley, JJ Coleman, and BC Hanley. *Theory for combined bending and torsion fatigue with data for SAE4340 steel*. Division of Engineering, Brown University, 1956. 145

A Fatemi, A Plaseied, AK Khosrovaneh, and D Tanner. Application of bi-linear log–log s–n model to strain-controlled fatigue data of aluminum alloys and its effect on life predictions. *International Journal of Fatigue*, 27(9):1040–1050, 2005. 146

Ali Fatemi and Darrell F Socie. A critical plane approach to multiaxial fatigue damage including out-of-phase loading. *Fatigue & Fracture of Engineering Materials & Structures*, 11(3):149–165, 1988. 147

Nadeem Ali Bhatti and Magd Abdel Wahab. Fretting fatigue crack nucleation: A review. *Tribology International*, 121:121–138, 2018. 149

Christopher D Lykins, Shankar Mall, and Vinod K Jain. Combined experimental–numerical investigation of fretting fatigue crack initiation. *International journal of fatigue*, 23(8):703–711, 2001b. 152

Mohammad Almajali. Effects of phase difference between axial and contact loads on fretting fatigue behavior of titanium alloy. Technical report, Air Force Inst of Tech Wright-Patterson AFB OH Scholl of Engineering and Management, 2006. 152

Jinxiang Liu, Jun Li, and Bo Wu. The cohesive zone model for fatigue crack growth. *Advances in Mechanical Engineering*, 5:737392, 2013. 163, 164, 167

Ani Ural, Venkat R Krishnan, and Katerina D Papoulia. A cohesive zone model for fatigue crack growth allowing for crack retardation. *International Journal of Solids and Structures*, 46(11-12):2453–2462, 2009. 163

O Nguyen, EA Repetto, Michael Ortiz, and RA Radovitzky. A cohesive model of fatigue crack growth. *International Journal of Fracture*, 110 (4):351–369, 2001. 164

KL Roe and Th Siegmund. An irreversible cohesive zone model for interface fatigue crack growth simulation. *Engineering fracture mechanics*, 70(2):209–232, 2003. 164, 165, 168

George Michael Winter. *A cohesive zone model approach to multiaxial fatigue*. PhD thesis, Purdue University, 2009. 165, 167, 172, 173, 177, 178

B Wang and T Siegmund. A numerical analysis of constraint effects in fatigue crack growth by use of an irreversible cohesive zone model. *International Journal of Fracture*, 132(2):175–196, 2005. 168

Reza Hojjati-Talemi, Magd Abdel Wahab, Eugenio Giner, and Mohamad Sabsabi. Numerical estimation of fretting fatigue lifetime using damage and fracture mechanics. *Tribology Letters*, 52(1):11–25, 2013. 173, 178, 183, 184, 185, 186, 187

ASM International. Handbook Committee. *Properties and selection: nonferrous alloys and special-purpose materials*, volume 2. Asm Intl, 1990. 177

Mohamad Sabsabi. *Modelado de grieta y estimación de vida en Fretting*

Fatiga mediante el Método de los Elementos Finitos Extendido X-FEM. PhD thesis, Universitat Politècnica de València, 2010. 180

Alberto Carpinteri and Marco Paggi. A unified interpretation of the power laws in fatigue and the analytical correlations between cyclic properties of engineering materials. *International Journal of Fatigue*, 31(10):1524–1531, 2009. 180

J Lankford. The influence of microstructure on the growth of small fatigue cracks. *Fatigue & Fracture of Engineering Materials & Structures*, 8(2):161–175, 1985. 180

Keisuke Tanaka. Fatigue crack propagation from a crack inclined to the cyclic tensile axis. *Engineering Fracture Mechanics*, 6(3):493–507, 1974. 181